DISSERTATION

ASSAY DEVELOPMENT FOR PATHOGEN DETECTION AT THE POINT-OF-NEED

Submitted by

Cody S. Carrell

Department of Chemistry

In partial fulfillment of the requirements

For the Degree of Doctor of Philosophy

Colorado State University

Fort Collins, Colorado

Fall 2020

Doctoral Committee:

Advisor: Charles S. Henry

Delphine K. Farmer
Andrew McNally
Kenneth F. Reardon

ABSTRACT

ASSAY DEVELOPMENT FOR PATHOGEN DETECTION AT THE POINT-OF-NEED

Infectious diseases are responsible for roughly one third of worldwide deaths, which disproportionately occur in low- and middle-income countries. Government health agencies recognize high quality diagnostics as a key tool to slow the spread and reduce the burden of disease in these countries. The same diagnostics that have minimized deaths from infectious disease in developed nations, however, cannot simply be implemented in all locations. Low- and middle-income countries lack the financial resources and infrastructure required to use the sophisticated instruments found in modern hospital laboratories. Instead of relying on current diagnostic technologies to reduce the burden of infectious disease, there is an urgent need to develop new technologies suited for the resource-limited settings they will be used in. The work described in this thesis aims to advance the capabilities of diagnostic sensors for use at the point-of-need.

Microfluidic devices have been used for decades to perform complex analysis using compact devices with small sample and reagent volumes. Their portability and low-cost make them ideal candidates for analysis in resource limited settings, but their fabrication is tedious and expensive. To improve the fabrication process, Chapter Two of this thesis describes two methods for simplified 3D-printing of microfluidic devices. The 3D printer and resin used are inexpensive and commercially available and the fabrication process is not limited by the need to remove uncured resin from enclosed channels. Instead, open-faced channels in 3D-printed pieces were silanized and sealed to a secondary substrate. Common microfluidic devices including a droplet generator and herringbone mixer were created with the new fabrication method to demonstrate the

strength of the seal and ability for the printer to create microfluidic channels. We envision this method being used for rapid prototyping and increased innovation in the field of microfluidic sensors.

Traditional polymer microfluidics are limited in their usefulness in point-of-need situations because they require a pump to drive flow. Paper-based microfluidics use capillary action to drive flow instead of a pump and have emerged as an easy-to-use and inexpensive alternative to traditional microfluidics in situations where a power source is not available. However, paper-based microfluidics often suffer from poor analytical performance, and efforts to improve result in increased complexity. Chapter Three of this thesis describes a paper-based device that increases the sensitivity of a *Salmonella* assay while retaining ease-of-use. The device combines paper-pads for reagent storage with a 3D-printed rotational manifold to perform an enzyme-linked immunosorbent assay (ELISA). Typically, this assay requires dozens of complex pipetting steps, but the rotary device simplifies this process into four semi-automated steps. A detection limit of 440 colony forming units/mL was found using the paper-based device.

As demonstrated in Chapter Three, common issues with paper-based microfluidics can be solved by integrating paper with other inexpensive components like 3D-printed polymer. In the final study in Chapter Four, we created a device to further simplify the steps of an ELISA using a combination of paper, polyester transparency film, and double-sided adhesive. The device, termed a disposable ELISA (dELISA), automatically performed the sequential reagent delivery and washing steps required for a traditional ELISA and require only two end user steps. The dELISA was then used to perform a serology assay for SARS-CoV-2 antibodies from whole-blood. The detection limit of the assay was 2.8 ng/mL for the dELISA, which was nearly identical to the detection limit found using a tradition well-plate assay (1.2 ng/mL).

ACKNOWLEDGEMENTS

First, I would like to thank my wife, Mollie Carrell, for her tremendous support during the four years of my Ph.D. A long day of failed experiments in the lab was much more tolerable knowing that I would be coming home to wonderful, caring partner every evening. She has made a great deal of sacrifices so that I could accomplish my goal of earning a Ph.D and I don't think I can thank her enough. I can't count the number of times I've been driven to the lab on days when it was too cold to bike, or the number of practice talks she's had to endure along the way. Mollie, you have always been there supporting me with a smile and I know that this journey would have been nearly impossible without you. In May, 2020 Mollie gave birth to our daughter, Charlotte Joy Carrell, in the midst of a pandemic, and I need to thank Charlotte as well for the motivation to push through the last few months of the Ph.D. I would also like to thank other family members for their support and love these last four years: My mother, Dr. Lori Carrell, for her valuable guidance as the other "Dr." in the family; my Father, Cliff Carrell, for reminding me to enjoy what Colorado has to offer and get out of the lab; and My in-laws, Tim and Colleen Merrill, for letting me drag their daughter half-way across the country.

Secondly, I would like to thank my advisor, Dr. Chuck Henry, for his support and guidance. I have never had a boss as understanding, patient, or kind as Chuck. Any future success of mine will forever be tied to the experience I had in the Henry Lab as a Ph.D. student. Chuck has created a culture in his lab that is accepting, inquisitive, supportive, hard-working, and ambitious. I've traveled and presented at four conferences including a conference in Taiwan, which was one of the highlights of my Ph.D. It is not lost on me that these travel opportunities were the result of a boss who paid for these trips because he cared about the development of his

students as scientists and public speakers. It has been a wonderful place to work and I feel fortunate to have had the opportunity to work for and with Chuck on such exciting and interesting projects. Early morning golf and hunting trips with Chuck were always a great way to start the workday and I am excited for many more post-graduation!

Finally, I would like to thank the members of the Henry group for their help and support over the last four years. It's been a fantastic group to work with and I deeply appreciate all of the edited papers, critiqued presentations, birthday cakes, and lunch trips. Specifically, I would like to thank Dr. Rob Channon for his encouragement, support, and friendship. As a first-year grad student, Rob set an example as a scientist and mentor that I strived to match during my graduate career. I attribute much of my success to the example he set, so thank you, Rob. I can't wait for Charlotte and James to finally meet!

TABLE OF CONTENTS

ABSTRACT…...…….ii

ACKNOWLEDGEMENTS……..iv

CHAPTER 1. INTRODUCTION.....1

1.1 Point-of-Care Pathogen Detection…….....…….1

1.2 Microfluidic Devices for Point-of-Care Diagnostics…….....2

1.3 Paper-based Microfluidic Devices…….....5

1.4 Improving µPAD Sensitivity and Functionality……....…..13

1.5 Hybrid passive flow solutions to address µPAD shortcomings…….....14

REFERENCES…….....15

CHAPTER 2: SEALING 3D-PRINTED PARTS TO POLY(DIMETHYLSILOXANE) FOR SIMPLE FABRICATION OF MICROFLUIDIC DEVICES.....25

2.1 Introduction…….....…….....25

2.2 Materials and Methods.....28

2.3 Results and Discussion.....30

2.4 Conclusion.....,.....40

REFERENCES.....42

CHAPTER 3: ROTARY MANIFOLD FOR AUTOMATING A PAPER-BASED *SALMONELLA* IMMMUNOASSAY.....46

3.1 Introduction.....46

3.2 Materials and Methods.....49

3.3 Results and Discussion.....54

3.4 Conclusion.....61

REFERENCES.....63

CHAPTER 4. POINT-OF-NEED DISPOSABLE ELISA SYSTEM FOR COVID-19 SEROLOGY TESTING....70

3.1 Introduction....71

3.2 Materials and Methods....74

3.3 Results and Discussion....77

3.4 Conclusion....84

REFERENCES.... 85

CHAPTER 5. CONCLUSIONS AND FUTURE DIRECTIONS....89

APPENDIX ONE: SUPPLEMENTARY INFORMATION - SEALING 3D-PRINTED PARTS TO POLY(DIMETHYLSILOXANE) FOR SIMPLE FABRICATION OF MICROFLUIDIC DEVICES....94

APPENDIX TWO: SUPPLEMENTARY INFORMATION - ROTARY MANIFOLD FOR AUTOMATING A PAPER-BASED *SALMONELLA* IMMMUNOASSAY....101

APPENDIX 3: SUPPLEMENTARY INFORMATION – POINT-OF-NEED DISPOSABLE ELISA SYSTEM FOR COVID-19 SEROLOGY TESTING....108

APPENDIX 4: SIMULTANEOUS ELECTROCHEMICAL DETECTION OF *E.COLI, SALMONELLA,* AND *LISTERIA* WITH A TRANSPARENCY AND PAPER-BASED ANALYTICAL DEVICE....109

APPENDIX 5: SARS-CoV-2 VIRAL ANTIGEN ASSAY USING THE dELISA....121

APPENDIX 6: A MICROFLUIDIC MAGNETOPHORETIC DUPLEX SPECIFIC NUCLEASE MICRO RNA ASSAY FOR LUNG CANCER SCREENING....126

CHAPTER 1. INTRODUCTION[1]

1.1 Point-of-Care Pathogen Detection

Infectious diseases are a leading cause of death worldwide.[1] As medicine and technology have advanced over the last two decades, the burden of infectious diseases relative to non-communicable diseases like heart-disease and stroke has decreased, especi[1]ally in developed countries. In low and middle income countries, however, infectious diseases remain a significant contributor to morbidity and mortality.[2] For example, HIV and tuberculosis caused over 3 million deaths in 2017.[3, 4] The World Health Organization (WHO) has long recognized inexpensive diagnostics as a critical tool to reduce the impact of infectious disease, and in 2018 published and Essential Diagnostics List that highlight the most important diagnostics still needing development.[5]

Although low-cost diagnostics have recently been focused on use in low and middle income countries, the corona virus pandemic of 2020 has also re-emphasized the significance of accurate and efficient pathogen detection in all countries regardless of socioeconomic status.[6] The countries with the best initial responses to the virus employed large-scale testing efforts to identify contagious individuals. Serology testing, or testing for antibodies that indicate prior infection and immunity, is also important to help to safely re-open economies and return to normalcy.[7] Diagnostic assays are a critical component to the current healthcare infrastructure and inform 70% of all clinical decisions, but are underrepresented in healthcare funding, composing only 2% of total healthcare spending.[8] In the case of SARS-CoV-2, testing methods included

[1] Contents of this section are based on a review article in which I was the first author, with modifications and edits for this document[26]

polymerase chain reaction (PCR) to identify specific RNA segments from the virus and enzyme linked immunosorbent assays (ELISAs) to detect antibodies against the virus. Although highly sensitive and specific, both methods are expensive, time consuming, and require trained end-users and a temperature-controlled laboratory. These same requirements are common for most diagnostic assays, which limits the accessibility of the technology to a select few in developed nations.

To slow the spread of infectious diseases and increase treatment efficiency, rapid and accurate pathogen detection is critical.[6, 9] Unfortunately, the economic disparities between populations that limit access to high quality diagnostic assays will not be solved any time soon, leaving most of the world's population susceptible to viral and bacterial outbreaks. Instead, new technologies that are designed to function in non-laboratory and resource-limited settings must be developed. Assays that can be performed at the point-of-care (POC) have been of significant interest to researchers for several decades. The two most common and successful POC assays are the pregnancy test and the glucose monitor. Both are simple to operate and quickly deliver vital information to the end user about their health at a relatively low cost. Additional characteristics of a successful POC assay are defined by the ASSURED criteria established by the WHO in 2012.[10] Assays that meet the ASSURED criteria should be **A**ffordable, **S**ensitive, **S**pecific, **U**ser-friendly, **R**apid and Robust, **E**quipment-free, and **D**eliverable to end users. It is difficult to meet all seven ASSURED guidelines for a given assay, so researchers must pick and choose the most important for the specific situation being addressed. Development of tests that meet these criteria is essential if we are to continue to decrease the burden of infectious disease across the globe.

1.2 Microfluidic Devices for Point-of-Care Diagnostics

A popular platform for POC assays is microfluidic devices.[11] Microfluidic devices manipulate sample and reagent flow through small micron sized channels to perform complex assays in a compact system. The small size of these devices (typically <5x5 cm) makes them relatively portable and low reagent volumes enable affordable analysis. Because of these advantages, microfluidics are frequently used for pathogen detection.[12] Importantly, precise and automated fluid manipulation eliminate the need for time-consuming culturing steps. Microfluidic devices have been developed to detect whole-cells, biomarkers, and biomolecules for bacteria, viruses, parasites, prions, and other infectious agents.[12, 13] These microfluidic systems use a variety of detection techniques including optical imaging, spectroscopy, electrochemistry, and fluorimetry, often performed with devices as portable and simple as a smartphone. In addition to analytical measurements, microfluidics have been used for drug discovery, cell culture, molecular biology, and many more applications.[14, 15] Although an immensely promising technology for point-of-care analysis, relatively few microfluidic devices have made the jump from bench to market.[16]

One reason for the lack of commercialization is that microfluidic fabrication is difficult. The most common fabrication technique for microfluidic devices is soft lithography, which is expensive, labor and time intensive, and complex, limiting the development of microfluidics to research laboratories and slowing progress for mass production.[17-19] Many labs have turned to 3D-printing as an alternative fabrication technique.[19] 3D printing began in the 1980s, but could not create channels with high enough resolution for microfluidics until recently.[20] Most printers for creating microfluidic devices use stereolithography (SLA), digital light processing (DLP) or direct ink writing (DIW) 3D-printers.[19] The most advanced printers have <10 µm resolution and have been used to directly print enclosed microfluidic channels, but these printers and their

corresponding resins are custom-made and/or expensive (>$100k). Of these techniques, SLA printers have become the preferred printer type for printing microfluidics.[19, 21] Here, a platform is lowered into a bath of liquid resin and the resin is locally cured with a UV laser. Once a layer is cured, the platform raises incrementally until all layers are printed (Figure 1.1). The resolution of SLA printers is limited by either the laser spot size and/or the minimum height the platform can be raised. For example, a popular and inexpensive SLA printer called the Form3 has a laser spot size of 85 µm (x,y resolution) and a minimum step height of 25 µm (z resolution). Because liquid resin is used, when enclosed fluidic channels are printed uncured resin becomes trapped in those channels. Consequently, tedious post-processing is required to remove uncured resin from enclosed channels, which can take days to fully clean.[22-24] The smaller the channel, the more difficult the resin is to remove, and the issue is considered a major limitation in the advancement of 3D-printing microfluidics.

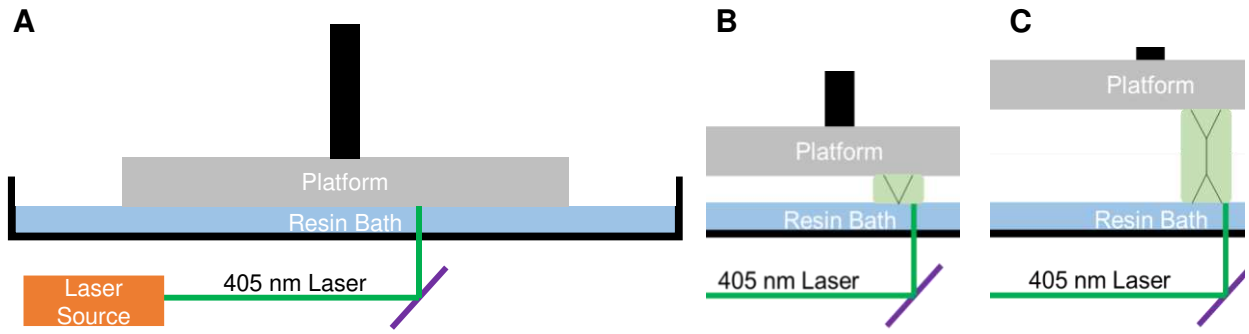

Figure 1.1. A) Typical setup of a stereolithography (SLA) printer. A platform sits in a bath of photo-curable resin and a 405 nm laser cures a pattern of resin onto the base of the platform. B) After each layer is cured, the platform slowly raises until the part is finished (C).

To circumvent the problems of printing enclosed, microfluidic-sized channels, Chapter 2 in this document will describe two methods to print open-faced channels in 3D-printed pieces and seal them to secondary substrates to form enclosed channels for microfluidic applications.[25] Importantly, the printer and resin used were inexpensive (~$2000, $150/L) and commercially

available. Instead of a fabrication process that takes multiple days to complete, devices can be made in a matter of hours and require no post-processing to remove uncured resin. To demonstrate the practicality of the fabrication method common microfluidic devices like droplet generators, gradient generators and H-cells were created. Ideally, this work will provide an alternative fabrication method that will lower the cost and labor barrier to allow more laboratories to begin researching microfluidics and improve access to microfluidic diagnostics in resource-limited settings.

1.3 Paper-based Microfluidic Devices (Contents of this section are based on a review article in which I was the first author, with modifications and edits for this document)[26]

Although versatile and widely used, microfluidics are not ideal systems for all POC applications because they require mechanical pumps to drive flow. These pumps are bulky, difficult to transport, and require a power source. As a result, they do not meet the "Equipment-free" and "Deliverable" criteria from the ASSURED guidelines. As an alternative to traditional microfluidics, microfluidic paper-based analytical devices (μPADs) were introduced in 2007 by Martinez et al.[27] Paper generates flow through capillary action from hydrophilic cellulose pores so no pumps are needed. Because of its availability, low cost, ease of safe handling and disposal, and inherent capillary flow, cellulosic paper has become increasingly popular for analytical applications since its introduction.[28-30] There have been numerous reviews of microfluidics and specifically μPADs in recent years from which one can identify several important common themes and future directions.[29-36]

From the initial report in 2007, the μPAD field rapidly expanded to include many more groups and key developments. Tens of thousands of papers have been published in the field, with an increasing number of publications each year until 2019 (Figure 1.2). New methods for

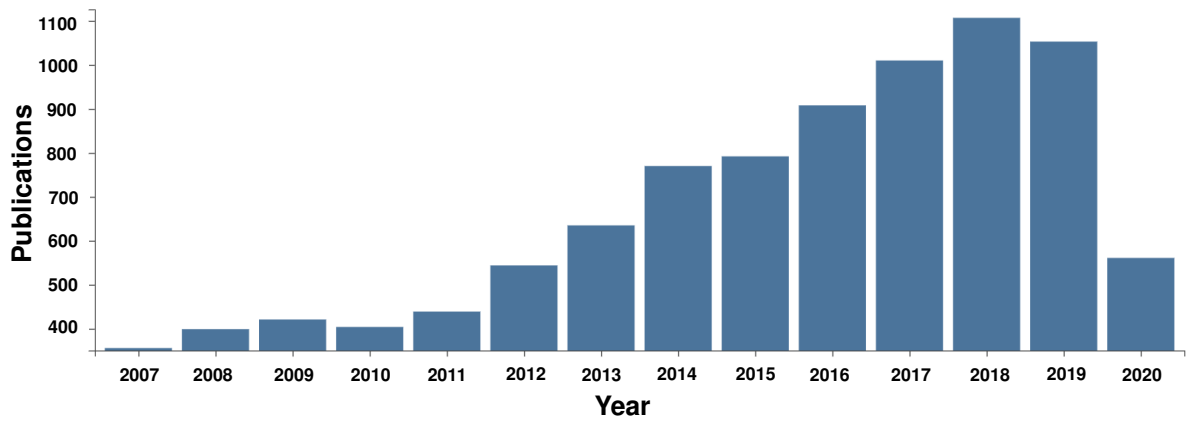

Figure 1.2 Publications per year for the search term "Paper based analytical devices" in Web of Science. Accessed 08.23.2020

fabricating devices appeared first, with a transition from photolithography (a complicated, expensive approach) to wax printing, screen-printing, and inkjet printing; these, in turn, expanded accessibility of the field to many researchers around the world. New methods for detection also appeared (the initial report used colorimetric detection), with the Henry group pioneering use of electrochemical detection,[37] the Whitesides group the use of fluorescence,[38] and the Yu group the use of chemiluminescence.[39] Areas of application also expanded from the initial work in point-of-care diagnostics to include efforts in food and environmental testing by the Henry group.[40, 41] The µPAD field has grown rapidly to the point where hundreds of articles are published each year describing the latest innovations. Despite this substantial growth, much work remains to move µPADs from academic curiosities to practical solutions for important global problems. In an effort to review the current state of µPADs, specific application areas were examined for more practical and less general and insights into future development. The application areas chosen for review were Medical Diagnostics, Environmental Monitoring, and Food Quality.

Medical Diagnostics

µPADs have shown tremendous potential as POC diagnostic tools for a wide variety of health issues. Such devices have recently been developed to detect many biomarkers and pathogens, including NO_2^- in saliva, Ebola virus RNA, Salmonella, Hepatitis C antibodies, virus DNA, and glucose.[42-47] While numerous diagnostic µPADs have been reported, there are pitfalls common to many that make them non-ideal for their intended use at the point-of-care in resource limited settings. These pitfalls include: 1) poor detection limits obtained in µPADs are particularly troublesome for biological analytes which are often relevant at sub-attomolar concentrations,[48] 2) common reagents used in biological assays (e.g. antibodies and enzymes) degrade easily in resource limited settings where storage conditions such as temperature and humidity are difficult to control[49] and 3) most existing µPADs test for one specific analyte rather than a suite of analytes. These problems must be addressed before µPADs can become commercialized POC diagnostic tools. Therefore, in the coming years we expect and advocate for µPAD research in this area to focus on improving sensitivity and detection limits, developing new techniques for long-term and stable storage of reagents on paper in uncontrolled conditions, and fabricating devices capable of multiplexed testing. We also expect the field to move towards preventative screening in addition to acute diagnostics, as healthcare experts have promoted in recent years.[50]

Many groups have addressed the pitfalls listed above by integrating new sensing motifs on PADs. For example, LODs on paper can be improved over traditional colorimetric detection through techniques like fluorescence or electrochemistry[51, 52]. However, in clinical diagnostics, these sensitive detection methods may still require some form of chemical amplification, such as enzyme or metal ion-based enhancement to further lower detection limits to clinically relevant levels.[53, 54] While such detection limits have been achieved, the chemical amplification procedures

are often unattractive in μPADs as they require expensive reagents, multiple steps to be carried out by the end user, and complex device fabrication methods.

Among the more sensitive detection techniques, electrochemical detection has emerged as a simple and portable detection format with the advent of smartphone controlled potentiostats.[55] In the earliest iterations of electrochemical μPADs, electrodes fabricated directly onto paper suffered from lowered sensitivity, by up to 40%, as a result of the cellulose fibers occupying a significant area of the electrode surface[56] This problem is associated with both screen/stencil printed carbon electrodes (SPCEs) and sputtered or printed metallic electrodes. Recently, Crooks et al. published several articles on their work with hollow-channel μPADs.[53, 57, 58] These hollow-channel μPADs demonstrated the incorporation of microwire electrodes in μPADs for the first time and provide ePADs with: 1) the capability to perform bulk solution electrochemistry under flow conditions; 2) electrodes which are amenable to surface modification external to the device, allowing for harsher pre-treatments without damaging and/or contaminating the paper substrate; and 3) faster flow rates than those obtained in single layer μPADs, permitting faster analysis times.[59, 60] Specifically, important to clinical diagnostics, Crooks et al. demonstrated the applicability of gold microwire electrodes modified with self-assembled monolayers (SAMs). SAMs are used extensively in electroanalysis of complex biological samples in order to achieve high sensitivity, high selectivity, and low detection limits of the target analyte[59] In our opinion, this work represents a significant milestone in the current and future development of ePADs capable of reaching the detection limits required for clinical diagnostics without the need for complicated chemical amplification methods.

The Henry group recently incorporated SAMs-modified gold microwire electrodes into a two-layer ePAD with quasi-steady flow providing highly sensitive and selective virus particle

detection via electrochemical impedance spectroscopy (EIS)[60] EIS is an attractive detection method in biosensing as it can detect the binding events that occur on a transducer surface. Surfaces can be modified to impart high selectivity to the binding of the target analyte, which is desirable in complex biological samples. Importantly, while EIS detection retains the sensitivity associated with electrochemical PADs, it is not necessary for the target analyte to be a redox-active species. [61] For these reasons, this work demonstrates significant progress in point-of-care biomedical diagnostic devices which provide low detection limits while retaining low cost, simple fabrication and operation, and high specificity. As research on new applications for μPADs continues to progress, we expect and advocate for the integration of sensing techniques like electrochemistry and fluorescence to improve detection limits and increase practicality of paper-based diagnostics in clinical settings.

Environmental Monitoring

Environmental analyses cover a wide range of potential analytes and sample matrices and often because of remote sampling locations it is not feasible to transport samples back to a laboratory for analysis The portability of μPADs makes them ideal for in-field testing, especially within the environmental sector where samples can be analyzed on site. However, there are many challenges associated with the optimization of these devices, including the need to improve sensitivity, specificity, reagent stability, and on-site data analysis. Depending on the target, there multiple considerations when designing μPADs for environmental analysis.

The devices need to detect analytes at levels at or below those set by regulatory agencies such as the U.S. Environmental Protection Agency (EPA) and the World Health Organization (WHO), which is especially critical for compounds that have negative effects on living organisms.[62, 63] The tests must also be highly selective and unaffected by complex sample matrices.[64, 65] Multiplexed

testing has been achieved on μPADs, but depending on the analytes, pretreatment may be required which increases cost and time, and decreases ease of use.[66, 67] Reagent stability is also critical, since the devices may need to be transported and used under a wide range of temperature, humidity, and sunlight conditions.[64, 67, 68] Finally, there has been significant progress in data processing, moving from large, expensive, lab-based instruments to smartphones and image analysis software. However, there are still many variables that need to be controlled to ensure reproducible data processing.[63, 64, 67]

Once these considerations are accounted for, there have been many examples of μPADs used successfully for environmental analysis. Some examples of work that have helped advance the field of environmental μPADs include: A smartphone application developed to process colorimetric signals for [nitrate] and pH in water samples;[63] Multiplexed electrochemical detection of heavy metals from particulate matter in air;[65] and ammonia detection from waste-water samples.[64] With further research, limits of detection, reagent stability, and specificity can be improved, making μPADs a viable option for on-site environmental analysis.

Food Quality and Safety

μPADs are increasingly used for food safety monitoring, especially in regions where such monitoring is not typically performed because of limited resources. In fact, more articles have been published on pathogen detection in the food industry than in any other field.[69] μPADs have been used to detect various analytes specific to food-safety such as amine vapors from fish, mycotoxins in cereals, and whole viruses and bacteria.[45, 70-78] Among these analytes bacteria detection has garnered the most attention among food-safety-related μPADs because pathogenic bacteria like *Escherichia coli* (E. *coli*) and *Salmonella typhimurium* (*Salmonella*) cause over a million foodborne illnesses per year in the United States alone.[79] Another reason research into POC

bacteria detection is needed is because the gold standard detection method for most bacteria is culturing.[80] Although reliable and well-established, culturing can take days to complete and requires trained end-users and a centralized laboratory.

Other common methods for bacteria detection besides culturing include polymerase chain reaction (PCR) and enzyme linked immunosorbent assays (ELISA). PCR is used to amplify DNA or RNA specific to a given bacteria (Figure 1.3a). PCR is a powerful technique that is extremely sensitive but requires a powered thermal cycler to reach temperatures near 100ºC, making point-of-need detection difficult. It can also take multiple hours to obtain results and requires complex sets of primers. Instead of detecting DNA, ELISAs are used to detect proteins or biomarkers specific to a given bacteria. Here, the target is captured by a capture antigen and labeled with a secondary protein conjugated to an enzyme. The enzyme label then reacts with a substrate to catalytically produce a detectable product (Figure 1.3b). However, ELISAs require a trained end user to perform ~10 pipetting steps with precise volumes and timing, and a bulky and expensive plate reader is used to quantify results through absorbance spectroscopy. Therefore, ELISAs are also not amenable to POC detection.

Both PCR and ELISA can achieve sensitive results because they amplify the signal. In other words, in these techniques for each individual target molecule or protein, millions more detectable products are created. The extent of amplification can be improved by increasing the number of cycles (PCR) or simply waiting for the reaction to produce more signal (ELISA). µPADs have long been criticized for poor sensitivity.[26, 30, 81] To improve sensitivity, many attempts have been made to adapt both ELISA and PCR onto paper-based platforms.[82-87] In our laboratory, I specifically worked on adapting ELISAs onto µPADs to achieve more sensitive detection without sacrificing the user-friendliness that makes µPADs so appealing in point-of-need analysis.

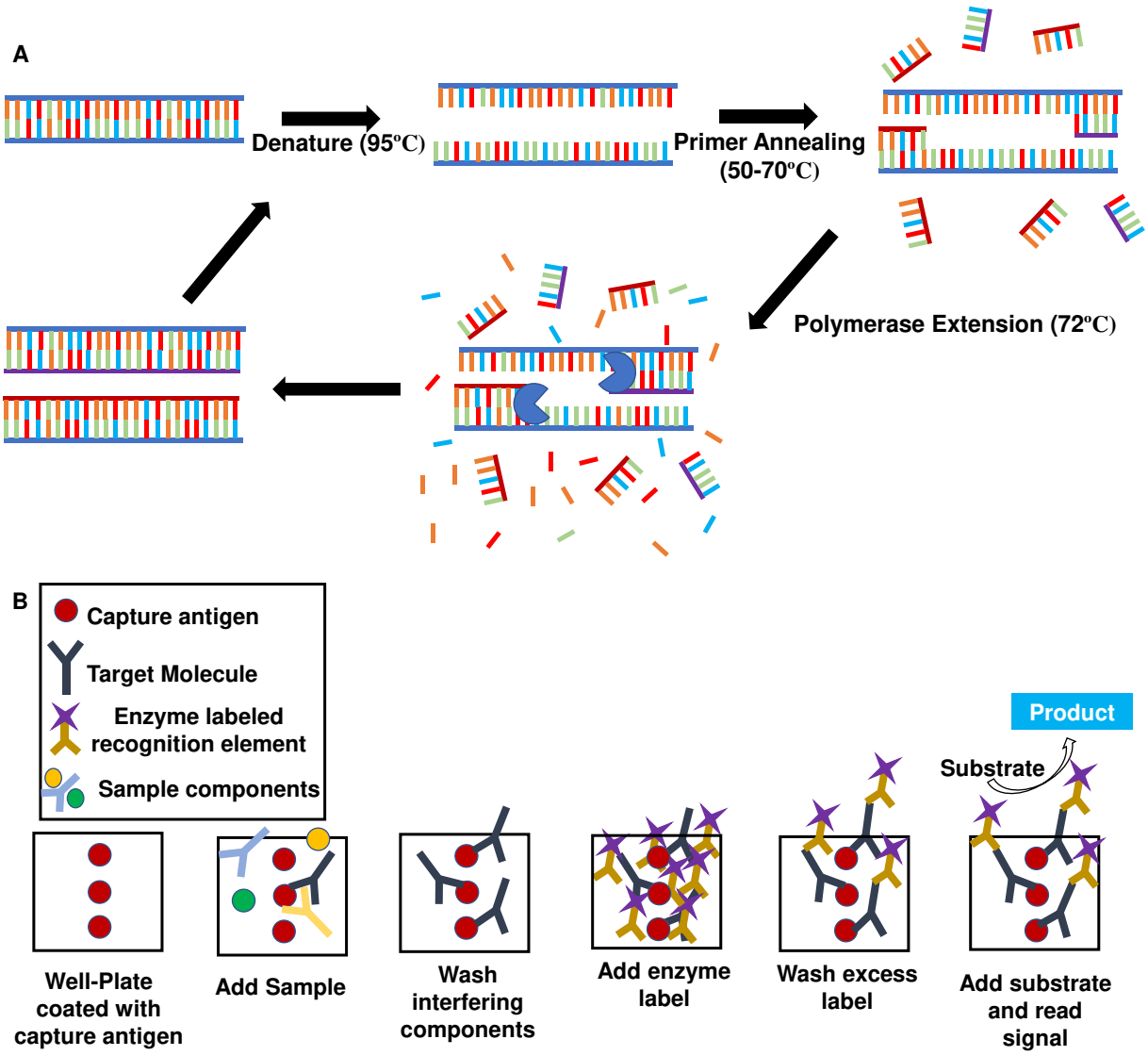

Figure 1.3. A) General method for PCR amplification of DNA. B) General scheme for running a well-plate ELISA.

1.4 Improving µPAD Sensitivity and Functionality

As mentioned earlier, the pregnancy test is an excellent example of a successful POC assay that meets many of the ASSURED criteria. The pregnancy is an example of a lateral flow assay (LFA), which is a popular tool to conduct POC analysis. LFAs have a similar format to an ELISA but use a single sample addition step to drive the entire assay and use nanoparticle labels to create a colorimetric signal instead of enzymes. These differences make the LFA extremely simple to

operate; however, their analytical performance is poor in comparison to ELISA.[88] LFAs perform more poorly than ELISAs for two reasons: 1) For each target molecule there is only one nanoparticle label and no signal amplification can occur; 2) The washing steps that reduce false positives and remove potential interferents are not possible with a single sample addition step. Therefore, although LFAs are an ideal POC assay from an ease-of-use perspective, they cannot perform the complicated steps required for highly sensitive results (pg/mL protein detection) and are not suitable for detection of many biomarkers that have low clinically relevant concentrations. There is a need for a system that is as easy to use as an LFA with the sensitivity and analytical performance of an ELISA

To that end, we created a μPAD system integrated into a 3D-printed manifold to simplify the pipetting steps typically associated with ELISAs.[85] Rather than pipetting, the device we developed delivered reagents to a detection zone by simply rotating the device through each step in the assay. After each rotation, buffer from a reservoir re-hydrated the reagents stored on paper pads and flowed them to a detection zone. The volume of buffer used in each step was controlled by the size of the waste-pad pump, which was optimized for each step of the assay. Washing steps were also integrated into the device by running only buffer through the detection zone into a large waste pad. The device demonstrated the ability to sequentially add and wash reagents from a test zone without precise and complicated pipetting steps. This change in format allows typical end-user with no laboratory experience to run an ELISA-type assay in remote settings.

In the proof-of-concept assay, we detected whole *Salmonella* cells after concentrating them using immunomagnetic separation (IMS). IMS is a popular method to capture target analytes and separate them from complex samples. Initially, this project was funded by the USDA to detect *Salmonella* from fecal samples in feed lots. Feces is a complex sample matrix that interferes with

colorimetric detection, so magnetic beads modified with anti-*Salmonella* antibodies were introduced to the sample. After a conjugation period, the magnetic beads were removed from the sample with a permanent magnet, the feces were discarded, and the beads, now conjugated to *Salmonella* from the sample, were reconstituted in clean buffer. IMS accomplishes two important tasks: 1) Removes potential interferents from the sample matrix; and 2) Concentrates the target analyte in a clean, buffered solution. Once cleaned and concentrated, the magnetic bead-*Salmonella* system was added to the rotational manifold and a sandwich immunoassay was performed using a β-galactosidase label. The enzyme label was used to produce a yellow to red color change in the presence of the substrate Chlorophenol-red- β-D-galactopyranoside, which was quantified with a smartphone camera and image analysis software developed specifically for this project.

IMS is a powerful technique when dealing with complex samples but requires additional complex steps that are not suited for point-of-need detection. IMS has been accomplished using traditional microfluidics where magnetic beads are moved between two parallel flow streams separated by a laminar flow boundary. However, the same functionality is not possible in μPADs because the magnetic particles are retained in the paper fibers and the flow is not fast enough. Our lab has presented a solution to this problem by creating fast-flow channels between two layers of paper.[89] The fast-flow μPADs create sustained flow that is 40x faster than one-layer paper devices and the gap between the paper layers can be used to transport larger particles like magnetic beads. The system described by Call et al. could therefore be used to simplify IMS and be integrated into a μPAD system like the rotary manifold to further improve ease-of-use. This concept of an integrated system for IMS will be discussed further in Chapter 5.

1.5 Hybrid passive flow solutions to address μPAD shortcomings

In 2007 μPADs were established by the Whitesides group, which created a new field for affordable point of need sensors.[27] There have been thousands of publications on μPADs in the 14 years since their introduction (Figure 1.2), but very few have reached the ultimate goal of commercialization and deployment in resource limited settings. The lack of success outside of laboratories is typically attributed to lack of sensitivity or complicated end-user steps. We believe that both problems can be solved if paper is combined with other inexpensive materials like transparency films, 3D printed materials, and/or adhesives. For example, the rotary manifold discussed above was made possible by combining paper devices for reagent storage with lamination sheets, transparency film, and 3D-printed polymer for device housing. Hydrophillic channels that create passive, pump-free flow can also be constructed with these materials.

The Henry Lab was exploring the possible uses for these devices when the COVID-19 pandemic began and was able to create a sensitive, easy to use, point-of-need SARS-CoV-2 assay using a hybrid-paper-transparency device. This device uses stacked channels made of double sided adhesive and transparency film to control flow and perform the sequential reagent delivery and washing steps needed for an ELISA. Paper pads are used to store reagents and a colorimetric readout on a nitrocellulose strip can be used to quantify Anti-SARS-CoV-2 antibodies or N protein. Importantly, all reagent addition and washing steps are performed automatically by the device and a single sample addition is the only end-user step required. The single use, disposable ELISA (dELISA) is described in Chapter 4.

REFERENCES

1. Michaud, C. M., Global Burden of Infectious Diseases. *Encyclopedia of Microbiology* **2009**, 444-454.

2. Murray, C. J.; Lopez, A. D., Measuring the global burden of disease. *New England Journal of Medicine* **2013,** *369* (5), 448-457.

3. Organization, W. H., *Global tuberculosis report 2013*. World Health Organization: 2013.

4. Unaids, UNAIDS data 2017. *Programme on HIV/AIDS* **2017**, 1-248.

5. Organization, W. H., *First WHO model list of essential in vitro diagnostics*. World Health Organization: 2019; Vol. 1017.

6. Sheridan, C., COVID-19 spurs wave of innovative diagnostics. *Nature Biotechnology* **2020,** *38* (7), 769-772.

7. Peeling, R. W.; Wedderburn, C. J.; Garcia, P. J.; Boeras, D.; Fongwen, N.; Nkengasong, J.; Sall, A.; Tanuri, A.; Heymann, D. L., Serology testing in the COVID-19 pandemic response. *The Lancet Infectious Diseases* **2020**.

8. Rohr, U.-P.; Binder, C.; Dieterle, T.; Giusti, F.; Messina, C. G. M.; Toerien, E.; Moch, H.; Schäfer, H. H., The Value of In Vitro Diagnostic Testing in Medical Practice: A Status Report. *PLoS One* **2016,** *11* (3), e0149856.

9. Rosenthal, P. J., The Importance of Diagnostic Testing during a Viral Pandemic: Early Lessons from Novel Coronavirus Disease (COVID-19). *Am J Trop Med Hyg* **2020,** *102* (5), 915-916.

10. Wu, G.; Zaman, M. H., Low-cost tools for diagnosing and monitoring HIV infection in low-resource settings. *Bulletin of the World Health Organization* **2012,** *90* (12), 914-920.

11. Pandey, C. M.; Augustine, S.; Kumar, S.; Kumar, S.; Nara, S.; Srivastava, S.; Malhotra, B. D., Microfluidics Based Point-of-Care Diagnostics. *Biotechnol J* **2018,** *13* (1).

12. Foudeh, A. M.; Didar, T. F.; Veres, T.; Tabrizian, M., Microfluidic designs and techniques using lab-on-a-chip devices for pathogen detection for point-of-care diagnostics. *Lab Chip* **2012,** *12* (18), 3249-3266.

13. Nasseri, B.; Soleimani, N.; Rabiee, N.; Kalbasi, A.; Karimi, M.; Hamblin, M. R., Point-of-care microfluidic devices for pathogen detection. *Biosensors and Bioelectronics* **2018,** *117*, 112-128.

14. Duncombe, T. A.; Tentori, A. M.; Herr, A. E., Microfluidics: reframing biological enquiry. *Nat. Rev. Mol. Cell Biol.* **2015,** *16* (9), 554-567.

15. Huh, D.; Hamilton, G. A.; Ingber, D. E., From 3D cell culture to organs-on-chips. *Trends in Cell Biology* **2011,** *21* (12), 745-754.

16. Chin, C. D.; Linder, V.; Sia, S. K., Commercialization of microfluidic point-of-care diagnostic devices. *Lab Chip* **2012,** *12* (12), 2118-2134.

17. Au, A. K.; Huynh, W.; Horowitz, L. F.; Folch, A., 3D-Printed Microfluidics. *Angew. Chem.-Int. Edit.* **2016,** *55* (12), 3862-3881.

18. Bhattacharjee, N.; Urrios, A.; Kanga, S.; Folch, A., The upcoming 3D-printing revolution in microfluidics. *Lab Chip* **2016,** *16* (10), 1720-1742.

19. Sochol, R. D.; Sweet, E.; Glick, C. C.; Wu, S.-Y.; Yang, C.; Restaino, M.; Lin, L., 3D printed microfluidics and microelectronics. *Microelectronic Engineering* **2018,** *189*, 52-68.

20. Kodama, H., Automatic method for fabricating a three-dimensional plastic model with photo-hardening polymer. *Review of scientific instruments* **1981,** *52* (11), 1770-1773.

21. Macdonald, N. P.; Cabot, J. M.; Smejkal, P.; Guijt, R. M.; Paull, B.; Breadmore, M. C., Comparing microfluidic performance of three-dimensional (3D) printing platforms. *Analytical chemistry* **2017,** *89* (7), 3858-3866.

22. Waheed, S.; Cabot, J. M.; Macdonald, N. P.; Lewis, T.; Guijt, R. M.; Paull, B.; Breadmore, M. C., 3D printed microfluidic devices: enablers and barriers. *Lab Chip* **2016,** *16* (11), 1993-2013.

23. Erkal, J. L.; Selimovic, A.; Gross, B. C.; Lockwood, S. Y.; Walton, E. L.; McNamara, S.; Martin, R. S.; Spence, D. M., 3D printed microfluidic devices with integrated versatile and reusable electrodes. *Lab Chip* **2014,** *14* (12), 2023-2032.

24. Samper, I. C.; Gowers, S. A.; Rogers, M. L.; Murray, D.-S. R.; Jewell, S. L.; Pahl, C.; Strong, A. J.; Boutelle, M. G., 3D printed microfluidic device for online detection of neurochemical changes with high temporal resolution in human brain microdialysate. *Lab Chip* **2019,** *19* (11), 2038-2048.

25. Carrell, C. S.; McCord, C. P.; Wydallis, R. M.; Henry, C. S., Sealing 3D-printed parts to poly(dimethylsiloxane) for simple fabrication of Microfluidic devices. *Analytica Chimica Acta* **2020,** *1124*, 78-84.

26. Carrell, C.; Kava, A.; Nguyen, M.; Menger, R.; Munshi, Z.; Call, Z.; Nussbaum, M.; Henry, C., Beyond the lateral flow assay: A review of paper-based microfluidics. *Microelectronic Engineering* **2019,** *206*, 45-54.

27. Martinez, A. W.; Phillips, S. T.; Butte, M. J.; Whitesides, G. M., Patterned paper as a platform for inexpensive, low-volume, portable bioassays. *Angew. Chem.-Int. Edit.* **2007,** *46* (8), 1318-1320.

28. Byrnes, S.; Thiessen, G.; Fu, E., Progress in the development of paper-based diagnostics for low-resource point-of-care settings. *Bioanalysis* **2013,** *5* (22), 2821-2836.

29. Xia, Y. Y.; Si, J.; Li, Z. Y., Fabrication techniques for microfluidic paper-based analytical devices and their applications for biological testing: A review. *Biosensors & Bioelectronics* **2016,** *77*, 774-789.

30. Yang, Y. Y.; Noviana, E.; Nguyen, M. P.; Geiss, B. J.; Dandy, D. S.; Henry, C. S., Paper-Based Microfluidic Devices: Emerging Themes and Applications. *Analytical Chemistry* **2017,** *89* (1), 71-91.

31. Ahmed, S.; Bui, M. P. N.; Abbas, A., Paper-based chemical and biological sensors: Engineering aspects. *Biosensors & Bioelectronics* **2016,** *77*, 249-263.

32. Akyazi, T.; Basabe-Desmonts, L.; Benito-Lopez, F., Review on microfluidic paper-based analytical devices towards commercialisation. *Analytica Chimica Acta* **2018,** *1001*, 1-17.

33. Cate, D. M.; Adkins, J. A.; Mettakoonpitak, J.; Henry, C. S., Recent Developments in Paper-Based Microfluidic Devices. *Analytical Chemistry* **2015,** *87* (1), 19-41.

34. Gong, M. M.; Sinton, D., Turning the Page: Advancing Paper-Based Microfluidics for Broad Diagnostic Application. *Chemical Reviews* **2017,** *117* (12), 8447-8480.

35. Lim, W. Y.; Goh, B. T.; Khor, S. M., Microfluidic paper-based analytical devices for potential use in quantitative and direct detection of disease biomarkers in clinical analysis. *Journal of Chromatography B-Analytical Technologies in the Biomedical and Life Sciences* **2017,** *1060*, 424-442.

36. Morbioli, G. G.; Mazzu-Nascimento, T.; Stockton, A. M.; Carrilho, E., Technical aspects and challenges of colorimetric detection with microfluidic paper-based analytical devices (mu PADs) - A review. *Analytica Chimica Acta* **2017,** *970*, 1-22.

37. Dungchai, W.; Chailapakul, O.; Henry, C. S., Electrochemical Detection for Paper-Based Microfluidics. *Analytical Chemistry* **2009,** *81* (14), 5821-5826.

38. Carrilho, E.; Phillips, S. T.; Vella, S. J.; Martinez, A. W.; Whitesides, G. M., Paper Microzone Plates. *Analytical Chemistry* **2009,** *81* (15), 5990-5998.

39. Yu, J.; Wang, S.; Ge, L.; Ge, S., A novel chemiluminescence paper microfluidic biosensor based on enzymatic reaction for uric acid determination. *Biosens. Bioelectron.* **2011,** *26* (7), 3284-3289.

40. Jokerst, J. C.; Adkins, J. A.; Bisha, B.; Mentele, M. M.; Goodridge, L. D.; Henry, C. S., Development of a Paper-Based Analytical Device for Colorimetric Detection of Select Foodborne Pathogens. *Analytical Chemistry* **2012,** *84* (6), 2900-2907.

41. Mentele, M. M.; Cunningham, J.; Koehler, K.; Volckens, J.; Henry, C. S., Microfluidic Paper-Based Analytical Device for Particulate Metals. *Analytical Chemistry* **2012,** *84* (10), 4474-4480.

42. Bhakta, S. A.; Borba, R.; Taba, M.; Garcia, C. D.; Carrilho, E., Determination of nitrite in saliva using microfluidic paper-based analytical devices. *Analytica Chimica Acta* **2014,** *809*, 117-122.

43. Magro, L.; Jacquelin, B.; Escadafal, C.; Garneret, P.; Kwasiborski, A.; Manuguerra, J. C.; Monti, F.; Sakuntabhai, A.; Vanhomwegen, J.; Lafaye, P.; Tabeling, P., Paper-based RNA detection and multiplexed analysis for Ebola virus diagnostics. *Sci Rep* **2017,** *7*.

44. Gabriel, E. F. M.; Garcia, P. T.; Lopes, F. M.; Coltro, W. K. T., Paper-Based Colorimetric Biosensor for Tear Glucose Measurements. *Micromachines* **2017,** *8* (4).

45. Srisa-Art, M.; Boehle, K. E.; Geiss, B. J.; Henry, C. S., Highly Sensitive Detection of Salmonella typhimurium Using a Colorimetric Paper-Based Analytical Device Coupled with Immunomagnetic Separation. *Analytical Chemistry* **2018,** *90* (1), 1035-1043.

46. Zhao, C.; Liu, X. Y., A portable paper-based microfluidic platform for multiplexed electrochemical detection of human immunodeficiency virus and hepatitis C virus antibodies in serum. *Biomicrofluidics* **2016,** *10* (2).

47. Li, X.; Scida, K.; Crooks, R. M., Detection of Hepatitis B Virus DNA with a Paper Electrochemical Sensor. *Analytical Chemistry* **2015,** *87* (17), 9009-9015.

48. Kelley, S. O., What Are Clinically Relevant Levels of Cellular and Biomolecular Analytes? *Acs Sensors* **2017,** *2* (2), 193-197.

49. Ramachandran, S.; Fu, E.; Lutz, B.; Yager, P., Long-term dry storage of an enzyme-based reagent system for ELISA in point-of-care devices. *Analyst* **2014,** *139* (6), 1456-1462.

50. Swan, M., Health 2050: The Realization of Personalized Medicine through Crowdsourcing, the Quantified Self, and the Participatory Biocitizen. *Journal of Personalized Medicine* **2012,** *2* (3), 93-118.

51. Liang, L. L.; Su, M.; Li, L.; Lan, F. F.; Yang, G. X.; Ge, S. G.; Yu, J. H.; Song, X. R., Aptamer-based fluorescent and visual biosensor for multiplexed monitoring of cancer cells in microfluidic paper-based analytical devices. *Sensors and Actuators B-Chemical* **2016,** *229*, 347-354.

52. Wu, Y. F.; Xue, P.; Hui, K. M.; Rang, Y. J., A paper-based microfluidic electrochemical immunodevice integrated with amplification-by-polymerization for the ultrasensitive multiplexed detection of cancer biomarkers. *Biosens. Bioelectron.* **2014,** *52*, 180-187.

53. Scida, K.; Cunningham, J. C.; Renault, C.; Richards, I.; Crooks, R. M., Simple, sensitive, and quantitative electrochemical detection method for paper analytical devices. *Analytical chemistry* **2014,** *86* (13), 6501–6507.

54. Hu, J.; Wang, S.; Wang, L.; Li, F.; Pingguan-Murphy, B.; Lu, T. J.; Xu, F., Advances in paper-based point-of-care diagnostics. *Biosensors and Bioelectronics* **2014,** *54*, 585-597.

55. Ainla, A.; Mousavi, M. P. S.; Tsaloglou, M.-N.; Redston, J.; Bell, J. G.; Fernández-Abedul, M. T.; Whitesides, G. M., Open-Source Potentiostat for Wireless Electrochemical Detection with Smartphones. *Analytical Chemistry* **2018,** *90* (10), 6240-6246.

56. Nie, Z.; Nijhuis, C. A.; Gong, J.; Chen, X.; Kumachev, A.; Martinez, A. W.; Narovlyansky, M.; Whitesides, G. M., Electrochemical sensing in paper-based microfluidic devices. *Lab on a Chip* **2010,** *10* (4), 477-483.

57. Renault, C.; Koehne, J.; Ricco, A. J.; Crooks, R. M., Three-dimensional wax patterning of paper fluidic devices. *Langmuir* **2014,** *30* (23), 7030-7036.

58. Renault, C.; Li, X.; Fosdick, S. E.; Crooks, R. M., Hollow-channel paper analytical devices. *Analytical chemistry* **2013,** *85* (16), 7976-7979.

59. Fosdick, S. E.; Anderson, M. J.; Renault, C.; DeGregory, P. R.; Loussaert, J. A.; Crooks, R. M., Wire, mesh, and fiber electrodes for paper-based electroanalytical devices. *Analytical chemistry* **2014,** *86* (7), 3659-3666.

60. Adkins, J. A.; Noviana, E.; Henry, C. S., Development of a Quasi-Steady Flow Electrochemical Paper-Based Analytical Device. *Analytical Chemistry* **2016,** *88* (21), 10639-10647.

61. Lisdat, F.; Schäfer, D., The use of electrochemical impedance spectroscopy for biosensing. *Anal. Bioanal. Chem.* **2008,** *391* (5), 1555.

62. Lin, Y.; Gritsenko, D.; Feng, S.; Teh, Y. C.; Lu, X.; Xu, J., Detection of heavy metal by paper-based microfluidics. *Biosens. Bioelectron.* **2016,** *83*, 256-266.

63. Lopez-Ruiz, N.; Curto, V. F.; Erenas, M. M.; Benito-Lopez, F.; Diamond, D.; Palma, A. J.; Capitan-Vallvey, L. F., Smartphone-Based Simultaneous pH and Nitrite Colorimetric Determination for Paper Microfluidic Devices. *Analytical Chemistry* **2014,** *86* (19), 9554-9562.

64. Jayawardane, B. M.; McKelvie, I. D.; Kolev, S. D., Development of a Gas-Diffusion Microfluidic Paper-Based Analytical Device (mu PAD) for the Determination of Ammonia in Wastewater Samples. *Analytical Chemistry* **2015,** *87* (9), 4621-4626.

65. Rattanarat, P.; Dungchai, W.; Cate, D.; Volckens, J.; Chailapakul, O.; Henry, C. S., Multilayer Paper-Based Device for Colorimetric and Electrochemical Quantification of Metals. *Analytical Chemistry* **2014,** *86* (7), 3555-3562.

66. Medina-Sanchez, M.; Cadevall, M.; Ros, J.; Merkoci, A., Eco-friendly electrochemical lab-on-paper for heavy metal detection. *Anal. Bioanal. Chem.* **2015,** *407* (28), 8445-8449.

67. Wang, H.; Li, Y.-j.; Wei, J.-f.; Xu, J.-r.; Wang, Y.-h.; Zheng, G.-x., Paper-based three-dimensional microfluidic device for monitoring of heavy metals with a camera cell phone. *Anal. Bioanal. Chem.* **2014,** *406* (12), 2799-2807.

68. Jayawardane, B. M.; Wongwilai, W.; Grudpan, K.; Kolev, S. D.; Heaven, M. W.; Nash, D. M.; McKelvie, I. D., Evaluation and Application of a Paper-Based Device for the Determination of Reactive Phosphate in Soil Solution. *Journal of Environmental Quality* **2014,** *43* (3), 1081-1085.

69. Lazcka, O.; Del Campo, F. J.; Munoz, F. X., Pathogen detection: a perspective of traditional methods and biosensors. *Biosensors and bioelectronics* **2007,** *22* (7), 1205-1217.

70. Adkins, J. A.; Boehle, K.; Friend, C.; Chamberlain, B.; Bisha, B.; Henry, C. S., Colorimetric and Electrochemical Bacteria Detection Using Printed Paper- and Transparency-Based Analytic Devices. *Analytical Chemistry* **2017,** *89* (6), 3613-3621.

71. Pang, B.; Zhao, C.; Li, L.; Song, X. L.; Xu, K.; Wang, J.; Liu, Y. S.; Fu, K. Y.; Bao, H.; Song, D. D.; Meng, X. J.; Qu, X. F.; Zhang, Z. P.; Li, J., Development of a low-cost paper-based ELISA method for rapid Escherichia coli O157:H7 detection. *Analytical Biochemistry* **2018,** *542*, 58-62.

72. Thuo, M. M.; Martinez, R. V.; Lan, W. J.; Liu, X. Y.; Barber, J.; Atkinson, M. B. J.; Bandarage, D.; Bloch, J. F.; Whitesides, G. M., Fabrication of Low-Cost Paper-Based Microfluidic Devices by Embossing or Cut-and-Stack Methods. *Chemistry of Materials* **2014,** *26* (14), 4230-4237.

73. Tseng, S. Y.; Li, S. Y.; Yi, S. Y.; Sun, A. Y.; Gao, D. Y.; Wan, D. H., Food Quality Monitor: Paper-Based Plasmonic Sensors Prepared Through Reversal Nanoimprinting for Rapid Detection of Biogenic Amine Odorants. *ACS Appl. Mater. Interfaces* **2017,** *9* (20), 17307-17317.

74. Kong, D. Z.; Liu, L. Q.; Song, S. S.; Suryoprabowo, S.; Li, A. K.; Kuang, H.; Wang, L. B.; Xu, C. L., A gold nanoparticle-based semi-quantitative and quantitative ultrasensitive paper sensor for the detection of twenty mycotoxins. *Nanoscale* **2016,** *8* (9), 5245-5253.

75. Kant, K.; Shahbazi, M.-A.; Dave, V. P.; Ngo, T. A.; Chidambara, V. A.; Than, L. Q.; Bang, D. D.; Wolff, A., Microfluidic devices for sample preparation and rapid detection of foodborne pathogens. *Biotechnol. Adv.* **2018**.

76. Yao, L.; Wang, L.; Huang, F. C.; Cai, G. Z.; Xi, X. G.; Lin, J. H., A microfluidic impedance biosensor based on immunomagnetic separation and urease catalysis for continuous-flow detection of E-coli O157:H7. *Sensors and Actuators B-Chemical* **2018,** *259*, 1013-1021.

77. Morales-Narvaez, E.; Naghdi, T.; Zor, E.; Merkoci, A., Photo luminescent Lateral-Flow Immunoassay Revealed by Graphene Oxide: Highly Sensitive Paper-Based Pathogen Detection. *Analytical Chemistry* **2015,** *87* (16), 8573-8577.

78. Park, J.; Shin, J. H.; Park, J. K., Pressed Paper-Based Dipstick for Detection of Foodborne Pathogens with Multistep Reactions. *Analytical Chemistry* **2016,** *88* (7), 3781-3788.

79. Scallan, E.; Hoekstra, R. M.; Angulo, F. J.; Tauxe, R. V.; Widdowson, M. A.; Roy, S. L.; Jones, J. L.; Griffin, P. M., Foodborne Illness Acquired in the United States-Major Pathogens. *Emerg. Infect. Dis* **2011,** *17* (1), 7-15.

80. Bohaychuk, V. M.; Gensler, G. E.; King, R. K.; Wu, J. T.; McMullen, L. M., Evaluation of detection methods for screening meat and poultry products for the presence of foodborne pathogens. *Journal of Food Protection* **2005,** *68* (12), 2637-2647.

81. Yamada, K.; Shibata, H.; Suzuki, K.; Citterio, D., Toward practical application of paper-based microfluidics for medical diagnostics: state-of-the-art and challenges. *Lab Chip* **2017,** *17* (7), 1206-1249.

82. Liu, F.; Liu, H.; Liao, Y.; Wei, J.; Zhou, X.; Xing, D., Multiplex detection and genotyping of pathogenic bacteria on paper-based biosensor with a novel universal primer mediated asymmetric PCR. *Biosensors and Bioelectronics* **2015,** *74*, 778-785.

83. Yakoh, A.; Chaiyo, S.; Siangproh, W.; Chailapakul, O., 3D Capillary-Driven Paper-Based Sequential Microfluidic Device for Electrochemical Sensing Applications. *ACS Sensors* **2019,** *4* (5), 1211-1221.

84. Jeong, S.-G.; Kim, J.; Jin, S. H.; Park, K.-S.; Lee, C.-S., Flow control in paper-based microfluidic device for automatic multistep assays: A focused minireview. *Korean Journal of Chemical Engineering* **2016,** *33* (10), 2761-2770.

85. Carrell, C. S.; Wydallis, R. M.; Bontha, M.; Boehle, K. E.; Beveridge, J. R.; Geiss, B. J.; Henry, C. S., Rotary manifold for automating a paper-based Salmonella immunoassay. *RSC Adv.* **2019,** *9* (50), 29078-29086.

86. Verma, M. S.; Tsaloglou, M.-N.; Sisley, T.; Christodouleas, D.; Chen, A.; Milette, J.; Whitesides, G. M., Sliding-strip microfluidic device enables ELISA on paper. *Biosensors and Bioelectronics* **2018,** *99*, 77-84.

87. Reboud, J.; Xu, G.; Garrett, A.; Adriko, M.; Yang, Z.; Tukahebwa, E. M.; Rowell, C.; Cooper, J. M., based microfluidics for DNA diagnostics of malaria in low resource underserved rural communities. *Proceedings of the National Academy of Sciences* **2019,** *116* (11), 4834-4842.

88. Posthuma-Trumpie, G. A.; Korf, J.; van Amerongen, A., Lateral flow (immuno) assay: its strengths, weaknesses, opportunities and threats. A literature survey. *Anal. Bioanal. Chem.* **2009,** *393* (2), 569-582.

89. Channon, R. B.; Nguyen, M. P.; Scorzelli, A. G.; Henry, E. M.; Volckens, J.; Dandy, D. S.; Henry, C. S., Rapid flow in multilayer microfluidic paper-based analytical devices. *Lab Chip* **2018,** *18* (5), 793-802.

CHAPTER 2: SEALING 3D-PRINTED PARTS TO POLY(DIMETHYLSILOXANE) FOR SIMPLE FABRICATION OF MICROFLUIDIC DEVICES

Microfluidics has revolutionized the fields of bioanalytical chemistry, cellular biology, and molecular biology. Advancements in microfluidic technologies, however, are often limited by labor, time, and resource-intensive fabrication methods, most commonly a form of photolithography. The advent of 3D printing has helped researchers fabricate proof-of-concept microfluidics more rapidly and at lower costs but suffers from poor resolution and tedious post-processing to remove uncured resin from enclosed channels. Additionally, custom resins and printers are often needed to create entirely enclosed channels, which increases cost and complexity of fabrication. In this work we demonstrate the ability to create microfluidic devices by covalently sealing 3D-printed parts with open-faced channels to polydimethylsiloxane (PDMS). Open-faced channels are easier to print than fully enclosed channels and can be printed using an inexpensive and commercially available stereolithography 3D printer and resin. The 3D-printed parts are sealed to PDMS, a common substrate used in traditional microfluidic fabrication, using two different techniques. The first involves coating the part with a commercially available silicone spray before sealing to PDMS via plasma treatment. In the second technique, the cured methacrylate resin is silanized with (3-Aminopropyl)triethoxysilane (APTES) before binding to PDMS with plasma treatment. Both methods create a strong seal between the two substrates, which is demonstrated with several types of microfluidic devices including droplet and gradient generators.

2.1 Introduction

Microfluidic devices are popular tools for diagnostic assays, single cell analysis, drug discovery, synthetic chemistry, molecular biology, organ-on-a-chip analysis, and many other applications.[1-7] Microfluidics are widely used across many fields because they offer advantages

such as portability, low-cost, high-throughput, decreased analysis time, and low sample volumes.[4] As the uses for microfluidics continues to grow, new fabrication techniques are continually developed to decrease the cost and manual labor involved in fabrication. Common fabrication techniques for microfluidic devices include soft-lithography, etching, hot-embossing, and injection molding.[8] Traditional fabrication methods, however, are often complex, expensive, and/or labor and time intensive.[9-11] Microfluidic research, and analytical chemistry in general, have recently been greatly enhanced by the advent of affordable benchtop 3D printers.[12] Rather than relying on traditional fabrication methods such as photolithography or hot embossing, microfluidic structures can be 3D-printed from a wide range of materials for rapidly prototyping iterative designs at a relatively low cost.[9-11, 13] Hundreds of 3D-printed microfluidic devices have been developed and published over the past decade including devices with stacked channels, gradient generators, cell culture devices, rapid mixers, and many others.[11, 14, 15]

3D-printed microfluidic devices do, however, suffer from resolution limitations of the printers, making it difficult to achieve small features or complicated structures. To reach channel dimensions smaller than 100x100 µm custom-built printers and/or resins are often necessary.[16-19] Using custom resins and home-built printers has allowed researchers to create channels as small as 18x20 µm.[19] Unfortunately, even with advanced resins and printers the process is still limited by the laser spot size (SLA printers) or pixel size (DLP printers) and uncured resin must be cleared from fully enclosed channels or printed with supports that also require removal.[13, 20-23] Support and/or resin removal may sound trivial but can take days to remove all uncured resin. An alternative fabrication method is to print open-faced channels and seal the 3D-printed part to a secondary substrate. Open-faced channels eliminate the necessity to clear uncured resin from enclosed channels after printing, which we hypothesize will allow smaller channels to be printed

without clogging. Open-faced 3D-printed channels have been used to create functioning microfluidic devices previously but are sealed with scotch-tape, which limits the capabilities of the device compared to sealing with PDMS.[22, 24]PDMS has many advantages as a material in microfluidic devices, such as its biocompatibility, optical transparency, and gas permeability.[22]

This work describes two methods to seal open-faced 3D-printed channels and PDMS to create permanently enclosed microfluidic channels. In each method, an inexpensive and commercially available printer and resin from Formlabs is used to create the devices. The printer and resin cost USD $2850 and $150/L respectively and are used frequently in academic and industrial labs.[15, 25] To seal the devices the surface of the 3D printed-piece (3DPP) is modified with silicone to create covalent siloxane (Si-O-Si) bonds between the 3D-printed surface and the surface of the PDMS through plasma treatment. The surface of the 3DPP is modified in two ways; the first uses a commercially available silicone spray to coat the 3DPP with silicone before sealing to PDMS. This method is rapid, simple, and ideal for proof of concept devices; however, the seal is not resistant to organic solvents and oils and the silicone spray is difficult to apply consistently and can distort channel dimensions. The second is a more robust method that covalently modifies the surface of the 3DPP with a silanizing agent before sealing to PDMS. Silanizing the surface of thermoplastics before binding to PDMS has been reported in the past, but to the best of our knowledge has not been demonstrated on 3D-printed materials.[26-28] The Formlabs clear resin is made of methacrylated monomers and oligimers, so the same technique used to bind thermoplastics can be applied to 3DPPs as well.[29] In this work microfluidic channels as small as 240x20 μm are demonstrated (Fig. 2.3, Table A1.1).

Both methods presented in this work are simple and inexpensive alternatives to current methods of 3D-printing microfluidics and traditional microfluidic fabrication techniques such as

soft lithography. Although this technique has not been used to create complex multi-layered microfluidic devices, it will significantly reduce the time and complexity needed to create conventional single-layer devices. The method will allow for integration of PDMS membranes to function as valves and pumps and for modification of channels with electrodes between the printing and sealing steps. Devices with integrated structures in the channels, such as the herringbone mixers demonstrated in this manuscript, can also be designed with CAD software and printed in one step. The increased ease of fabrication will allow researchers to rapidly prototype new microfluidic designs and let research groups that do not have the necessary cleanroom facilities for soft lithography perform microfluidic research with an inexpensive 3D-printer.

2.2 Materials and Methods

2.2.1 3D Printing

The 3D printer used was a Form 2 from Formlabs. All 3D-printed pieces were printed using Formlabs Clear V4 resin. The 3D-printed parts were all designed in Onshape, a cloud-based CAD software. PDMS and curing agent was purchased as a kit (DOW Sylgard 184, Krayden Inc. Denver, CO). 3-(Aminopropyl)triethoxysilane (APTES) was purchased from Sigma-Aldrich (Milwaukee, WI).

2.2.2 Silicone Spray Sealing Procedure

After printing the open faced 3D printed channels, PDMS was cured at a 10:1 or 15:1 PDMS:Curing-agent ratio. The PDMS was poured into a mold to ensure a consistent thickness (1.6 mm) for all experiments. The PDMS was cured in an 80°C oven for 1 h and pieces were cut with a scalpel blade to the same size as the 3DPP. The 3DPPs were sprayed with one light coat of silicone spray (MG Chemicals Burlington, Ontario) from 6-8 inches away. After letting the spray dry for 1 h, the coated 3DPP and matching piece of PDMS were both plasma treated in air with an

18 W Harrick PDC-32G Plasma Cleaner (Ithica, NY) for 30 s. The two pieces were pressed together by hand immediately after plasma treatment and further pressed with a 7 lb weight for 30 min. The spray sealing method is illustrated in Figure 2.1.

2.2.3 Silanization Sealing Procedure.

An aqueous APTES solution from between 1-12% v/v is mixed together for 10 min with a stir bar. The 3DPP is rinsed in isopropyl alcohol and DI water, and is then plasma treated in air using an 18 W Harrick PDC-32G Plasma Cleaner for 30 s. Immediately after plasma treatment the 3DPP is submerged in the APTES solution for 20 min to silanize the surface. After 20 min, the 3DPP is taken out of the APTES solution, rinsed in a beaker of DI water, and dried under nitrogen. A PDMS piece of the same size as the 3DPP is cleaned with isopropyl alcohol and DI water before use and particles on the surface of the PDMS are removed with a piece of scotch tape. The PDMS is then plasma treated for 30 s. Immediately after plasma treatment, the silanized 3DPP and the PDMS are pressed together by hand for one min. They are further pressed for 30 min under a 7 lb weight. The silanization method is illustrated in Figure 2.1.

2.2.4 Surface Characterization

The surfaces of the modified 3DPPs were characterized with a Physical Electronics-5800 X-ray Photo Electron Spectrometer (Chanhassen, MN). A Zemetrics ZeGage Optical Profilometer (Tuscson, AZ) was used to map the surface of 3DPPs and other substrates to determine their surface roughness and the channel dimensions. Contact angle experiments were performed using a Dino-Lite digital microscospe and DinoCapture software (Dunwell Tech, Torrance, CA).

2.2.5 Device Demonstration

In all devices 1.6mm OD and 0.7mm ID tubing from Western Analytical Products (Boise, ID) was used with New Era syringe pumps (Farmingdale, NY). Flow rates differed between

experiments and devices and are specified in the experimental section below. The tubing was connected to the devices by inserting the tubing into a hole printed in the 3DPP. Once inserted, the tubing was sealed into place with Loctite Epoxy. A Dino-lite digital microscope was used to image the devices and NIH ImageJ was used to analyze the images for quantitative results. CAD images of all device designs used in this manuscript are shown in Figure A1.1.

2.3 Results and Discussion

2.3.1 Binding concept and mechanism

In this work two methods to seal a 3DPP with open channels to PDMS to create enclosed microfluidic channels are proposed. The general concept of sealing an open-faced channel is illustrated in Figure 2.1A. The first sealing method (Fig. 2.1B) involves spraying the surface of

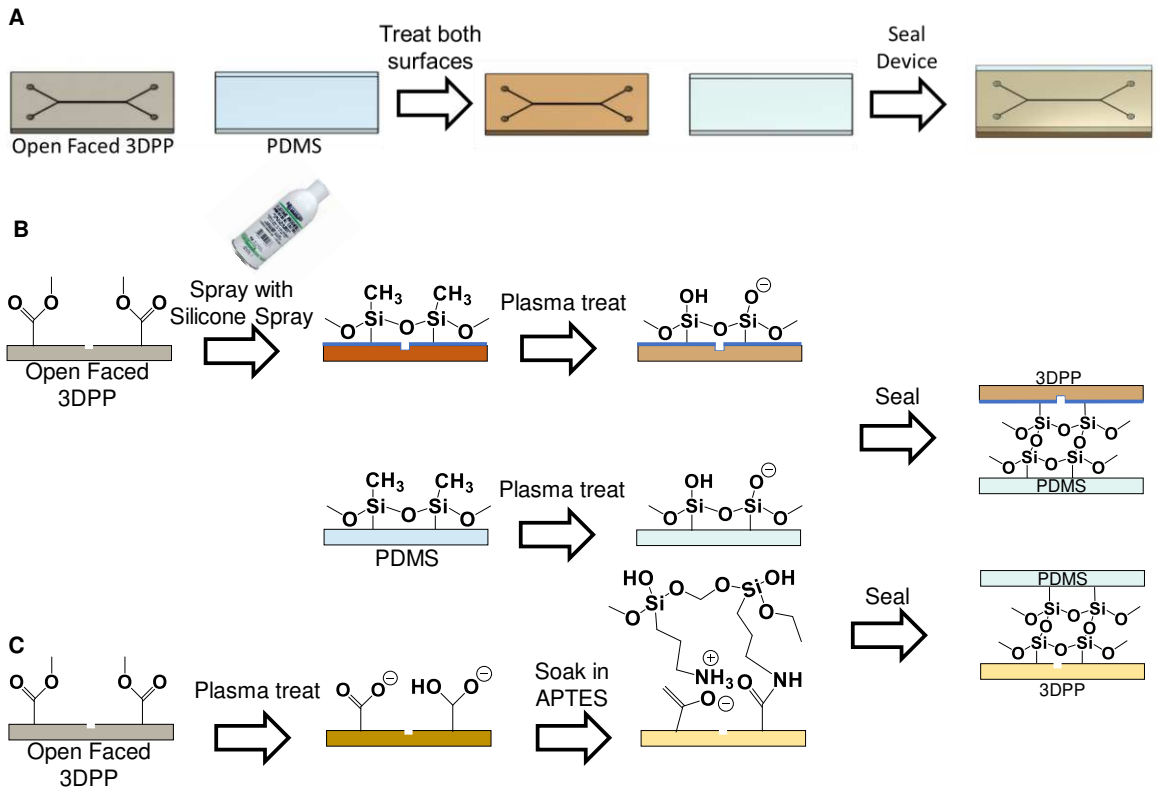

Figure 2.1. General concept of creating a microfluidic device from open faced channels on a 3DPP and PDMS. Silicone spray method (A), and APTES modification method (B).

the 3DPP with a commercially available silicone spray. The spray is typically used to protect electronic components in circuit boards and can be used to increase the clarity of the printed "clear" resin. While improving the clarity, the spray also coats the surface with silicone. Although the content of the spray is proprietary the presence of silicone on the surface after spraying was confirmed with XPS and contact angles (Fig. 2.2A and A1.2 respectively). Figure 2.2A shows the XPS spectra of the surface of the 3DPP sprayed with silicone spray. The spray-modified spectrum contains two silicon peaks at 102 and 152 eV that are not present in the spectrum of a bare 3DPP (Fig. 2.2B). Additionally, the O1s peak on the un-modified piece at 532 eV is ~2/3 the intensity of the same peak in 2.2A, indicating the presence of additional oxygen groups from silicone (Si-O-Si). Therefore, Si and Si-O are available for binding at the surface of the spray-modified 3DPPs like they are on glass, a common substrate bound to PDMS to make microfluidic channels. Additionally, after spraying the 3DPP with Silicone spray the contact angle increased from 67° to 83° (Fig. A1.2). Depending on the structure of the silicone polymer in the spray, the surface will either become more or less hydrophilic. Because the contents are proprietary, it is not possible to predict whether the contact angle should increase or decrease, but the results in Figure A1.2 indicate that the 3DPP is coated with a silicone polymer that is more hydrophobic than the methacrylate-based resin.

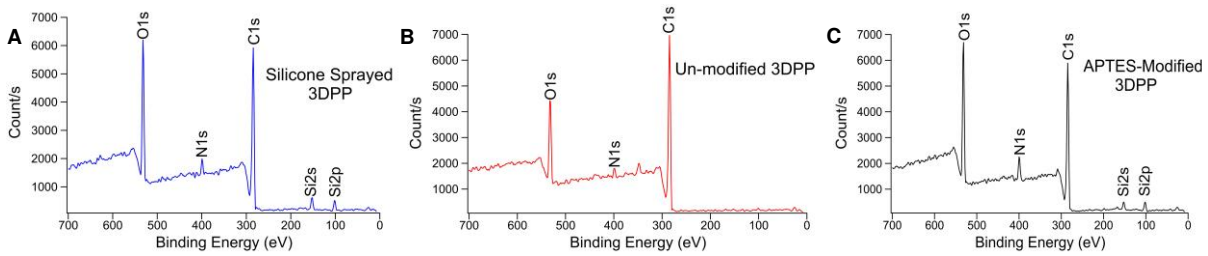

Figure 2.2. XPS spectra of APTES-modified (A), Silicone spray-modified (B), and bare (C) 3DPPs.

To bind PDMS to a 3DPP with silicone spray, a thin coat of the silicone spray is sprayed onto the surface of the 3DPP and dried. The thickness of the silicone spray coating was measured by spraying a coating on a glass slide partly covered with a piece of scotch tape. When the tape is removed, the height of the ledge formed at the tape-spray interface was measured with an optical profilometer. The thickness of the spray coating was 6.5±4.3 μm (Fig. A1.3, n=5) but can vary between users because of inconsistent spray methods (Amount sprayed, distance sprayed from, etc.) as indicated by the large relative standard deviation. The data collected for Figure A1.3 was obtained with one user spraying five different devices on the same day. The variation in spray thickness is expected to increase with multiple sprayers. Both the coated 3DPP and a complementary PDMS piece are plasma treated in air and pressed together by hand. They are further pressed with a weight for 30 min before use. The plasma treatment activates the surface of both pieces as shown in Figure 2.1B. When pressed together immediately after plasma treatment, covalent Si-O-Si bonds bind the PDMS and 3DPP together. The spray method is a rapid and simple fabrication technique that creates a strong seal between the two substrates (Fig. A1.4). Unfortunately, when the spray is applied, a silicon-containing film simply dries on top of the 3DPP and no covalent bonds form between the Si in the spray and the cured resin of the 3DPP. The PDMS is therefore only covalently bonded to the spray film and not directly to the 3DPP. The film is also soluble in organic solvents and oils commonly used in microfluidic droplet generators like mineral oil and perfluorinated oils. Therefore, the seal fails when non-aqueous solvents are used in the channels. Additionally, the film can significantly distort the channel dimensions and is difficult to apply reproducibly and evenly (Fig. 2.3, Table A1.1). As shown in Table S1, depending on the size of the channel the spray can distort the channel depth as much 40 μm and the width as much as 120 μm. To decrease the thickness of the spray, one could theoretically dilute the spray

in a compatible solvent and spray using a commercial sprayer. Due to the limitations of the Si-spray method, we attempted to directly silanize the surface of the 3DPP for a more robust seal without channel distortion.

Silanization of thermoplastics followed by subsequent bonding to PDMS has been previously described in the literature as a way to create microfluidic channels.[26, 28, 30] The specific contents of the 3D printing resin used in this project is proprietary, but according to the safety data sheet contains "methacrylated oligomers and monomers, and photoinitiator(s)".[29] Therefore, it was hypothesized that the surface of the 3DPP could be silanized. To silanize the 3DPP, printed devices were plasma treated and soaked in a 10% solution of aqueous APTES (Fig 2.1C). Modification of the surface with APTES was confirmed using XPS and contact angle studies. The contact angle decreased from 66° to 43° after modification, which is expected due to the polar silanol groups of APTES (Fig. A1.2). The decrease in contact angle is also consistent with other literature values after silanization of thermoplastics with APTES.[27] Figure 2.2C shows the XPS spectra of the surface of the APTES-modified 3DPP. Here, two silicon peaks are found at 102 and 152 eV that are not present in the spectrum of a bare 3DPP (Fig. 2.2B). Additionally, the O1s and N1s peak in 2.2B are larger than they are on the un-modified spectrum, indicating the presence of APTES ($C_9H_{23}NO_3Si$) on the surface. After drying, a complementary piece of PDMS is plasma treated in air and both pieces are pressed together by hand followed by a weight for 30 min before use. Although APTES modification is a more involved process, the surface of the 3DPP is covalently modified with APTES so the seal can withstand organic solvents and oils and the channels are not distorted like they are with the spray (Fig. 2.3 and Table A1.2), resulting in a more permanent and robust seal.

2.3.2 Bonding Optimization

The sealing process was next optimized to maximize adhesion strength. To evaluate the adhesion strength, we manually attempted to peel the PDMS from the 3DPP after sealing and rated the seal as “Strong”, “Weak” or “No Seal”. A rating of Strong indicates that the PDMS ripped during removal and/or that PDMS was stuck on the surface of the 3DPP (Fig. A1.4). A rating of Weak indicates that the PDMS could be removed by hand without ripping, but still required some force to remove. A rating of No Seal indicates that the PDMS could be removed without any force. Both sealing methods were compared to the sealing of PDMS to glass, which is one of the most common methods to make microfluidic devices. Here a glass microscope slide and PDMS are both plasma treated and pressed together by hand. The seal between glass and PDMS was stronger than either of the methods proposed in this paper (removal not possible without immediate ripping of PDMS). The most notable difference between glass and the 3DPP is that glass much smoother than 3D printed materials (Area roughness of 0.03±0.02 vs 2.84±0.43 µm respectively, n=3). In this work, the SLA printer creates 3DPPs in 25 µm thick layers (Z-resolution) using a laser with a spot size of 140 µm (XY-resolution). The discrete layers create ridges on the surface of the 3DPP (Fig. A1.5). PDMS is typically made with a 10:1 ratio of PDMS:Curing agent. At this ratio, it was hypothesized that the PDMS was too rigid to fill in the valleys on the surface of the 3DPP and the seal only occurred at the peaks. To test this hypothesis, a more flexible PDMS with a 15:1 ratio was tested alongside the 10:1 ratio using the APTES sealing method. All devices sealed with a 10:1 ratio had Weak or No Seal ratings, and devices sealed with a 15:1 ratio had Strong or Weak ratings.

In previous work, thermoplastics were treated with 1% solutions of APTES before binding to PDMS.[28] Here, a 10% solution of APTES was used for modification, as the 1% solution produced a poor seal that resulted in a No Seal rating. To determine the optimal concentration of

APTES for binding to 3DPPs, the contact angle after modification was measured for four different concentrations (Fig. A1.6). A smaller contact angle indicated more complete surface coverage with APTES, and above 10% APTES the contact angle did not continue to decrease. The contact angle results were confirmed with the seal rating system described above: The 1% solution produced a poor seal that resulted in a No Seal rating, and at 10% APTES and above, devices had a Strong seal. The difference in the necessary APTES concentration can be attributed to the increased surface area and roughness of the 3DPP vs other thermoplastics (e.g. poly(methyl methacrylate).

At higher concentrations of APTES, a rinsing step after modification was vital to a proper seal. If thorough rinsing in DI water was not performed before sealing to PDMS, a thin film of APTES would dry on the 3DPP surface. When the plasma activated PDMS was pressed onto the 3DPP, it would only react with the APTES at the surface of the film instead of the APTES bound to the 3DPP. Rinsing the modified 3DPP in DI water before drying removed the film so that the PDMS could bind directly to the 3DPP.

2.3.3 Characterization of 3D-Printed Channels

The resolution in SLA printers is either limited to the z-direction step size or the laser spot size. The SLA printer used in this work has a minimum z-resolution of 25 µm and a laser spot size (x,y resolution) of 140 µm, which was the limiting factor in achieving channels of the same size that were printed. To determine the minimum achievable channel size, a microfluidic device with seven straight channels of varying widths was printed and sealed by both methods. Each channel was designed to have a depth of 200 µm and widths from 500 to 75 µm (Fig. 2.3A). After printing the channels, an optical profilometer was used to determine the channel dimensions of the 3DPP. As shown in Figure 2.3 and Table A1.1 and A1.2, the measured dimensions are significantly different from the printed dimensions. The only channel where measured dimensions were similar

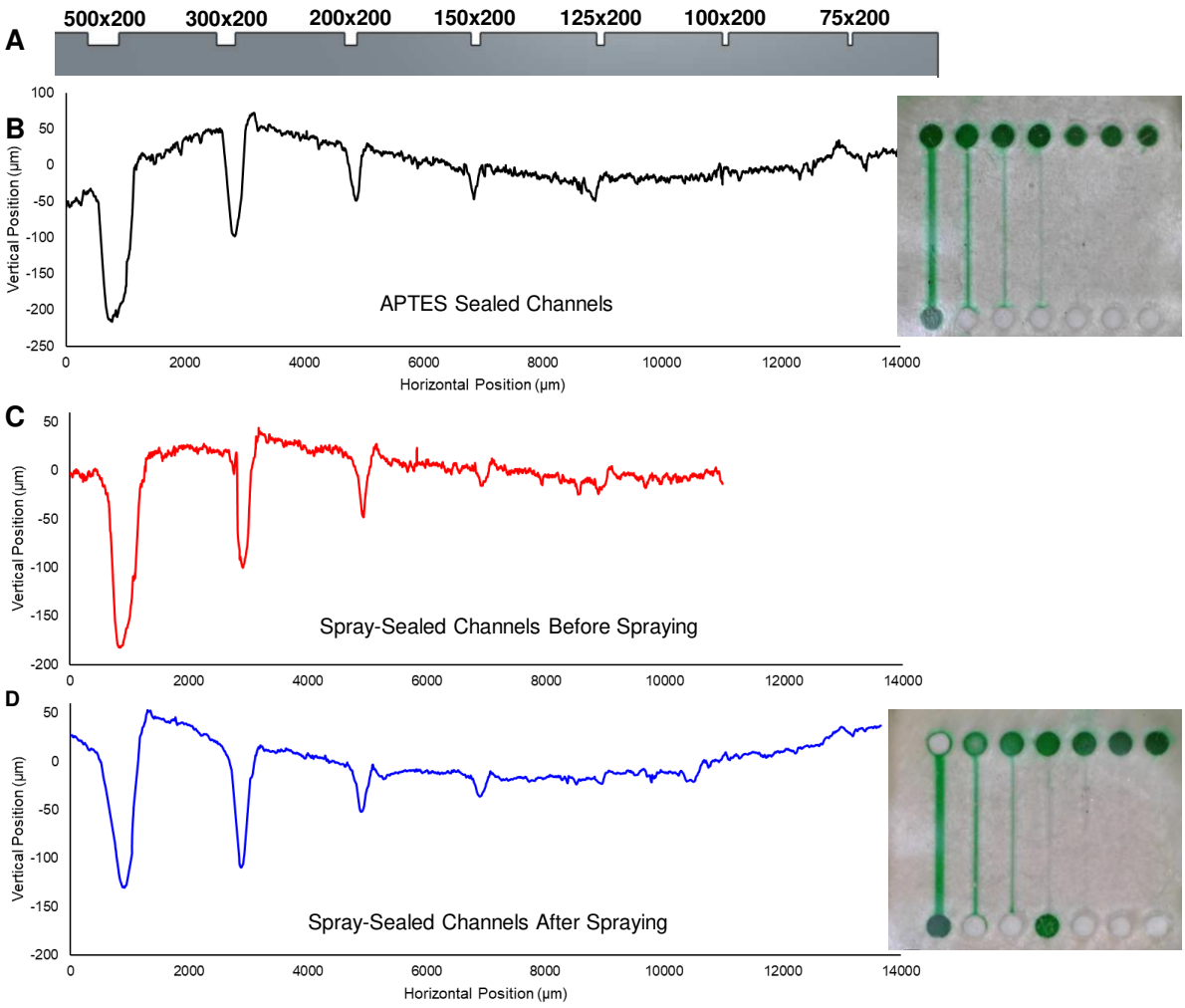

Figure 2.3. Cross sectional view of CAD design for channels of different depths (A). Optical profilometer profile for channels that were sealed with APTES and the sealed channels filled with green food coloring (B). Optical profilometer profile for channels before (C) and after (D) spraying with silicone spray and sealed channels filled with green food coloring.

to the printed dimensions was the largest channel. Here the intended dimensions were 500x200 µm and the actual dimensions were 626±71 x 180±12 µm (n=6) channel. All other channels have a significantly shallower depth than the 200 µm designed depth. As the specified width and aspect ratio of the channel decreased, the actual depth decreased until a specified width of 125 µm, where no channels were visible.

The inconsistencies between specified and actual dimensions in channels is due to the 140 µm laser spot size and is consistent with other 3D-printed microfluidic channels.[21] The device orientation in the printer was angled at 45°, so the X,Y resolution impacted both the channel depth and width. When the specified width was smaller than the laser spot size, channels were either non-existent or much smaller than expected. However, understanding this behavior will allow for printing desired dimensions by adjusting the specified dimensions to larger than what is desired. For example, to print a channel with dimensions of ~150x50 µm, channel dimensions of 200x200 µm would be specified (Fig. 2.3A,B). The minimum channel dimensions that could be sealed without blockages or leakages were 228 µm wide x 20 µm deep (Fig. 2.3E). Importantly, when fully enclosed channels with the same dimensions as those in Figure 2.3 were printed on the Form2, all channels were clogged with cured resin and not even the largest channel (500x200µm) could hold solution. Figure A1.7 shows a cross-sectional view of a 3DPP with fully enclosed channels that was cut in half with a laser cutter, and no channels can be seen. Here, we confirmed our hypothesis that open-faced 3DPPs sealed to PDMS enable the creation of smaller channels than printing fully enclosed channels.

SLA printers may create ridges on the surface of 3DPPs, depending on the printer, settings, and orientation of the printed device.[31] To decrease surface roughness and improve sealing, 3DPPs in nine different orientations were printed to determine which printed the smoothest surface (Fig. A1.8). The nine orientations were printed with a 25 µm z-resolution and a 50 µm z-resolution (18 total devices). Interestingly, the z-resolution did not impact the surface roughness. Instead the printing orientation affected both the surface roughness and the accuracy of the channel dimensions. In Figure A1.8 the channels were designed as 150 µm deep, and only three of the nine printing orientations resulted in channels >140 µm deep. The three orientations that gave the most

accurate channel dimensions also gave the smoothest surface. Of these three orientations, two had a large peak (~40 µm high) adjacent to all channels (Fig. A1.8D), which made the seal near the channel inconsistent. The only orientation that did not contain the peak was orientation number 7. Printing orientation number 7 from Figure A1.8 was used for all remaining devices in this paper.

2.3.4 Demonstration of Microfluidic Devices

To demonstrate the capabilities of the sealing techniques described above, we created four common microfluidic devices: An H-cell with a laminar flow barrier; H-cell with printed grooves and protrusions for mixing; a gradient generator; and a droplet generator. The many uses for these devices have been discussed elsewhere in the literature.[32,33] Figure 2.4 shows images and results of two devices sealed with the silicone spray method. The first device (2.4A-C) is an H-cell device that demonstrated laminar flow and diffusional mixing at different flow rates. The gradient generator (2.4D) was chosen to demonstrate the ability to seal large microfluidic devices (8cmx5cm) with complex channel configurations. A droplet generator with a spray-seal was created, but the seal could not withstand the mineral oil that was used to generate droplets.

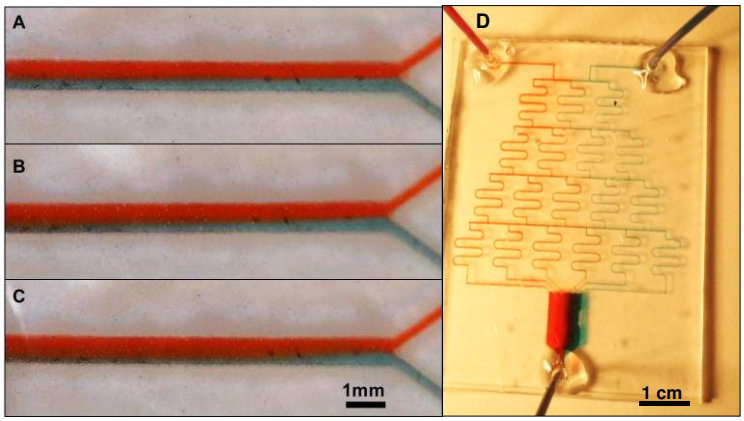

Figure 2.4. Laminar flow demonstration in an H-cell device at different flow rates (A-C). No diffusional mixing is observed at flow rates above 5 µL/min (A), slight mixing at 2 µL/min (B), and significant mixing at 0.5 µL/min (C). Gradient generator with two inlets and six outlets (D)

Figure 2.5 shows images and results of four devices sealed via APTES silanization. Figure 2.5A and B show two H-cell devices with the same channel dimensions. In A, a laminar flow barrier between the two fluids is observed because the channel is smooth. To demonstrate the ability to print structures within a microfluidic channel, herringbone patterned protrusions and indents (150 wide by 150 µm high/deep) were printed to create a mixing device. The channel containing the herringbone structures was 750 wide x 300 µm deep. The mixing capability of the device is clearly shown in 5B where yellow and blue fluids were mixed along the length of the channel and turned the solution green. In 5C we show the gradient generated from a gradient generator to show the ability to seal large devices (8x5cm). The channels here are 300 wide x 250 deep µm. Figure 2.5D and E show the results of a droplet generator that created water in oil droplets. Channel dimensions vary in this device but the smallest features (200x250 µm) occur at the t-junction where the aqueous dispersed phase meets the continuous phase. The droplets are dyed blue with food coloring and decrease in size as the oil:water flow rate ratio increases as

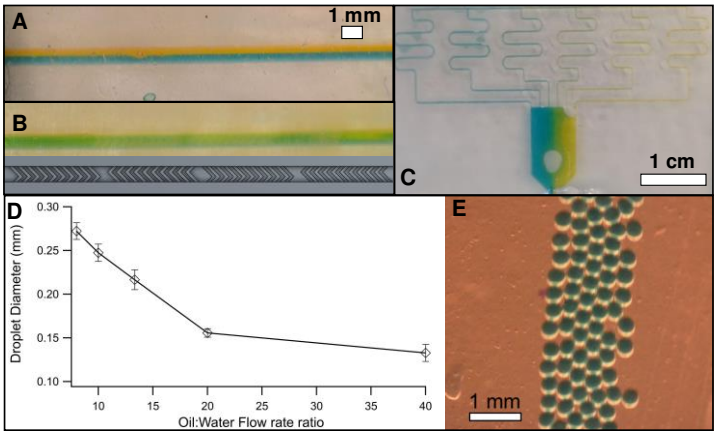

Figure 2.5. H-Cell device demonstrating laminar flow at high flow rates (80 µL/min) (A). Mixing device with herringbone-shaped indents and protrusions printed into the surface of a microfluidic channel demonstrating the mixing capabilities of yellow and blue dye (B). A CAD rendering of the herringbone pattern in a channel is shown below the image of the channel. A gradient generator highlighting the gradient generated in the device (C). Droplet size from a droplet generator as a function of Oil:Water flow rate ratio (D). Droplets generated with a 200 µL/min oil flow rate and a 20 µL/min water flow rate.

expected.[34] The CAD files for all devices are included in the supplementary information as a zip file.

2.4 Conclusion

In this work two separate methods were developed to seal open-faced 3D printed channels with PDMS to create microfluidic channels. In the first method, a commercially available silicone spray is used to coat the surface of the 3DPP before plasma treating and sealing to PDMS. This method is rapid, simple, and creates a strong seal, but deteriorates in the presence of organic solvents and channel dimensions are distorted by the spray. In the second method the 3DPP surface is silanized with APTES before sealing to PDMS. Although slightly more tedious to fabricate, the APTES seal can withstand non-aqueous solvents and is not distorted by a spray. Although 3D printed microfluidics are becoming more and more sophisticated, they also require expensive and/or custom 3D printers and resins. In this work we used a common and inexpensive stereolithography printer and resin from FormLabs to demonstrate the capabilities of our sealing methods. Additionally, fully enclosed 3D printed microfluidics require time-intensive post-processing to remove trapped resin from the channels. Our open-faced design solves this problem, and only requires a short bath in isopropyl alcohol to remove excess resin from the surface. Currently this work is limited by the large feature sizes capable with the Form2 printer. Importantly, this is a limitation of the printer and not the sealing method presented. This fabrication method also enables channel modification before sealing with external components like electrodes. Future work will explore this capability along with creating 3-dimensional structures by sealing together multiple devices. The sealing methods described in this work will enable labs with limited resources to rapidly prototype new microfluidic devices without worrying about cost.

Publication Disclosure: This chapter was published in *Analytical Chimica Acta.*[35] I was the first author and was the sole writer of the published work. All experiments were conducted by myself or one of the other listed authors.

REFERENCES

1. He, Y.; Wu, Y.; Fu, J. z.; Gao, Q.; Qiu, J. j., Developments of 3D printing microfluidics and applications in chemistry and biology: a review. *Electroanalysis* **2016,** *28* (8), 1658-1678.

2. Su, W.; Gao, X.; Jiang, L.; Qin, J., Microfluidic platform towards point-of-care diagnostics in infectious diseases. *Journal of Chromatography A* **2015,** *1377*, 13-26.

3. Wheeler, A. R.; Throndset, W. R.; Whelan, R. J.; Leach, A. M.; Zare, R. N.; Liao, Y. H.; Farrell, K.; Manger, I. D.; Daridon, A., Microfluidic device for single-cell analysis. *Analytical chemistry* **2003,** *75* (14), 3581-3586.

4. Duncombe, T. A.; Tentori, A. M.; Herr, A. E., Microfluidics: reframing biological enquiry. *Nat. Rev. Mol. Cell Biol.* **2015,** *16* (9), 554-567.

5. Rackus, D. G.; Shamsi, M. H.; Wheeler, A. R., Electrochemistry, biosensors and microfluidics: a convergence of fields. *Chem. Soc. Rev.* **2015,** *44* (15), 5320-5340.

6. Huh, D.; Hamilton, G. A.; Ingber, D. E., From 3D cell culture to organs-on-chips. *Trends in Cell Biology* **2011,** *21* (12), 745-754.

7. Casadevall i Solvas, X.; deMello, A., Droplet microfluidics: recent developments and future applications. *Chem. Commun.* **2011,** *47* (7), 1936-1942.

8. Tsao, C. W., Polymer Microfluidics: Simple, Low-Cost Fabrication Process Bridging Academic Lab Research to Commercialized Production. *Micromachines* **2016,** *7* (12), 11.

9. Au, A. K.; Huynh, W.; Horowitz, L. F.; Folch, A., 3D-Printed Microfluidics. *Angew. Chem.-Int. Edit.* **2016,** *55* (12), 3862-3881.

10. Bhattacharjee, N.; Urrios, A.; Kanga, S.; Folch, A., The upcoming 3D-printing revolution in microfluidics. *Lab Chip* **2016,** *16* (10), 1720-1742.

11. Sochol, R. D.; Sweet, E.; Glick, C. C.; Wu, S.-Y.; Yang, C.; Restaino, M.; Lin, L., 3D printed microfluidics and microelectronics. *Microelectronic Engineering* **2018,** *189*, 52-68.

12. Gross, B.; Lockwood, S. Y.; Spence, D. M., Recent Advances in Analytical Chemistry by 3D Printing. *Analytical Chemistry* **2017,** *89* (1), 57-70.

13. Waheed, S.; Cabot, J. M.; Macdonald, N. P.; Lewis, T.; Guijt, R. M.; Paull, B.; Breadmore, M. C., 3D printed microfluidic devices: enablers and barriers. *Lab Chip* **2016,** *16* (11), 1993-2013.

14. Shallan, A. I.; Smejkal, P.; Corban, M.; Guijt, R. M.; Breadmore, M. C., Cost-Effective Three-Dimensional Printing of Visibly Transparent Microchips within Minutes. *Analytical Chemistry* **2014,** *86* (6), 3124-3130.

15. Knowlton, S.; Yu, C. H.; Ersoy, F.; Emadi, S.; Khademhosseini, A.; Tasoglu, S., 3D-printed microfluidic chips with patterned, cell-laden hydrogel constructs. *Biofabrication* **2016,** *8* (2).

16. Gong, H.; Beauchamp, M.; Perry, S.; Woolley, A. T.; Nordin, G. P., Optical approach to resin formulation for 3D printed microfluidics. *RSC Adv.* **2015,** *5* (129), 106621-106632.

17. Gong, H.; Woolley, A. T.; Nordin, G. P., High density 3D printed microfluidic valves, pumps, and multiplexers. *Lab Chip* **2016,** *16* (13), 2450-2458.

18. Beauchamp, M. J.; Nordin, G. P.; Woolley, A. T., Moving from millifluidic to truly microfluidic sub-100-μm cross-section 3D printed devices. *Anal. Bioanal. Chem.* **2017,** *409* (18), 4311-4319.

19. Gong, H.; Bickham, B. P.; Woolley, A. T.; Nordin, G. P., Custom 3D printer and resin for 18 mu m x 20 mu m microfluidic flow channels. *Lab Chip* **2017,** *17* (17), 2899-2909.

20. Munshi, A. S.; Chen, C.; Townsend, A. D.; Martin, R. S., Use of 3D printing and modular microfluidics to integrate cell culture, injections and electrochemical analysis. *Analytical methods* **2018,** *10* (27), 3364-3374.

21. Samper, I. C.; Gowers, S. A.; Rogers, M. L.; Murray, D.-S. R.; Jewell, S. L.; Pahl, C.; Strong, A. J.; Boutelle, M. G., 3D printed microfluidic device for online detection of neurochemical changes with high temporal resolution in human brain microdialysate. *Lab Chip* **2019,** *19* (11), 2038-2048.

22. Chen, C.; Mehl, B. T.; Munshi, A. S.; Townsend, A. D.; Spence, D. M.; Martin, R. S., 3D-printed microfluidic devices: fabrication, advantages and limitations—a mini review. *Analytical Methods* **2016,** *8* (31), 6005-6012.

23. Erkal, J. L.; Selimovic, A.; Gross, B. C.; Lockwood, S. Y.; Walton, E. L.; McNamara, S.; Martin, R. S.; Spence, D. M., 3D printed microfluidic devices with integrated versatile and reusable electrodes. *Lab Chip* **2014,** *14* (12), 2023-2032.

24. Comina, G.; Suska, A.; Filippini, D., Low cost lab-on-a-chip prototyping with a consumer grade 3D printer. *Lab Chip* **2014,** *14* (16), 2978-2982.

25. Hinman, S. S.; McKeating, K. S.; Cheng, Q., Plasmonic Sensing with 3D Printed Optics. *Analytical Chemistry* **2017,** *89* (23), 12626-12630.

26. Vlachopoulou, M. E.; Tserepi, A.; Pavli, P.; Argitis, P.; Sanopoulou, M.; Misiakos, K., A low temperature surface modification assisted method for bonding plastic substrates. *J. Micromech. Microeng.* **2009,** *19* (1).

27. Sunkara, V.; Cho, Y. K., Investigation on the Mechanism of Aminosilane-Mediated Bonding of Thermoplastics and Poly(dimethylsiloxane). *ACS Appl. Mater. Interfaces* **2012,** *4* (12), 6537-6544.

28. Sunkara, V.; Park, D. K.; Hwang, H.; Chantiwas, R.; Soper, S. A.; Cho, Y. K., Simple room temperature bonding of thermoplastics and poly(dimethylsiloxane). *Lab Chip* **2011,** *11* (5), 962-965.

29. Clear. In *Photoreactive Resin for Form 1, Form 1+, Form 2*, Formlabs: Somerville, MA, 2016.

30. Tennico, Y. H.; Koesdjojo, M. T.; Kondo, S.; Mandrell, D. T.; Remcho, V. T., Surface modification-assisted bonding of polymer-based microfluidic devices. *Sensors and Actuators B-Chemical* **2010,** *143* (2), 799-804.

31. Beauchamp, M.; Gong, H.; Woolley, A.; Nordin, G., 3D printed microfluidic features using dose control in X, Y, and Z dimensions. *Micromachines* **2018,** *9* (7), 326.

32. Grosche, M.; Zoheir, A. E.; Stegmaier, J.; Mikut, R.; Mager, D.; Korvink, J. G.; Rabe, K. S.; Niemeyer, C. M., Microfluidic Chips for Life Sciences-A Comparison of Low Entry Manufacturing Technologies. *Small*, 9.

33. Parittotokkaporn, S.; Dravid, A.; Bansal, M.; Aqrawe, Z.; Svirskis, D.; Suresh, V.; O'Carroll, S. J., Make it simple: long-term stable gradient generation in a microfluidic microdevice. *Biomed. Microdevices* **2019,** *21* (3), 10.

34. Xu, J.; Li, S.; Tan, J.; Wang, Y.; Luo, G., Controllable preparation of monodisperse O/W and W/O emulsions in the same microfluidic device. *Langmuir* **2006,** *22* (19), 7943-7946.

35. Carrell, C. S.; McCord, C. P.; Wydallis, R. M.; Henry, C. S., Sealing 3D-printed parts to poly(dimethylsiloxane) for simple fabrication of Microfluidic devices. *Analytica Chimica Acta* **2020,** *1124*, 78-84.

CHAPTER 3: ROTARY MANIFOLD FOR AUTOMATING A PAPER-BASED *SALMONELLA IMMMUNOASSAY*

Foodborne pathogens are responsible for hundreds of thousands of deaths around the world each year. Rapid screening of agricultural products for these pathogens is essential to reduce and/or prevent outbreaks and pinpoint contamination sources. Unfortunately, current detection methods are laborious, expensive, time-consuming and require a central laboratory. Therefore, a rapid, sensitive, and field-deployable pathogen-detection assay is needed. We previously developed a colorimetric sandwich immunoassay utilizing immuno-magnetic separation (IMS) and chlorophenol red-β-D-galactopyranoside for *Salmonella* detection on a paper-based analytical device (μPAD); however, the assay required many sample preparation steps prior to the μPAD as well as laboratory equipment, which decreased user-friendliness for future end-users. As a step towards overcoming these limitations in resource-limited settings, we demonstrate a reusable 3D-printed rotational manifold that couples with disposable μPAD layers for semi-automated reagent delivery, washing, and detection in 65 minutes. After IMS to clean the sample, the manifold performs pipette-free reagent delivery and washing steps in a sequential order with controlled volumes, followed by enzymatic amplification and colorimetric detection using automated image processing to quantify color change. *Salmonella* was used as the target pathogen in this project and was detected with the manifold in growth media and milk with detection limits of 4.4×10^2 and 6.4×10^2 CFU/mL respectively. The manifold increases user friendliness and simplifies immunoassays resulting in a practical product for in-field use and commercialization.

3.1 Introduction

Foodborne pathogens pose a major health risk around the world. Each year they are responsible for 600 million infections and over 400,000 deaths around the world (9.4 million and

1,300 in the US).[1-2] Screening for specific pathogens could prevent large and deadly outbreaks; however, traditional pathogen detection assays are inadequate for testing large volumes of samples in a timely manner.[3] The most effective screening tests should be inexpensive, portable, rapid, and easy to use such that the assay can be performed in the field by an untrained end user.[4]

Foodborne pathogen detection is typically accomplished using culture-based methods.[5] Culture-based methods are well established, selective, sensitive, and benefit from decades of data to cross reference. Despite these advantages, culturing can take days to complete, requires trained laboratory personnel, transportation to a central laboratory for analysis, and is prone to false negatives due to viable but non-culturable pathogens.[3-4, 6] Therefore, culturing is an ill-suited tool to screen for foodborne pathogens, especially in resource-limited settings.

To decrease testing times, numerous rapid assays have been developed, including lateral flow immunoassays (LFAs), polymerase chain reaction (PCR), loop mediated isothermal amplification (LAMP), and enzyme linked immunosorbent assays (ELISAs). Other rapid assays have used nanomaterials and specific recognition elements like aptamers, phages, or antibodies for capture and detection.[5, 7] While faster than culture-based methods, PCR and ELISA are both expensive, require complex instrumentation, and are unsuitable for in-field testing.[8] LAMP is a promising tool for resource limited settings, but it still requires heating to 65°C, four sets of primers, and trained technicians for most detection techniques.[9] Finally, LFAs have been used for decades to detect pathogens, antibodies, and small biomarkers.[10-11] Although they are well established diagnostic tools, LFAs consistently suffer from poor detection limits without pre-enrichment steps such as culturing or PCR amplification.[11-12] Additionally, complex food sample matrices are difficult to use in an LFA format without significant sample pre-treatment or cleaning.

Microfluidic paper-based analytical devices (μPADs) have become a common platform for point-of-care and field-based assays.[13-17] μPADs are small, portable, inexpensive, easy to dispose of, frequently require no external instrumentation, and can effectively store reagents.[14, 16, 18-19] Recently, μPADs have been used to detect multiple foodborne pathogens with the goal of creating a simple screening test.[20-23] In these works, traditional antibody-based immunoassays, enzymatic detection, and electrochemical methods were adapted for use in μPADs. Although they are a promising technology, μPADs frequently suffer from inadequate sensitivity and high detection limits compared to traditional methods like PCR and ELISA.[14] To improve detection limits and sensitivity in traditional immunoassays, washing steps and signal enhancement reagents are used.[3, 24-25] However, these steps require timed and sequential delivery of reagents and/or washing agents, which μPADs are not typically designed to do without significant manual intervention from the end user.

Several groups have successfully demonstrated sequential reagent delivery in μPADs. Fu et al. accomplished this in 2010 with a 2D μPAD containing multiple inlets,[26] and Govindarajan et al. introduced folding, or origami, μPADs in 2012, where reagents are delivered in each folding step.[27] Since then, many other devices have been proposed including key shaped devices, sliding μPADs, rotating devices, dissolving sugar bridges, and complex channel geometries.[26, 28-32] Although they accomplish the goal of sequential reagent delivery, many of these devices suffer from inconsistent results, as the end user is ultimately performing the folding or sliding, and others require multiple pipetting steps to continually add buffer.[33] Additionally, the more complex channels necessary for sequential delivery in these systems can result in lost analyte to the cellulose fibers and decreased sensitivity.[24] Instead of relying on paper alone for reagent delivery, several groups have developed paper-plastic hybrid devices for pathogen detection.[34-36] In this work we

propose a μPAD housed in a re-usable 3D-printed rotational manifold capable of reproducible sequential reagent delivery for the detection of *Salmonella* via an immuno-magnetic separation (IMS) sandwich immunoassay.

Among foodborne pathogens, *Salmonella* is the most harmful, causing more worldwide infections (>90 million) and deaths (~155,000) than any other foodborne pathogen.[37] Therefore, *Salmonella* was chosen as the target in this study and the manifold was used to detect *Salmonella* in growth media and milk. Milk was used as a real-world sample as milk-borne infections are common in unpasteurized, raw milk.[38] Specificity against *E. Coli* and other bacteria naturally found in milk was also demonstrated. To simplify the assay, we employed colorimetric detection using an enzymatic reaction that cleaves chlorophenol red-β-D-galactopyranoside (CPRG) to chlorophenol red (CPR), which is indicated by a yellow to red color change. The color change can be qualitatively observed by the naked eye or quantitatively analyzed through image analysis. We used a flood fill algorithm and analysis system that lowered the limit of detection by an order of magnitude over previous color analysis techniques. Our target limit of detection (LOD) was ≤ 10^2 colony forming units (CFU)/mL, which has been reported as the infectious dose of *Salmonella* in food samples.[39-40] This LOD was realized in milk and media samples and is also the lowest detection limit that has been realized for direct colorimetric detection of *Salmonella* on a paper-based sensor with no pre-enrichment.[41-42] By combining a 3D-printed manifold with paper layers we have increased the capabilities of a μPAD without sacrificing user-friendliness. We believe that many of the pitfalls of traditional μPADs may be solved by integrating inexpensive plastic platforms or manifolds like the one described here.

3.2 Materials and Methods

3.2.1 Rotational Manifold

The 3D-printed manifold was printed using a FormLabs Form2 printer with their Clear V2 resin. All 3D-printed parts were designed in OnShape, a cloud-based CAD software. The paper channels, waste-pads, and sample layers are made of Fusion 5 paper, a conjugate-release membrane from GE healthcare (Waukesha, WI). The reagent layer and sample layers were made from Fusion 5 pieces, 3M transparency sheets, and 10 mil Fellowes® lamination sheets. The two layers are sealed using a TruLam laminator at 360°F. The surfaces of the reagent and sample layers are coated in Never-Wet®, a hydrophobic spray-on product from Rust-Oleum®. All designs for the two layers and paper pieces were created in CorelDraw (Fig. A2.1) and were cut with a 30W CO_2 laser cutter (Epilog Model 10000).

3.2.2 IMS Assay Reagents

The reagents used in the *Salmonella* immunoassay include: Dynabeads™ M-280 Tosylactivated (Invitrogen™, purchased from Thermo Fisher Scientific, Milwaukee, WI); Anti-*Salmonella* typhimurium 0-4 monoclonal mouse antibody (Abcam, Cambridge, MA ab8274); *Salmonella* antibody-biotin conjugate (Invitrogen™, purchased from Thermo Fisher Scientific); Streptavidin- β-galactosidase conjugate (Invitrogen™, purchased from Thermo Fisher Scientific), and Chlorophenol Red- β -D-galactopyranoside (purchased from Sigma Aldrich, St. Louis, MS). The bacterial strains used in this work were *Salmonella enterica serovar Typhimurium* and *Escherichia Coli* DH5α. The cells were grown in a difco (*Salmonella*) and LB (*E. Coli*) media for 12 h to a final concentration ~10^8 CFU/mL. After each growth the cell concentration was quantified by serial dilution and plating. The cells were spiked into and diluted in growth media or milk at the desired concentrations before running the assay with the manifold. The milk used was DairyGold ultra-high pasteurized whole milk. The buffer used in the manifold was a 1x solution of phosphate buffered saline (PBS) at pH 7.4 diluted in Milli-Q water. 2.5-4.5 µm pink

fluorescent magnetic beads from SpheroTech (Product #FP-4058-2) were used to perform the bead retention studies with a Dino-Lite EDGE fluorescent digital microscope at an excitation wavelength of 575 nm.

3.2.3 Assay Steps

One mL of liquid sample is incubated with 5 µL of 5 mg/mL magnetic bead-*Salmonella* antibody conjugate for 15 min at room temperature in a microcentrifuge tube. After a washing step using an external DynaMag-2 (Thermo Fisher Scientific) magnet for IMS, the magnetic bead-antibody-*Salmonella* conjugate is reconstituted in 60 µL of PBS buffer. A 15 µL aliquot of the concentrated solution was placed on the sample layer and the remainder of the assay (enzyme labeling and detection) is performed in the rotational manifold.

3.2.4 Device Operation

The manifold consists of four 3D printed pieces: the manifold top, center, and bottom, and the sample layer insert (Fig. 3.1). The top, center, and bottom pieces are all held together by bolts and springs. The springs allow the center piece to rotate while the top and bottom pieces are held in place. The center piece contains a slot for the reagent card. Within the reagent card are eight reagent channels and waste pads. The reagent card is made of five layers: a transparency sheet

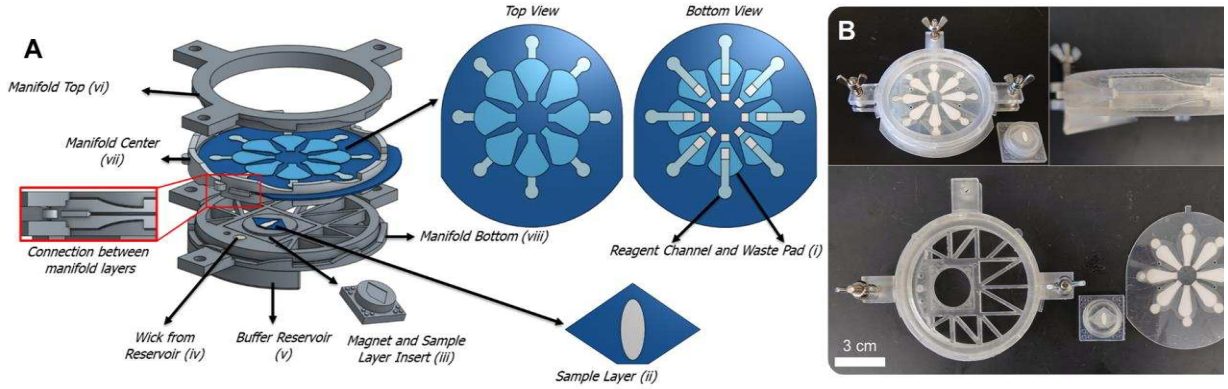

Figure 3.1. CAD rendering (A) and images (B) of the rotational manifold. In the CAD renderings all gray portions are 3D printed, dark blue are lamination or transparency sheets, and white are exposed Fusion 5 paper, and light blue are Fusion 5 paper covered by lamination or transparency sheets

with a hydrophobic coating, the paper reagent channels, a 3 mil lamination sheet, the paper waste pads, and a 10 mil lamination sheet. The waste pads and sample layers are stacked on top of each other but are separated by the 3 mil lamination sheet. Four reagent channels store reagents and four are empty channels used for washing. Two reagent and two washing channels are needed to run the assay in the current format, so eight total channels allow two tests to be run with one reagent card. In the four channels needed, the first channel contains 0.4 µg of biotin-labeled *Salmonella* antibody that is deposited and dried prior to the assay; the second is empty for washing; the third contains 0.2 µg of dried Streptavidin β-galactosidase; and the fourth is empty. 5 µL aliquots of 40 µg/mL and 80 µg/mL Streptavidin β-galactosidase and biotin-ab are added to the reagent channels to obtain 0.2 µg and 0.4 µg of dried reagent respectively. These reagents are all added and dried before the assay is run so the end-user does not need to perform the reagent addition steps.

When the manifold is assembled, the reagent layer rotates with the center piece and the sample layer insert remains stationary. As the center piece rotates, the top and bottom pieces move vertically while keeping pressure on the center piece. After a 45° rotation the center piece clicks into a slot and the top and bottom pieces collapse down with it. A video in the supplementary information shows the device rotation, clicking mechanism, and flow through the layers.

With each rotation, an opening in the reagent layer is aligned with a wick in the bottom piece of the manifold and the next reagent layer and waste pad are aligned with the sample layer. The wick sits in a buffer reservoir and, buffer flows through the reagent channel, through sample layer, and into a waste pad. The flow through the system either delivers a reagent to the sample layer or simply washes excess reagent away from the sample layer. Magnetic beads, and anything conjugated to them, will not wash through the sample layer because of a magnet that's fitted

underneath the sample layer in the sample layer insert. The end-user knows to rotate the device after the waste pad is saturated (~2 min).

3.2.5 Colorimetric Detection

The final step of the assay is to add 25 μL of a colorimetric substrate (CPRG) to the sample layer with a pipette. In the presence of β-galactosidase, and therefore *Salmonella*, CPRG (Yellow) will be turned over to CPR (Red). The [CPR] can be monitored via image capture and analysis. The image of the colored sample layer is taken inside a light box. The light box consists of two shells. The inner shell houses the sample layer and is made of clear acrylic. The acrylic was sanded until cloudy to diffuse light and prevent glare on the sample. The outer shell covers the first and is made of black acrylic so no ambient light can reach the sample layer. The outer shell contains 35 white and warm white LEDs built into the walls and powered by a 9V battery. The inner and outer shells contain an opening for a smartphone to capture an image (Fig. A2.2).

In this work we used a Samsung Galaxy S7 smartphone to capture static images of the sample layer at different time points. In the past, our group has frequently used manual processing with NIH ImageJ to quantify color changes.[42-45] To decrease the manual labor associated with ImageJ we used a flood-fill algorithm available in the OpenCV computer vision library.[46] Flood-fill identifies the color pixels in our sample region by employing a recursive region growing process. The regions grow out from a seed known to be in the sample. Flood-fill adds pixels relatively similar in color until no more similar pixels are adjacent to the region. In our case this means it stops at the edge of the oval paper that bounds our sample. The average RGB color values in the resulting set of pixels is then analyzed for each sample.[47] When compared to manual analysis using NIH ImageJ, the automated algorithm returned nearly identical results (Fig. A2.3). We define the signal in each trial as the difference in color between the blank and the sample. To

quantify this difference the vector length in 3D RGB space between our blank RGB coordinates and the sample RGB coordinates (ΔRGB) was calculated using Equation 1 as previously described.[48-49]

$$\Delta RGB = \sqrt{(R_s - R_0)^2 + (G_s - G_0)^2 + (B_s - B_0)^2} \qquad (1)$$

Where R_S, G_S, and B_S are the RGB values for the sample being tested, and R_0, G_0, and B_0 are the RGB values for each blank. The magnitude of the signal was larger for ΔRGB versus a single-color channel, thus increasing sensitivity. Additionally, equation 1 yields 9 data points with only 3 repeats: ΔS_1Bl_1, ΔS_1Bl_2, ΔS_1Bl_3, ΔS_2Bl_1, ΔS_2Bl_2, ΔS_2Bl_3, ΔS_3Bl_1, ΔS_3Bl_2, ΔS_3Bl_3, where S and Bl are the sample and the blank respectively and the number denotes the trial. The larger signal and number of data points resulted in an order of magnitude improvement in detection limit when compared to the use of a single channel (Fig. A2.4).

3.3 Results and Discussion

3.3.1 Assay Steps and Design

In a previous publication we presented an immuno-magnetic separation sandwich immunoassay for *Salmonella* detection.[42] The chemistry of the immunoassay remains the same in this work and is discussed in depth in our previous publication. Briefly, *Salmonella* is isolated from a sample using *Salmonella*-antibody labeled magnetic beads. After a short incubation with the sample the beads are removed from solution with an external magnet, washed, and reconstituted in a small volume of buffer to concentrate the sample. A secondary *Salmonella*-antibody labeled with biotin is then introduced to the *Salmonella*-magnetic bead complex solution. After an incubation and washing step, streptavidin-labeled β-galactosidase is added to the

Salmonella-magnetic bead-biotin conjugate solution. Finally, after another incubation and washing step a small volume of the *Salmonella*-magnetic bead-biotin-β-galactosidase conjugate solution reacts with the substrate CPRG. After a set reaction time, a color change from yellow to red indicates the presence of β-galactosidase, and therefore *Salmonella.* Previously, all steps of the assay were performed in solution in a microcentrifuge tube until the final step, where a small aliquot of magnetic bead-*Salmonella*-enzyme conjugate was added to a paper spot with dried substrate. The assay worked but required thirteen pipetting steps. To improve ease-of-use, we designed a rotational manifold to minimize pipetting steps by washing and delivering reagents to the test zone (Fig. 3.2). Here, the initial step of sample incubation with antibody-labeled magnetic beads remains in-solution to ensure a sufficient number of bacteria are available for conjugation to the magnetic beads. After the bacteria is isolated from the sample, a 15 µL aliquot of the magnetic bead-bacteria complex is added to a small paper sample-layer and the remaining steps

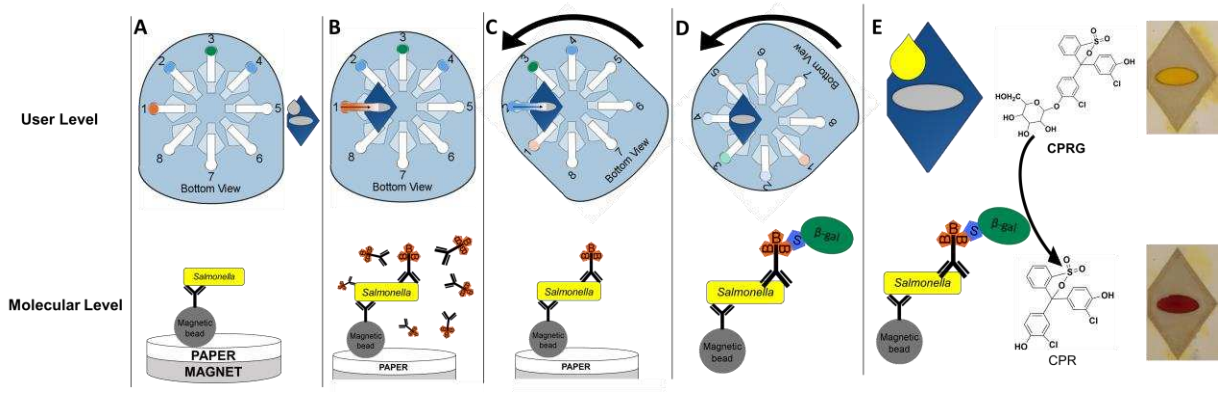

Figure 3.2. Schematic demonstrating the concept of sequential reagent delivery using a rotating reagent storage card and a stationary sample layer A) Add sample containing magnetic beads conjugated to your target analyte to the sample layer. B) Add the sample layer to the device. Biotinylated antibodies will be introduced. C) Rotate the device to a washing step used to remove excess biotinylated antibodies. D) Continue rotating until streptavidin β-galactosidase has been introduced and washed. E) Remove sample layer, add substrate CPRG, and observe color change

are completed in the device.

3.3.2 Device Design and Operation

Schematic drawings and a photograph of the manifold are shown in Figure 3.1. An important feature of the device is that the buffer volume delivered in each step can be controlled by changing the size of the waste pad. Fusion 5 paper holds 0.422±0.006 µL/mm^2 (Fig. A2.5), so by changing the surface area of the waste pad the volume of buffer used in each step can be customized. Volume control of each reagent delivery and washing step is critical when using the device for different assays that may need more thorough washing. Flow through each layer of the device is illustrated in Figure 3.3. The sample layer sits on the 3D-printed sample layer insert, which fits into the bottom manifold piece with lego-style fittings. A magnet screws into the bottom of the insert and is positioned directly underneath the sample layer. The magnet ensures that the magnetic beads are not washed away during reagent delivery and washing steps (Fig. A2.6). Using magnetic beads and magnets to create a test zone allowed us to use membranes other than nitrocellulose, which is expensive and has a short shelf life.[50] Additionally, the sample in the

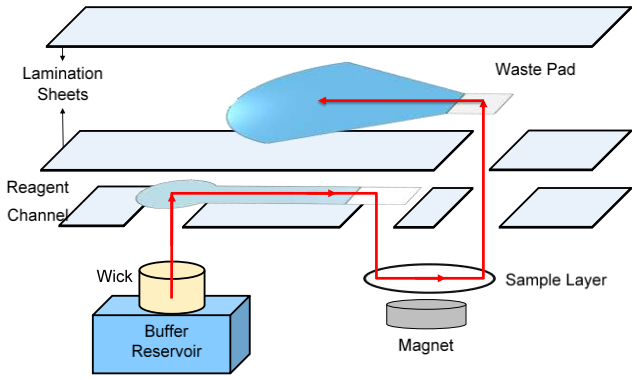

Figure 3.3. Flow through the device begins in the buffer reservoir where PBS is wicked through a paper wick into the reagent channel. Buffer flows through the reagent channel and delivers reagents to the conjugated system on the sample layer before washing away excess reagents to the waste pad.

manifold is stationary on the sample layer and therefore will not be lost to the membrane during flow through the device as is the case in traditional LFAs. Sample loss to paper channels is a problem in paper-based devices,[24, 51] and a stationary sample can improve detection limits.

After the final washing step, the insert and sample layer are removed from the device. 25 µL of 2.5 mM CPRG is pipetted onto the sample layer containing the conjugated system and the substrate reacts with any enzyme present for 40 min. A picture is then taken of the sample layer inside the light box. The image is analyzed as described in the materials and methods to determine the *Salmonella* concentration. Using the rotational manifold, the number of pipetting steps needed to complete the IMS sandwich immunoassay was decreased from thirteen to four, which significantly reduces labor and complexity for the end user. Each sample addition step requires ~1 second of user input (rotating the device) compared to traditional pipetting and IMS that can take multiple minutes per step. Additionally, the waste generated during each step of a traditional in-solution IMS assay exceeds 1 mL, while our assay uses roughly 0.1 mL/step, reducing cost and storage needs.

3.3.2 Assay Optimization and Parameters

Paper type: Fusion 5 was chosen as the paper type for all portions of the manifold: reagent layer, waste pad, and sample layer. Fusion 5 was developed as a substrate for all portions of an LFA.[52] In our device, Fusion 5 demonstrated faster flow and lower noise from non-specific enzyme adsorption than other papers tested (Whatman I and IV). The faster flow rates increased washing efficiency and decreased assay time. Additionally, Fusion 5 contains plastic binder meant to stabilize its mechanical properties, allowing us to laminate the reagent layer under high pressure and heat without decreasing flow rates.

Sample Layer: A major challenge in developing the rotational manifold and corresponding assay was minimizing the noise in the blank signal. Although using Fusion 5 helped improve washing, β-galactosidase would consistently get trapped on the edges or ends of the sample layer. To overcome this challenge, we blocked the surface of the sample layer with 10 µL of 5 mg/mL bovine serum albumin (BSA) and updated the shape to an oval. The benefit of an oval sample layer is that there are no corners where the enzyme can be trapped. Once these changes were implemented, the washing efficiency of the device was improved, and blank samples remained yellow after all washing steps were performed (Fig. 3.4).

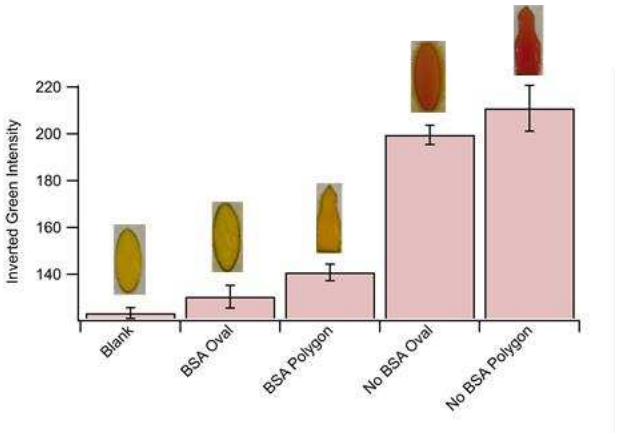

Figure 3.4. Effect of sample layer shape and blocking with BSA. The blank sample was an image of the sample layer with CPRG without any β-Galactosidase ever introduced. All other samples had β-Galactosidase washed through the sample layer into the waste pads

Reaction times: The initial sample incubation with the magnetic beads was 15 min. In more complex samples this incubation may need to be lengthened; however, in our liquid sample matrices 15 min was sufficient. The reaction times for each reagent delivery step were roughly 2 min, or the time it took for the waste pad to completely saturate. Once saturated, flow through the waste pad stopped and no new reagents reached the immobilized magnetic bead complex, eliminating any benefit of longer incubation. The shape of the waste pad was fan-like to provide continuous capillary pressure and more constant flow rates.[53] Finally, the substrate and enzyme

reacted for 40 min. In optimization studies of CPRG and β-galactosidase the longer the wait time the higher the signal, so long as the sample layer did not dry out. Above 25 µL of substrate, the sample layer began to leak, and at 25 µL the sample began to dry out after 60 min (Fig. A2.7). The 40-min reaction time was a compromise between assay speed and sensitivity. If total assay time was not a concern, one could lower detection limits by increasing the reaction time and minimizing evaporation with a small air-tight enclosure. With the 40-min reaction, the entire assay can be performed in roughly 65 min. In samples with higher bacteria concentrations, a qualitative color change could be observed in as little as 5 min after adding the substrate. To reach a lower limit of detection, however, 40 min of reaction time was needed to differentiate between the blank and the lowest bacteria concentration.

Image Capture: An image captured by a smartphone was used to quantify *Salmonella.* Smartphones are an excellent tool for in-field measurements as most end-users will already own a smartphone, cutting down on the cost of the assay and increasing user-friendliness. Additionally, numerous papers on colorimetric µPADs use a smartphone for detection.[54] We correct for differences in ambient lighting with a custom light box that contains an opening for a smart phone to take a picture. The light-box improved consistency between images (Table S1). The %RSD of three identical blank images of the sample layer taken in three different ambient light settings decreased from 19.9% without the box to 3.3% in the box.

3.3.3 Colorimetric Salmonella Detection

A *Salmonella* detection assay was used to test the functionality of the manifold. Here, *Salmonella* cultured in Difco nutrient broth was diluted to concentrations spanning from 10^2 to 10^7 CFU/mL. The results are shown in Figure 3.5 (n=3). The data was fit to a 4-parameter logistic curve (Equation SI) with a χ^2=13.02 (α=0.05, $\chi_{critical}$=15.51).[55] The logistic fit was chosen because

the antibody binding kinetics of the sandwich immunoassay are the limiting steps. The LOD was calculated by finding 3×SD + mean of the blank and plugging it into the fit equation. An LOD of 4.40×10^2 CFU/mL was realized using the manifold. In our previous entirely in-solution assay, we found a LOD on the same order of magnitude, which demonstrates the capabilities of our device to perform a multi-step immunoassay on a μPAD.[42]

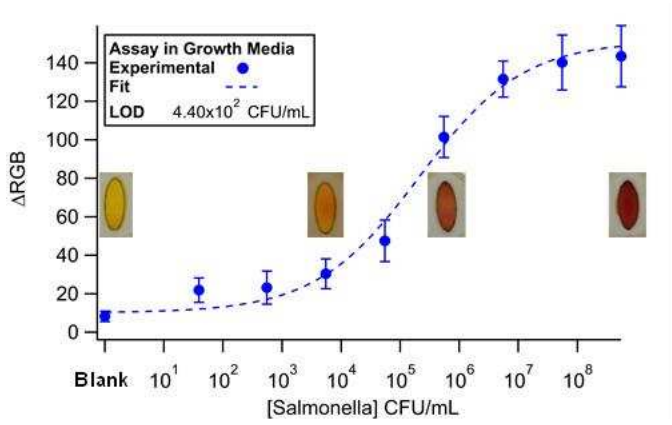

Figure 3.5: Dose response curve (n=3) for *Salmonella* in media detected using the rotational manifold. The curve was fit to a 4-parameter logistic model and a LOD of 2.9×10^3 was achieved

2.3.4 Specificity and Real-World Samples

To confirm the specificity of our *Salmonella* assay, 10^7 CFU/mL DH5 α *E. Coli* in media was tested with the device using *Salmonella* specific antibodies (Fig. 3.6A). The low signal for E. Coli samples demonstrates the specificity of the assay. A low signal also indicates efficient washing throughout the system as E. Coli produces β-galactosidase naturally, and any excess enzyme would increase the signal. Finally, the assay was run using milk spiked with *Salmonella* (Fig. 3.6B). In milk, we found a detection limit of 6.36×10^2 CFU/mL. The data was once again fit to a 4-parameter logistic curve (χ^2=4.13, α=0.05, $\chi_{critical}$=14.07) and the LOD found using the fit equations and 3×SD + the mean of the blank. Although the detection limit is slightly higher, the assay performed nearly as well in milk versus growth media. The small difference in LOD could

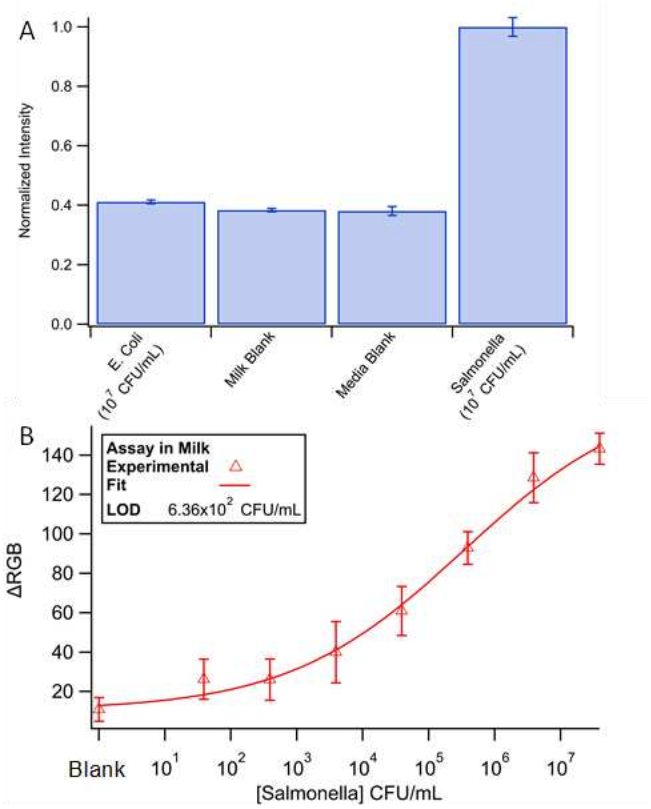

Figure 3.6. (A) Specificity study using *E. Coli* at 10^7 CFU/mL compared to blank samples in milk, growth media, and a positive *Salmonella* sample. **(B)** Dose-response curve (n=3) of *Salmonella* in milk detected using the rotational manifold. The curve was fit to a 4-parameter logistic model and a LOD of 6.4×10^2 CFU/mL was achieved.

be attributed to decreased antibody binding efficiency in the first step of the assay due to non-specific adsorption of other biomolecules in milk onto the magnetic beads. The international microbiological criteria for dairy products states that *Salmonella* should have a concentration of <1 cell per mL.[56] The only way to meet the required LOD with our device, and any other inexpensive point-of-care system, is through some form of pre-enrichment like culturing. Although we believe that the rotary manifold is an innovative way to perform IMS as a rapid screening tool, further technologies will need to be developed to meet the strict requirements of the food safety industry.

3.4. Conclusions and Future Directions

The field of microfluidic paper-based devices has grown tremendously over the last 10 years in academic settings. There are many reasons for the disconnect between published works and commercial products, but the most commonly cited argument is poor sensitivity and specificity in µPADs.[14, 19] Attempts to improve these criteria are often successful but result in assays that are far too complicated for their intended use at the point-of care with untrained end-users. We believe that coupling µPADs with other inexpensive materials could enhance sensitivity and specificity without sacrificing usability. In this work we designed a 3D-printed rotational manifold to perform multiple reagent delivery and washing steps in a sequential order. The washings steps increase sensitivity over traditional LFAs and the manifold ensures that the additional steps do not infringe on usability. The manifold was used to detect *Salmonella*, however with a simple change of reagents could be used to detect a large host of other pathogens, proteins, and/or biomarkers. In the future we will continue working with this device to detect additional biomolecules in a multiplexed format. We also recognize that although we simplified testing and reduced manual input, the four pipetting steps still required are not ideal. Some liquid transfer will always be necessary in an IMS assay, however, future work will be dedicated to decreasing user intervention further. For example, work has begun to implement a motorized rotational mechanism and further automate image capture and analysis with a web-based interface. With devices like the one described here, we anticipate an increase in new µPADs on the market.

Acknowledgements

Funding for this project was provided by the United States Department of Agriculture, Grant Number #16-74000589 through the National Wildlife Research Center. The authors would also

like to thank the members of the Henry and Geiss laboratories and Dr. Alan Franklin for their guidance throughout the project.

Publication Disclosure: This chapter was published in *RSC Advances.*[57] I was the first author and was primary writer of the published work. All experiments were conducted by myself or one of the other listed authors.

REFERENCES

1. Scallan, E.; Hoekstra, R. M.; Angulo, F. J.; Tauxe, R. V.; Widdowson, M. A.; Roy, S. L.; Jones, J. L.; Griffin, P. M., Foodborne Illness Acquired in the United States-Major Pathogens. *Emerg. Infect. Dis* **2011,** *17* (1), 7-15.

2. Group, F. D. B. E. R., WHO Estimates of the Global Burden of Foodborne Diseases. Organization, W. H., Ed. 2015.

3. Law, J. W. F.; Ab Mutalib, N. S.; Chan, K. G.; Lee, L. H., Rapid methods for the detection of foodborne bacterial pathogens: principles, applications, advantages and limitations. *Front. Microbiol.* **2015,** *5*, 19.

4. Velusamy, V.; Arshak, K.; Korostynska, O.; Oliwa, K.; Adley, C., An overview of foodborne pathogen detection: In the perspective of biosensors. *Biotechnol. Adv.* **2010,** *28* (2), 232-254.

5. Bohaychuk, V. M.; Gensler, G. E.; King, R. K.; Wu, J. T.; McMullen, L. M., Evaluation of detection methods for screening meat and poultry products for the presence of foodborne pathogens. *Journal of Food Protection* **2005,** *68* (12), 2637-2647.

6. P. K. Mandal, A. K. B., K. Choi and U. K. Pal, Methods for Rapid Detection of Foodborne Pathogens: An Overview. *American Journal of Food Technology* **2011,** *6* (2), 15.

7. Chen, J.; Andler, S. M.; Goddard, J. M.; Nugen, S. R.; Rotello, V. M., Integrating recognition elements with nanomaterials for bacteria sensing. *Chem. Soc. Rev.* **2017,** *46* (5), 1272-1283.

8. Zhao, X.; Lin, C. W.; Wang, J.; Oh, D. H., Advances in Rapid Detection Methods for Foodborne Pathogens. *J. Microbiol. Biotechnol.* **2014,** *24* (3), 297-312.

9. Mori, Y.; Notomi, T., Loop-mediated isothermal amplification (LAMP): a rapid, accurate, and cost-effective diagnostic method for infectious diseases. *J. Infect. Chemother.* **2009,** *15* (2), 62-69.

10. Zhao, Y.; Wang, H. R.; Zhang, P. P.; Sun, C. Y.; Wang, X. C.; Wang, X. R.; Yang, R. F.; Wang, C. B.; Zhou, L., Rapid multiplex detection of 10 foodborne pathogens with an up-converting phosphor technology-based 10-channel lateral flow assay. *Sci Rep* **2016,** *6*.

11. Posthuma-Trumpie, G. A.; Korf, J.; van Amerongen, A., Lateral flow (immuno) assay: its strengths, weaknesses, opportunities and threats. A literature survey. *Anal. Bioanal. Chem.* **2009,** *393* (2), 569-582.

12. Hu, J.; Wang, S. Q.; Wang, L.; Li, F.; Pingguan-Murphy, B.; Lu, T. J.; Xu, F., Advances in paper-based point-of-care diagnostics. *Biosens. Bioelectron.* **2014,** *54*, 585-597.

13. Martinez, A. W.; Phillips, S. T.; Butte, M. J.; Whitesides, G. M., Patterned paper as a platform for inexpensive, low-volume, portable bioassays. *Angew. Chem.-Int. Edit.* **2007,** *46* (8), 1318-1320.

14. Yamada, K.; Shibata, H.; Suzuki, K.; Citterio, D., Toward practical application of paper-based microfluidics for medical diagnostics: state-of-the-art and challenges. *Lab Chip* **2017,** *17* (7), 1206-1249.

15. Martinez, A. W.; Phillips, S. T.; Whitesides, G. M.; Carrilho, E., Diagnostics for the Developing World: Microfluidic Paper-Based Analytical Devices. *Analytical Chemistry* **2010,** *82* (1), 3-10.

16. Yang, Y. Y.; Noviana, E.; Nguyen, M. P.; Geiss, B. J.; Dandy, D. S.; Henry, C. S., Paper-Based Microfluidic Devices: Emerging Themes and Applications. *Analytical Chemistry* **2017,** *89* (1), 71-91.

17. Xia, Y. Y.; Si, J.; Li, Z. Y., Fabrication techniques for microfluidic paper-based analytical devices and their applications for biological testing: A review. *Biosens. Bioelectron.* **2016,** *77*, 774-789.

18. Lopez-Marzo, A. M.; Merkoci, A., Paper-based sensors and assays: a success of the engineering design and the convergence of knowledge areas. *Lab Chip* **2016,** *16* (17), 3150-3176.

19. Carrell, C.; Kava, A.; Nguyen, M.; Menger, R.; Munshi, Z.; Call, Z.; Nussbaum, M.; Henry, C., Beyond the lateral flow assay: A review of paper-based microfluidics. *Microelectronic Engineering* **2019,** *206*, 45-54.

20. Kant, K.; Shahbazi, M.-A.; Dave, V. P.; Ngo, T. A.; Chidambara, V. A.; Than, L. Q.; Bang, D. D.; Wolff, A., Microfluidic devices for sample preparation and rapid detection of foodborne pathogens. *Biotechnol. Adv.* **2018**.

21. Jokerst, J. C.; Adkins, J. A.; Bisha, B.; Mentele, M. M.; Goodridge, L. D.; Henry, C. S., Development of a Paper-Based Analytical Device for Colorimetric Detection of Select Foodborne Pathogens. *Analytical Chemistry* **2012,** *84* (6), 2900-2907.

22. Bhardwaj, J.; Devarakonda, S.; Kumar, S.; Jang, J., Development of a paper-based electrochemical immunosensor using an antibody-single walled carbon nanotubes bio-conjugate modified electrode for label-free detection of foodborne pathogens. *Sensors and Actuators B-Chemical* **2017,** *253*, 115-123.

23. Park, J.; Shin, J. H.; Park, J. K., Pressed Paper-Based Dipstick for Detection of Foodborne Pathogens with Multistep Reactions. *Analytical Chemistry* **2016,** *88* (7), 3781-3788.

24. Nguyen, M. P.; Meredith, N. A.; Kelly, S. P.; Henry, C. S., Design considerations for reducing sample loss in microfluidic paper-based analytical devices. *Analytica Chimica Acta* **2018,** *1017*, 20-25.

25. Fu, E.; Kauffman, P.; Lutz, B.; Yager, P., Chemical signal amplification in two-dimensional paper networks. *Sensors and Actuators B-Chemical* **2010,** *149* (1), 325-328.

26. Fu, E.; Lutz, B.; Kauffman, P.; Yager, P., Controlled reagent transport in disposable 2D paper networks. *Lab Chip* **2010,** *10* (7), 918-920.

27. Govindarajan, A. V.; Ramachandran, S.; Vigil, G. D.; Yager, P.; Bohringer, K. F., A low cost point-of-care viscous sample preparation device for molecular diagnosis in the developing world; an example of microfluidic origami. *Lab Chip* **2012,** *12* (1), 174-181.

28. Channon, R. B.; Nguyen, M. P.; Scorzelli, A. G.; Henry, E. M.; Volckens, J.; Dandy, D. S.; Henry, C. S., Rapid flow in multilayer microfluidic paper-based analytical devices. *Lab Chip* **2018,** *18* (5), 793-802.

29. Apilux, A.; Ukita, Y.; Chikae, M.; Chailapakul, O.; Takamura, Y., Development of automated paper-based devices for sequential multistep sandwich enzyme-linked immunosorbent assays using inkjet printing. *Lab Chip* **2013,** *13* (1), 126-135.

30. Liu, H.; Li, X.; Crooks, R. M., Paper-Based SlipPAD for High-Throughput Chemical Sensing. *Analytical Chemistry* **2013,** *85* (9), 4263-4267.

31. Lutz, B.; Liang, T.; Fu, E.; Ramachandran, S.; Kauffman, P.; Yager, P., Dissolvable fluidic time delays for programming multi-step assays in instrument-free paper diagnostics. *Lab Chip* **2013,** *13* (14), 2840-2847.

32. Sun, X. E.; Li, B. W.; Tian, C. Y.; Yu, F. B.; Zhou, N.; Zhan, Y. H.; Chen, L. X., Rotational paper-based electrochemiluminescence immunodevices for sensitive and multiplexed detection of cancer biomarkers. *Analytica Chimica Acta* **2018,** *1007*, 33-39.

33. Fu, E.; Downs, C., Progress in the development and integration of fluid flow control tools in paper microfluidics. *Lab Chip* **2017,** *17* (4), 614-628.

34. Lafleur, L.; Stevens, D.; McKenzie, K.; Ramachandran, S.; Spicar-Mihalic, P.; Singhal, M.; Arjyal, A.; Osborn, J.; Kauffman, P.; Yager, P.; Lutz, B., Progress toward multiplexed sample-to-result detection in low resource settings using microfluidic immunoassay cards. *Lab Chip* **2012,** *12* (6), 1119-1127.

35. Tang, R. H.; Yang, H.; Choi, J. R.; Gong, Y.; Hu, J.; Wen, T.; Li, X. J.; Xu, B.; Mei, Q. B.; Xu, F., Paper-based device with on-chip reagent storage for rapid extraction of DNA from biological samples. *Microchimica Acta* **2017,** *184* (7), 2141-2150.

36. Jalal, U. M.; Jin, G. J.; Shim, J. S., Paper-Plastic Hybrid Microfluidic Device for Smartphone-Based Colorimetric Analysis of Urine. *Analytical Chemistry* **2017,** *89* (24), 13160-13166.

37. Majowicz, S. E.; Musto, J.; Scallan, E.; Angulo, F. J.; Kirk, M.; O'Brien, S. J.; Jones, T. F.; Fazil, A.; Hoekstra, R. M.; Int Collaboration Enteric Dis, B., The Global Burden of Nontyphoidal Salmonella Gastroenteritis. *Clinical Infectious Diseases* **2010,** *50* (6), 882-889.

38. Oliver, S. P.; Boor, K. J.; Murphy, S. C.; Murinda, S. E., Food Safety Hazards Associated with Consumption of Raw Milk. *Foodborne Pathog. Dis.* **2009,** *6* (7), 793-806.

39. Blaser, M. J.; Newman, L. S., A REVIEW OF HUMAN SALMONELLOSIS .1. INFECTIVE DOSE. *Reviews of Infectious Diseases* **1982,** *4* (6), 1096-1106.

40. Kothary, M. H.; Babu, U. S., Infective dose of foodborne pathogens in volunteers: A review. *Journal of Food Safety* **2001,** *21* (1), 49-73.

41. Li, C. Z.; Vandenberg, K.; Prabhulkar, S.; Zhu, X. N.; Schneper, L.; Methee, K.; Rosser, C. J.; Almeide, E., Paper based point-of-care testing disc for multiplex whole cell bacteria analysis. *Biosens. Bioelectron.* **2011,** *26* (11), 4342-4348.

42. Srisa-Art, M.; Boehle, K. E.; Geiss, B. J.; Henry, C. S., Highly Sensitive Detection of Salmonella typhimurium Using a Colorimetric Paper-Based Analytical Device Coupled with Immunomagnetic Separation. *Analytical Chemistry* **2018,** *90* (1), 1035-1043.

43. Boehle, K. E.; Gilliand, J.; Wheeldon, C. R.; Holder, A.; Adkins, J. A.; Geiss, B. J.; Ryan, E. P.; Henry, C. S., Utilizing Paper-Based Devices for Antimicrobial-Resistant Bacteria Detection. *Angew. Chem.-Int. Edit.* **2017,** *56* (24), 6886-6890.

44. Boehle, K. E.; Carrell, C. S.; Caraway, J.; Henry, C. S., Paper-Based Enzyme Competition Assay for Detecting Falsified beta-Lactam Antibiotics. *Acs Sensors* **2018,** *3* (7), 1299-1307.

45. Adkins, J. A.; Boehle, K.; Friend, C.; Chamberlain, B.; Bisha, B.; Henry, C. S., Colorimetric and Electrochemical Bacteria Detection Using Printed Paper- and Transparency-Based Analytic Devices. *Analytical Chemistry* **2017,** *89* (6), 3613-3621.

46. Bradski, G., The OpenCV library. *Dr Dobbs Journal* **2000,** *25* (11), 120-+.

47. Boehle, K. E.; Doan, E.; Henry, S.; Beveridge, J. R.; Pallickara, S. L.; Henry, C. S., Single board computing system for automated colorimetric analysis on low-cost analytical devices. *Analytical Methods* **2018,** *10* (44), 5282-5290.

48. Murdock, R. C.; Shen, L.; Griffin, D. K.; Kelley-Loughnane, N.; Papautsky, I.; Hagen, J. A., Optimization of a Paper-Based ELISA for a Human Performance Biomarker. *Analytical Chemistry* **2013,** *85* (23), 11634-11642.

49. Shen, L.; Hagen, J. A.; Papautsky, I., Point-of-care colorimetric detection with a smartphone. *Lab Chip* **2012,** *12* (21), 4240-4243.

50. Sajid, M.; Kawde, A. N.; Daud, M., Designs, formats and applications of lateral flow assay: A literature review. *Journal of Saudi Chemical Society* **2015,** *19* (6), 689-705.

51. Li, X.; Ballerini, D. R.; Shen, W., A perspective on paper-based microfluidics: Current status and future trends. *Biomicrofluidics* **2012,** *6* (1).

52. Jones, K., FUSION 5: A New Platform For Lateral Flow Immunoassay Tests. *Lateral Flow Immunoassay* **2009**, 115-129.

53. Adkins, J. A.; Noviana, E.; Henry, C. S., Development of a Quasi-Steady Flow Electrochemical Paper-Based Analytical Device. *Analytical Chemistry* **2016,** *88* (21), 10639-10647.

54. Zhang, D. M.; Liu, Q. J., Biosensors and bioelectronics on smartphone for portable biochemical detection. *Biosens. Bioelectron.* **2016,** *75*, 273-284.

55. Christopoulos, T. K.; Diamandis, E. P., Theory of immunoassays. *Immunoassay* **1996**, 25-50.

56. Scientific Criteria to Ensure Safe Food. National Academies Press: Washington, DC, 2003. https://www.ncbi.nlm.nih.gov/books/NBK221563/.

57. Carrell, C. S.; Wydallis, R. M.; Bontha, M.; Boehle, K. E.; Beveridge, J. R.; Geiss, B. J.; Henry, C. S., Rotary manifold for automating a paper-based Salmonella immunoassay. *RSC Adv.* **2019,** *9* (50), 29078-29086.

CHAPTER 4. POINT-OF-NEED DISPOSABLE ELISA SYSTEM FOR COVID-19 SEROLOGY TESTING

A disposable enzyme-linked immunosorbent assay (dELISA) device for at-home or doctor's office use was developed to detect SARS-CoV-2 antibodies. Serology testing for SARS-CoV-2 antibodies is currently run using well-plate ELISAs in centralized laboratories. However, the scale of serology testing needed for epidemiological and clinical screening studies will overwhelm existing clinical laboratory resources. Instead, a point-of-need device that can be used at home or in doctor's offices for COVID-19 serology testing must be developed and is one of four target products prioritized by the World Health Organization. Lateral flow assays are common and easy to use, but lack the sensitivity needed to reliably detect SARS-CoV-2 antibodies in clinical samples. This work describes a disposable ELISA device that is as simple to use as a lateral flow assay, but as sensitive as a well-plate ELISA. The device utilizes capillary-driven flow channels made of transparency films and double-sided adhesive combined with paper pumps to drive flow. The geometry of the channels and storage pads enables automated sequential washing and reagent addition steps with two simple end-user steps. An enzyme label is used to produce a colorimetric signal instead of a nanoparticle label in order to amplify signal and increase sensitivity, while the integrated washing steps decrease false positives and increase reproducibility. Naked-eye detection can be used for qualitative results or a smartphone camera for quantitative analysis. The device can detect antibodies at 2.8 ng/mL from whole blood, which was very close the concentration of detectable target in a well-plate ELISA (1.2 ng/mL). In this study the dELISA system was used to detect SARS-CoV-2 antibodies, but we believe that the device represents a fundamental step forward in point-of-care technology that will enable sensitive detection of many other analytes outside of a centralized laboratory.

4.1 Introduction

SARS-CoV-2, the causative agent of COVID-19, has infected at least 32 M people and caused the deaths of over 980,000 worldwide (September 25, 2020).[1] The SARS-CoV-2 virus represents a dire threat to public health and the global economy. SARS-CoV-2 is highly infectious, making isolation one of the most effective methods of slowing disease spread. As societies attempt to return to normal, the question of how to determine who can leave isolation and return to work safely must be addressed. This question is difficult to answer because it is unclear who has been infected and recovered and is therefore immune, given the high prevalence of asymptomatic individuals. Serology assays that detect the presence of anti-SARS-CoV-2 antibodies can be used to help answer these questions.[2]

To detect active infections, the approved SARS-CoV-2 detection methods rely on nucleic acid amplification technologies like PCR and LAMP to detect viral RNA.[3] While these methods are sensitive and specific, they are also expensive and complicated. The Medicare reimbursement cost for the CDC approved RT-qPCR assay is $100 and many labs report that this rate is insufficient.[4] More importantly, nucleic acid methods detect active infections and cannot determine who has been infected previously. Serological assays that detect antibodies are required to determine prior infection status and are traditionally done in laboratory settings using enzyme-linked immunosorbent assays (ELISA) or at the point of care using lateral flow assays (LFAs). These assays can also determine candidates for convalescent plasma donation, an increasingly important treatment strategy.[2] While traditional ELISAs have superior analytical performance, they require expensive equipment and samples must be shipped to a centralized laboratory for testing. The volume of serology tests needed in the US alone for a robust serosurvey of different populations will overwhelm clinical laboratory resources and samples may take days or weeks to

process. Additionally, at ~$60/sample the cost of a test would be a significant financial burden to individuals, insurance companies and/or governments.[5] The World Health Organization has outlined four key target product profiles in the effort to fight the pandemic, and one is a point of care serology assay that takes < 20 min to perform, can be used by an untrained person, and costs < $12.[6] Traditional LFAs meet these requirements, but are lacking the analytical performance needed for such critically important testing.

LFAs use a series of porous membranes to wick sample across a detection zone. Target analyte is captured on a nitrocellulose membrane using a capture agent and is typically labeled with nanoparticles that form a colored line for naked-eye detection.[7] LFAs can be performed in a matter of minutes, require no external instrumentation, cost ~$5 per device, and can be used outside of a centralized laboratory. Several LFAs have been developed to detect SARS-CoV-2 antibodies but results from these devices are not trusted in large scale surveys because of poor clinical sensitivity and specificity.[8] Commercially available LFAs for SARS-CoV-2 serology testing report sensitivities of 80-96% and specificities of 80-99%, which are lower than the desired sensitivities and specificities outlined by the WHO (>95% and >99% respectively).[9-11] Further, in a study comparing six commercial rapid LFAs to an ELISA for COVID-19 serology testing, the ELISA outperformed all six LFAs for clinical sensitivity and specificity.[12] In that study the most sensitive LFA reported a sensitivity of 60% while the ELISA reported 79% sensitivity for the same samples. LFAs will inherently perform more poorly than ELISAs for two reasons: 1) They cannot wash excess reagent and/or sample from the detection zone to mitigate non-specific adsorption, and 2) nanoparticle labels cannot amplify colorimetric signal like enzymatic reporters. Previous attempts to create simplified ELISAs for use at the point-of-need have been successful, but require multiple timed steps,[13, 14] have inefficient washing,[15] are inconsistent because of end-user

intervention, and can take over one hour,[16] limiting their practicality in at-home settings.[13, 17-19] There is a pressing need for a SARS-CoV-2 serology test that is as easy to use as a one-step LFA with the sensitivity and specificity of an ELISA.

This chapter describes a disposable ELISA system (dELISA) that automatically performs sequential washing and reagent addition steps using capillary-driven flow in hydrophilic channels and paper pumps for colorimetric detection of SARS-CoV-2 antibodies. The dELISA uses a recently developed pump-free microfluidic device to achieve automated and sequential sample transport, plasma separation from whole-blood, reagent delivery, and washing steps.[20] Individual steps of the assay are controlled through simple but highly effective valving and flow control structures in a laminate device with capillary-driven channels for fluid transport previously reported by our group.[20, 21] The channel geometry in the laminate device enables programmable flow of sample, washing buffer, and reagents for sequential delivery to a detection zone on a nitrocellulose membrane. These processes are performed with only two end-user steps: sample addition followed by buffer addition. Sequential flow of reagents and washing buffer stands in contrast to an LFA where all steps occur within the sample matrix without washing. The device is made of a combination of PET films, pressure sensitive adhesive, and nitrocellulose. As a result, devices are inexpensive (~$1) and can be made in large quantities. This chapter discusses the flow control methods embedded in the dELISA along with the colorimetric assay that was designed specifically for use in the device. Anti-SARS-CoV-2 IgG nucleocapsid protein (anti-N protein) was detected using the N protein as a capture probe and a horseradish peroxidase secondary antibody (HRP-Ab) as the label. The chromogenic substrate 3,3'-Diaminobenzidine (DAB) was used for colorimetric detection. The performance of the disposable ELISA assay was compared to standard well-plate ELISA and antibodies were detected from whole blood, a common matrix for

serology testing. Although the application of the device in this manuscript is serology testing for Covid-19, the technology will open the possibility of at-home ELISA testing for many more targets.

4.2 Materials and Methods

4.2.1 Device Construction

The fluidic channels in the device are constructed from 3M™ 9962 polyester film, which is 99 µm thick and coated with a proprietary hydrophilic coating on both sides. Four layers of the 9962 film are cut using a CO_2 laser cutter (Epilog, Zing 1000) to form channels for flow. These layers were designed in CorelDRAW X4. 3M™ MP467 double-sided adhesive is used between each piece of 9962 film to bind the film together and to form a gap between the layers. Each piece of double-sided adhesive is 50 µm thick and are patterned with the same CO_2 laser cutter. Three layers of double-sided adhesive are laminated between the layers of 9962 film to create the final device as shown in Figure 4.1. Layers are shown in more detail in Figure A3.1. 3×5 mm^2 glass fiber pads (Millipore Sigma, GXDX203000) were used as conjugate release membranes and the secondary antibody and substrate were dried and stored on these pads. The pads are inserted into the device before the final 9962 film layer is sealed on top. A plasma separation membrane (Vivid GX Membrane, Pall Corporation) was integrated above the main channel between the buffer inlet and the nitrocellulose. Finally, a 3×15 mm^2 nitrocellulose membrane (GE FF120) striped with capture antigen is inserted into the end of the channel and a waste pad made of GE CF4 membrane is placed at the end of the nitrocellulose. To demonstrate sequential delivery and washing in the device tartrazine (yellow dye, 1870 µM) and erioglaucine (blue dye, 800 µM) were used.[21]

4.2.2 Anti-SARS-CoV-2 Assay

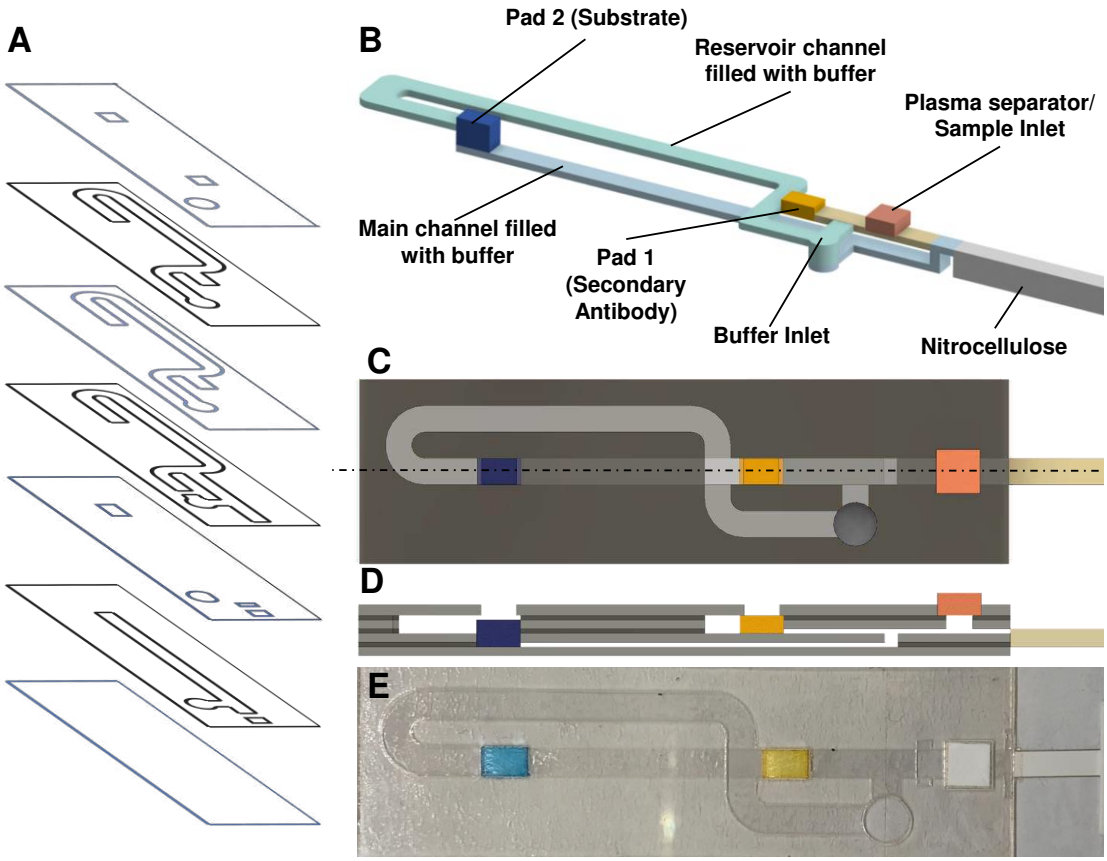

Figure 4.1. A) Designs for each layer of the device. Blue layers are transparency sheets and black layers are double-sided adhesive B) Three-dimensional representation of the channels and reagent pads within the device. C) Top view device schematic. D) Cross-sectional view of device cut along the dashed line in C. E) Top view of a real device.

The anti-SARS-CoV-2 immunoassay used SARS-CoV-2 nucleocapsid protein (N protein AA133-419) as the capture antigen. Recombinant SARS-CoV-2 N protein was produced as previously described.[22] Briefly, a bacteria-codon optimized gBlock was cloned into a pET28a bacterial expression with a C-terminal 6xHis tag. Recombinant protein was expressed in BL21(DE3) pLysS *E. coli* and purified by nickel affinity and size exclusion chromatography in 50 mM HEPES buffer (pH 7.4) and 500mM NaCl throughout purification to reduce aggregation. Protein purity and quality was verified by SDS-PAGE gel electrophoresis. N protein was striped onto the nitrocellulose strip with a reagent dispenser (Claremont Bio). The striping solution contained 45 mM trehalose, 4.5% glycerol, and 0.5 mg/mL N protein. The trehalose and glycerol

were used to improve storage capability. Roughly 120 ng of N protein was added to each 3 mm nitrocellulose strip. The secondary antibody was an anti-mouse-IgG conjugated to horse radish peroxidase (HRP) (Abcam ab97040, Lot no. 3327554). The antibody was diluted to 5 µg/mL in a solution of 0.01 M FeSO4-EDTA, 4% Trehalose, and 0.1% BSA to improve long term storage.[23] Two 5 µL aliquots of the secondary antibody solution (50 ng) were sequentially dried onto a 3x5 glass fiber pad. The colorimetric substrate used was 3,3'-Diaminobenzidine (DAB). Pierce™ DAB Substrate kit from ThermoFisher, which included a 10x solution of DAB and a peroxide buffer, was used for the substrate and washing buffer. 15µL of the 10x DAB solution was added to a 3x5 glass fiber pad in three 5µL aliquots and air dried at 37ºC for 20 min. The peroxide buffer was adjusted to a pH of 6.5 with sodium hydroxide and Tween-80 (Fisher Scientific) was added to a concentration of 0.1%.

To start the assay, 10 µL of sample is added to the Vivid plasma separation membrane (sample pad). The target analyte used was SARS-CoV-2 nucleocapsid antibody (GeneTex Cat. No. GTX632269 Lot No. 43936). The target antibody was diluted in phosphate buffer pH 7.2 or single donor human whole blood (Innovative Research) to concentrations ranging from 0.01 ng/mL to 100 µg/mL. After the sample is added to the sample pad, 75 µL of wash buffer is added to the buffer inlet (Figure 4.1). Once buffer has been added, the waste pad pumps the buffer through the system for ~20 min at which point the nitrocellulose membrane is imaged using a Motorola One smartphone. The color intensity at the test line is quantified using NIH ImageJ. Here, the image of the test line is converted to grayscale and inverted. The grayscale intensity across the test line is divided by the intensity adjacent to the test line to obtain a "gray ratio" for quantification. The ratio is used to reduce any error caused by variation in lighting. Lighting for this project was also stabilized with a 16 LED light box for consistency.[24, 25]

4.2.3 Well-plate ELISA

The analytical performance of the dELISA was compared to a traditional well-plate ELISA using the same capture antigen, target, and secondary antibody. In the well-plate ELISA, polystyrene plates were coated with 50 µL of 0.2 µg/mL N protein overnight on a shaker at 4°C and then blocked with 4% dry non-fat milk powder in 1X PBS and 0.1% Tween-20 at RT. 50 µL of the target antibody solution (GeneTex Cat. No. GTX632269 Lot No. 43936) was incubated in the wells for 1 h at RT on a shaker followed by washing 3X with 0.1%Tween-20 in PBS (200 µL). The secondary antibody is the same used in the dELISA (Abcam ab97040), and 50 µL of 0.1 µg/mL was incubated in each well for 1 h. The wells were washed 3X before addition of the 50 µL 1-step Ultra TMB substrate (Thermo Fisher Scientific, 34028). After 4 min the reaction was quenched with 1 M H_2SO_4 and absorbance readings were taken with a Perkin Elmer Victor X5 plate reader at 450 nm.

3. Results and Discussion

4.3.1 Automated sequential flow design

The dELISA contains laminate flow channels for programmable reagent release and washing that generates sequential flow, a nitrocellulose membrane strip where the sandwich immunoassay is performed, and a waste pad to drive flow (Figure 4.1a). Importantly, the flow channel was designed in a multi-layered format to achieve sequential delivery of the sample, buffer, and reagents to the nitrocellulose membrane after two simple end-user steps. The assay steps are as follows: 1) Sample addition by user; 2) buffer addition by user; 3) sample is washed through nitrocellulose membrane with washing buffer via capillary-driven flow and target is conjugated to proteins on detection zone; 4) rehydrated secondary antibody flows through the nitrocellulose membrane strip and conjugates to captured target 5) wash buffer removes excess

secondary antibody from the nitrocellulose membrane strip; 6) rehydrated substrate flows through the nitrocellulose membrane strip, reacts with enzymatic label and produces a visible-by-eye color change.

The flow channel is divided into two sections: the main channel (lower) and the reservoir channel (upper). The sample and reagent inlets were placed in order of delivery to the detection zone along the main straight channel (Figure 4.1b). The sample is added to the main channel through the plasma separation membrane while the reagents dried in the glass pad are rehydrated with buffer for delivery through the main channel. The timing of the sample and reagent delivery was controlled by adjusting the distance between the nitrocellulose and each reagent inlet. The opening above the glass fiber pads prevents air bubbles from forming in the main channel and helps maintain consistent flow. The reservoir channel, which connects upstream of each reagent pad, supplies the buffer solution to rehydrate reagents and generate flow in the main channel. Although the buffer channels are connected upstream of the glass pads, the buffer inlet is placed downstream of the glass pads so the buffer can fill both the main channel and the reservoir channel upon buffer addition. This channel geometry also makes the device more compact. Since the two reagent channels have different vertical positions, buffer can fill the main channel without being affected by the glass pads (Figure 4.1c). Finally, a burst valve was implemented under the separation membrane, which releases the sample and buffer into the main channel at the same time without air bubbles.[21] The burst valve initiates flow in a channel only after two separate channels meet to ensure proper flow timing.

To visualize these automated sequential steps, food dye was used in place of immunoassay reagents, (Figure 4.2). In addition to the still images in Figure 4.2b, a video showing the flow is included in the supplementary information. Here, blue dye is added to the sample pad, yellow dye

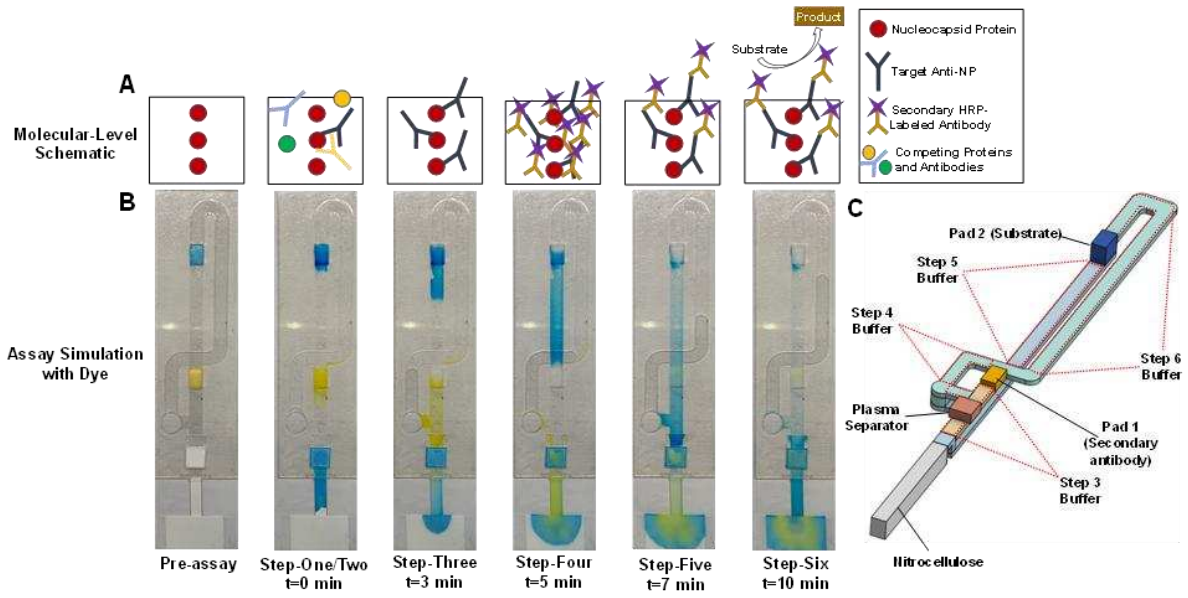

Figure 4.2. A) Molecular level representation of detection zone during different stages of the assay. B) Simulation of assay steps in the device using blue dye to mimic the sample and substrate, and yellow to mimic the secondary antibody. C) Three-dimensional representation of the channels in the device and how the reagents and buffer in the channels are used in different stages of the assay.

is dried on glass pad 1 to simulate the secondary antibody, and blue dye is dried on glass pad 2 to simulate the substrate. After sample and buffer addition (steps 1 and 2) all channels are filled via capillary action, and the sample, secondary antibody, and substrate are connected via buffer. Once the channels are filled, the nitrocellulose strip and waste pad pumps the sample, buffer, and immunoassay reagents through the device. Because the sample is placed at the front of the device it is programmed to pass through the nitrocellulose membrane first and the target is captured on the test line. Next, the buffer between the sample inlet and pad 1 (yellow) will flow through the nitrocellulose membrane and wash away excess sample constituents that might interfere with the remaining assay (step 3). The pressure difference from pad one to the nitrocellulose membrane is larger than that of the difference between the pad two (blue) and the nitrocellulose membrane, so the rehydrated enzyme label from the yellow pad flows through next and any target analyte on the test line will capture the enzyme label (step 4). Once the buffer above pad one is

depleted, the flow from the blue pad to the nitrocellulose begins. The rehydrated substrate stored on pad two will be preceded by a slug of buffer between pads 1 and 2 in the main channel (step 5). Once the buffer has washed away excess label, the substrate reaches the test line and reacts with the enzyme label to produce a visible color change (step 6). After flow stops (~20 min) the color change is detected with the naked eye for qualitative detection, or imaged (smartphone camera) for quantitative information. The volume of buffer used to wash the sample or reagents through the nitrocellulose membrane can be controlled by changing the length of channels for any given assay. In the current device design, the total volume of washing buffer was 75 µL and the assay takes 20 min to run.

4.3.2 Anti-SARS-CoV-2 Assay Optimization

Once sequential reagent delivery and washing steps were confirmed, an immunoassay for anti-SARS-CoV-2 antibodies was performed using the dELISA device. Separate glass fiber pads were used to store the secondary antibody and substrate. A drying buffer (section 2.2) was used to dilute the secondary antibody to improve storage capabilities.[23] The assay parameters mentioned in section 2.2 were optimized, and the key results for washing buffer pH, capture antigen concentration, secondary antibody concentration, and DAB concentration are shown in Figure 4.3 with a blue star indicating the conditions chosen for the final assay. One of the struggles of running a sandwich immunoassay in the dELISA vs. a well-plate ELISA is that assay conditions must be constant instead of optimized for each individual sample addition or washing step. For example, a commercial peroxide buffer was used as the washing buffer to improve the activity of HRP with DAB, but the buffer was adjusted from a pH of 5.5 to 6.5 for the final assay. While changing from 5.5 to 6.5 decreased the HRP activity, it improved the antibody-antigen binding, which had a larger

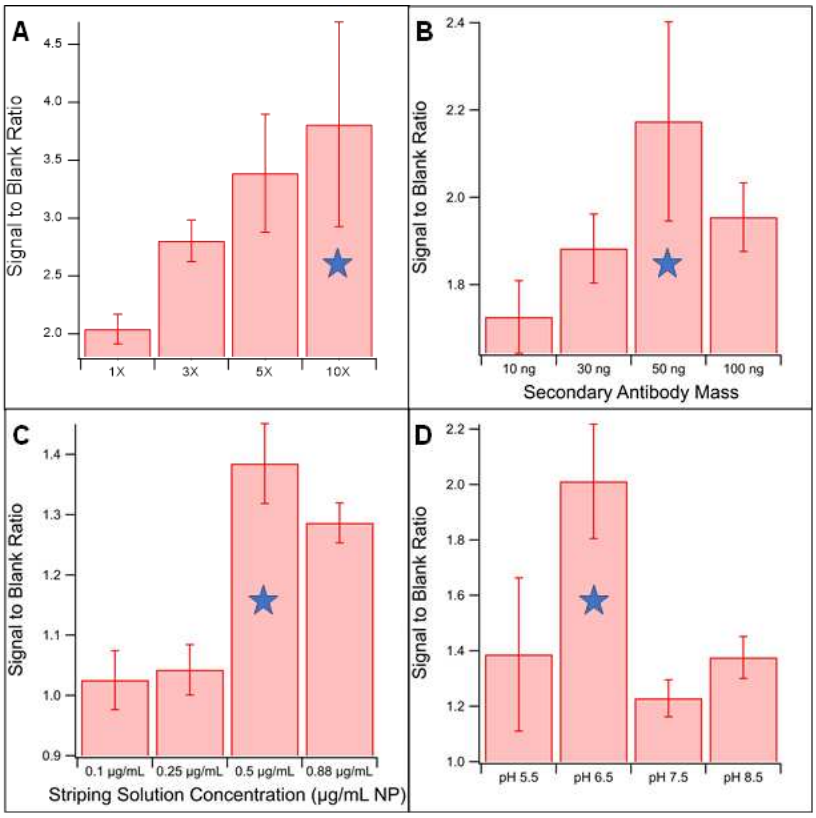

Figure 4.3. Optimization results for (A) Commercial DAB solution concentration dried on pad 2; (B) mass of secondary antibody dried on pad 1; (C) concentration of striping solution; (D) pH of washing buffer. Star represents the condition used for final assay

impact on assay sensitivity. 1 µg/mL target antibody was used during the optimization experiments as that concentration falls within the linear range of the assay.

4.3.3 Assay from Whole-Blood

Whole blood was used as the sample matrix because plasma from whole blood is the most common matrix for serology testing. In an at-home setting blood could be obtained with a lancet to prick a finger and draw a drop of blood, similar to diabetic glucose testing. To ensure that red blood cells do not interfere with the colorimetric readout on the nitrocellulose membrane, they must be removed using a plasma separation membrane. In the dELISA device, the membrane is integrated just upstream of the nitrocellulose membrane (Fig. 4.1). After adding 10 µL of sample to the plasma separation membrane, red blood cells are captured in the membrane and plasma

flows into the device and through the nitrocellulose. Video S2 in the supplementary information captures this process along with the rest of the assay. A dose-response curve was generated using blood spiked with anti-N protein antibody (Figure 4.4a). The data was fit to a four-parameter logistic curve as is common for sandwich immunoassays (Equation S1).[26] The detection limit using the dELISA in blood was 2.8 ng/mL, which is sensitive enough to detect anti-N protein IgG

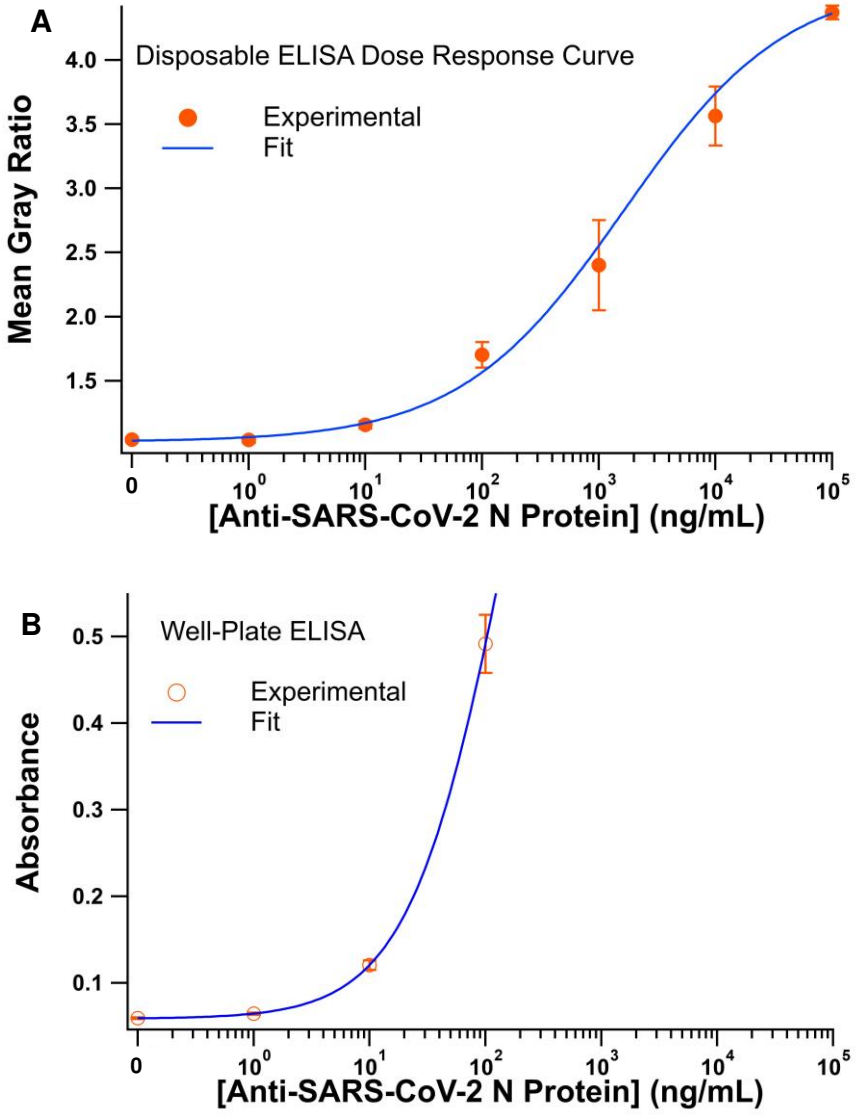

Figure 4.4. A) Dose-response curve of anti-N protein spiked into whole human blood using the dELISA. B) Dose-response curve of anti-N protein obtained with a well-plate ELISA. The data for both curves was fit to a 4-parameter logistic curve

from clinical samples (>10 µg/mL).[27] The detection limit was calculated using Eq S2. Future studies will focus on using the dELISA with real patient samples to establish a clinical sensitivity and specificity for the device.

In upcoming clinical studies, the results will be validated with a well-plate ELISA, so in this work results were also compared to a well-plate ELISA using the same antigen and secondary antibody. The results for the well-plate ELISA are shown in Figure 4.4b. The well-plate ELISA dose-response curve was once again fit with a 4-parameter logistic curve and a detection limit of 1.2 ng/mL was calculated. The detection limit of the dELISA (2.8 ng/mL) is roughly the same as the detection limit in the dELISA (1.2 ng/mL). These results exceeded expectations for the dELISA considering that a well-plate ELISA uses absorbance values from a plate reader, while our device quantifies results using images from a smartphone. The advantages of the dELISA over a traditional well-plate assay include faster assay time (2.5 h versus 20 min), decreased end-user steps (13 vs 2), increased portability, decreased cost, and increased ease of use. Hands-on time and preparation time are also significantly less in the dELISA than the well-plate ELISA. Most importantly, the dELISA is a true at-home test that can be run outside of a centralized laboratory by an untrained end-user. These advantages are common for POC assays but are typically offset by sacrificing analytical performance. This is not the case for the dELISA, which has the sensitivity of a well-plate ELISA and is as easy to use as an LFA.

The question of whether the dELISA could be used to detect Anti-SARS-CoV-2 antibodies from real blood or nasopharyngeal samples is yet to be answered, but the detection limits presented here are promising as well-plate ELISAs have been used to detect actual SARS-CoV-2 antibodies types at higher concentrations.[27] Well-plate ELISAs and even LFAs have detected lower concentrations of antibodies previously, but we believe the limiting factor in the current dELISA

setup is the capture antigen and secondary antibody and their specificity toward the particular commercial Anti-NP used. To improve results further a thorough screening of suitable secondary antibody for clinical anti-NP similar to the work presented by Cate et al. would need to be conducted.[28] Additionally, the drying procedure for the secondary antibody could be improved through lyophilization, and increasing the sample volume would increase sensitivity, but also increase assay time.

4.4 Conclusion and Future Directions.

This chapter describes a system that enables ELISA-level performance in a disposable and easy-to-use device. The dELISA was used to detected anti-SARS-CoV-2 antibodies from whole blood with a detection limit of 2.8 ng/mL, which is nearly the same as a traditional well-plate ELISA (1.2 ng/mL). The dELISA can achieve such sensitive results with a colorimetric read-out because an enzyme label is used to amplify the signal and sequential washing and reagent addition steps are performed automatically after sample and buffer addition. Qualitative detection can be performed with the naked eye, or a smartphone can be used to capture quantitative information. Future iterations of the device will use electrochemical sensing as a more quantitative alternative to colorimetric detection. Amid the current pandemic, next steps will focus on improving the assay for more robust serology testing that includes IgM, IgA and IgG antibodies, and simplifying use by integrating a housing and blister pouches for buffer storage. We will also design an assay for soluble nucleocapsid protein from nasal swabs so an active infection can be identified as well as a previous infection. Eventually, we envision this technology will be used in resource-limited settings to detect analytes such as influenza, malaria, or other viral proteins, biomarkers for chronic

illness such as heart failure or cancer, and/or other antibodies at levels that were previously undetectable outside a centralized laboratory.

Publication Disclosure: This chapter was published in *ChemRXIV*. I am the co-first author with Dr. Ilhoon Jang. All experiments were conducted by myself or one of the other listed authors.

REFERENCES

1. COVID-19 Dashboard. John's Hopkins University Center for Systems Science and Engineering (CSSE): 2020.

2. Shen, C.; Wang, Z.; Zhao, F.; Yang, Y.; Li, J.; Yuan, J.; Wang, F.; Li, D.; Yang, M.; Xing, L., Treatment of 5 critically ill patients with COVID-19 with convalescent plasma. *Jama* **2020,** *323* (16), 1582-1589.

3. CDC Diagnostic Tests for COVID-19. https://www.cdc.gov/coronavirus/2019-ncov/lab/testing.html (accessed 27 July, 2020).

4. CMS Increases Medicare Payment for High-Production Coronavirus Lab Tests. https://www.cms.gov/newsroom/press-releases/cms-increases-medicare-payment-high-production-coronavirus-lab-tests-0#:~:text=Medicare%20will%20pay%20laboratories%20for,the%20spread%20of%20COVID%2D19. (accessed 28 July, 2020).

5. Dalvie, M. A.; Sinanovic, E.; London, L.; Cairncross, E.; Solomon, A.; Adam, H., Cost analysis of ELISA, solid-phase extraction, and solid-phase microextraction for the monitoring of pesticides in water. *Environ Res* **2005,** *98* (1), 143-50.

6. COVID-19 Target product profiles for priority diagnostics to support response to the COVID-19 pandemic v.0.1. Organization, W. H., Ed. 2020.

7. Posthuma-Trumpie, G. A.; Korf, J.; van Amerongen, A., Lateral flow (immuno) assay: its strengths, weaknesses, opportunities and threats. A literature survey. *Anal. Bioanal. Chem.* **2009,** *393* (2), 569-582.

8. Krammer, F.; Simon, V., Serology assays to manage COVID-19. *Science* **2020,** *368* (6495), 1060-1061.

9. Li, Z.; Yi, Y.; Luo, X.; Xiong, N.; Liu, Y.; Li, S.; Sun, R.; Wang, Y.; Hu, B.; Chen, W., Development and clinical application of a rapid IgM-IgG combined antibody test for SARS-CoV-2 infection diagnosis. *Journal of medical virology* **2020**.

10. Lou, B.; Li, T.-D.; Zheng, S.-F.; Su, Y.-Y.; Li, Z.-Y.; Liu, W.; Yu, F.; Ge, S.-X.; Zou, Q.-D.; Yuan, Q., Serology characteristics of SARS-CoV-2 infection since exposure and post symptom onset. *European Respiratory Journal* **2020**.

11. Lassaunière, R.; Frische, A.; Harboe, Z. B.; Nielsen, A. C.; Fomsgaard, A.; Krogfelt, K. A.; Jørgensen, C. S., Evaluation of nine commercial SARS-CoV-2 immunoassays. *Medrxiv* **2020**.

12. Ong, D. S. Y.; de Man, S. J.; Lindeboom, F. A.; Koeleman, J. G. M., Comparison of diagnostic accuracies of rapid serological tests and ELISA to molecular diagnostics in patients with suspected coronavirus disease 2019 presenting to the hospital. *Clin Microbiol Infect* **2020,** *26* (8), 1094.e7-1094.e10.

13. Carrell, C. S.; Wydallis, R. M.; Bontha, M.; Boehle, K. E.; Beveridge, J. R.; Geiss, B. J.; Henry, C. S., Rotary manifold for automating a paper-based Salmonella immunoassay. *RSC Adv.* **2019,** *9* (50), 29078-29086.

14. Verma, M. S.; Tsaloglou, M.-N.; Sisley, T.; Christodouleas, D.; Chen, A.; Milette, J.; Whitesides, G. M., Sliding-strip microfluidic device enables ELISA on paper. *Biosensors and Bioelectronics* **2018,** *99*, 77-84.

15. Apilux, A.; Ukita, Y.; Chikae, M.; Chailapakul, O.; Takamura, Y., Development of automated paper-based devices for sequential multistep sandwich enzyme-linked immunosorbent assays using inkjet printing. *Lab Chip* **2013,** *13* (1), 126-135.

16. Fridley, G. E.; Le, H.; Yager, P., Highly sensitive immunoassay based on controlled rehydration of patterned reagents in a 2-dimensional paper network. *Analytical chemistry* **2014,** *86* (13), 6447-6453.

17. Jeong, S.-G.; Kim, J.; Jin, S. H.; Park, K.-S.; Lee, C.-S., Flow control in paper-based microfluidic device for automatic multistep assays: A focused minireview. *Korean Journal of Chemical Engineering* **2016,** *33* (10), 2761-2770.

18. Preechakasedkit, P.; Siangproh, W.; Khongchareonporn, N.; Ngamrojanavanich, N.; Chailapakul, O., Development of an automated wax-printed paper-based lateral flow device for alpha-fetoprotein enzyme-linked immunosorbent assay. *Biosensors and Bioelectronics* **2018,** *102*, 27-32.

19. Yakoh, A.; Chaiyo, S.; Siangproh, W.; Chailapakul, O., 3D Capillary-Driven Paper-Based Sequential Microfluidic Device for Electrochemical Sensing Applications. *ACS Sensors* **2019,** *4* (5), 1211-1221.

20. Jang, I.; Carrão, D. B.; Menger, R. F.; Moraes de Oliveira, A. R.; Henry, C. S., Pump-Free Microfluidic Rapid Mixer Combined with a Paper-Based Channel. *ACS Sensors* **2020,** *5* (7), 2230-2238.

21. Ilhoon, J.; David S., D.; Brian J., G.; Charles, H.; Hyunwoong, K.; Simon, S., *Flow Control in a Laminate Capillary-Driven Microfluidic Device*. 2020.

22. Fagre, A.; Lewis, J.; Eckley, M.; Zhan, S.; Rocha, S. M.; Sexton, N. R.; Burke, B.; Geiss, B.; Peersen, O.; Kading, R.; Rovnak, J.; Ebel, G. D.; Tjalkens, R. B.; Aboellail, T.; Schountz, T., SARS-CoV-2 infection, neuropathogenesis and transmission among deer mice: Implications for reverse zoonosis to New World rodents. *bioRxiv* **2020**, 2020.08.07.241810.

23. Ramachandran, S.; Fu, E.; Lutz, B.; Yager, P., Long-term dry storage of an enzyme-based reagent system for ELISA in point-of-care devices. *Analyst* **2014,** *139* (6), 1456-1462.

24. Henry, C. S.; Feeny, R.; Franklin, A. B.; Carrell, C., Rotary manifold for paper-based immunoassays. Google Patents: 2020.

25. Boehle, K. E.; Doan, E.; Henry, S.; Beveridge, J. R.; Pallickara, Sangmi L.; Henry, C. S., Single board computing system for automated colorimetric analysis on low-cost analytical devices. *Analytical Methods* **2018,** *10* (44), 5282-5290.

26. Christopoulos, T. K.; Diamandis, E. P., Theory of immunoassays. *Immunoassay* **1996**, 25-50.

27. Ma, H.; Zeng, W.; He, H.; Zhao, D.; Yang, Y.; Jiang, D.; Zhou, P.; Qi, Y.; He, W.; Zhao, C.; Yi, R.; Wang, X.; Wang, B.; Xu, Y.; Yang, Y.; Kombe Kombe, A. J.; Ding, C.; Xie, J.; Gao, Y.; Cheng, L.; Li, Y.; Ma, X.; Jin, T., COVID-19 diagnosis and study of serum SARS-CoV-2 specific IgA, IgM and IgG by chemiluminescence immunoanalysis. *medRxiv* **2020**, 2020.04.17.20064907.

28. David, C.; Helen, H.; Veronika, G.; Joshua D, B.; H Gleda, H.; Brianda, B.-L.; Ben D, G.; Caitlin E, A.; Ethan, S.; Samantha, K.; Ryan, G.; Rafael, R.; Crissa, B.; Sam A, B.; John T, C.; Puneet K, D.; David, S. B.; Bernhard H, W.; Kevin P, N., *Antibody Screening Results for Anti-Nucleocapsid Antibodies Towards the Development of a SARS-CoV-2 Nucleocapsid Protein Antigen Detecting Lateral Flow Assay*. 2020.

29. Carrell, C.; Jang, I.; Link, J.; Terry, J.; Scherman, M.; Call, Z.; Panraksa, Y.; Dandy, D. S.; Geiss, B. J.; Henry, C., Point-of-Need Disposable ELISA System for COVID-19 Serology Testing. **2020**.

CHAPTER 5. CONCLUSIONS AND FUTURE DIRECTIONS

There is an urgent need to develop and deploy sensors for pathogen detection at the point-of-need. The Coronavirus pandemic of 2020 has re-emphasized the importance of pathogen diagnostics in developed nations, but low- and middle-income countries have been disproportionately impacted infectious diseases for decades. Lack of access to high-quality diagnostics is a major contributor to the disparity between nations regarding the burden of infectious disease. Building the infrastructure required for advanced diagnostics in low- and middle-income countries is not financially feasible, so the diagnostics themselves must be designed to function in resource limited settings. Ideal assays meet the ASSURED criteria outlined by the WHO. These assays are **A**ffordable, **S**ensitive, **S**pecific, **U**ser-friendly, **R**apid and Robust, **E**quipment-free, and **D**eliverable to end users. Traditional and paper-based microfluidics have emerged as technologies that could potentially meet the WHO criteria, but have not made the transition from the laboratory to the market. Lack of commercialization stems from multiple problems, but some include insufficient sensitivity and specificity, poor usability, and difficult manufacturing.

The reports in this thesis discuss microfluidic devices that were designed to improve sensitivity and specificity, simplify assays for the end-user, and create a more time and cost-effective manufacturing method. First, a method for designing and creating traditional microfluidics from open-faced 3D-printed pieces was presented. Here, microfluidic channels were printed with an open-faced design and the 3D printed pieces were subsequently bound to a secondary PDMS substrate to create enclosed channels. Importantly, a commercially available and affordable 3D printer and resin were used to print all pieces. The fabrication method accomplished

two goals, both of which simplified the fabrication process over traditional microfluidics. First, complex stereolithography was replaced with 3D-printing to decrease the number of steps, time and cost needed to create a finished product. Second, because the channels were not printed as enclosed channels, no resin uncured resin was trapped, and resin removal was vastly simplified. Future studies regarding this project should investigate methods to modify the channels after printing and before sealing. The ability to modify channels before sealing is a major advantage of printing open-faced channels versus enclosed channels that was not attempted in the initial study. Specifically, modifying the channels with electrodes for electrochemical sensing would be of significant interest to the field of 3D-printed microfluidics. We envision this method will be used to increase access to microfluidic research in laboratories with limited resources to potentially improve the use of microfluidics as point-of-need diagnostic tools.

The second project discussed in this thesis involves a pump-free paper-based microfluidic device as an alternative to traditional microfluidics, which require pumps to drive flow. Microfluidic paper-based analytical devices μPADs have garnered significant research interest in the years since their introduction in 2007, and their history, applications, advantages, and disadvantages were thoroughly discussed in Chapter One. The most cited disadvantage for μPADs is their poor sensitivity. Efforts to address sensitivity in μPADs have worked but are offset by a decrease in ease-of-use. Chapter Three offers a solution that improves the sensitivity of a *Salmonella* assay through immunomagnetic separation and enzyme labeling while simplifying the end-user steps using a 3D-printed rotational housing. While the device was only used to detect *Salmonella*, it could be used to detect many other targets requiring immunomagnetic concentration from complex samples, or to simply run an enzyme linked immunosorbent assay (ELISA) if magnetic separation is not necessary.

The logical next step for the rotational manifold is to attempt multiplexed detection of different bacteria species. However, multiplexing would require manipulation of the magnetic beads in the paper flow channels. One negative of μPADs is that they cannot transport large particles like bacteria or magnetic beads because the particles become trapped in the paper fibers. Instead, we hypothesized that a hybrid device with hydrophilic channels made of polyester transparency film and double-sided adhesive, and paper pads for reagent storage, could be used to transport beads and accomplish multiplexed bacteria detection after immunomagnetic separation. Here, electrochemical detection was also chosen rather than colorimetric to improve sensitivity. Further details and preliminary data for the multiplexed bacteria detection project can be found in Appendix 4. Although this technology is not completely developed or characterized, the initial data discussed in Appendix 4 shows promise for highly sensitive bacteria detection. Once the initial multiplexed project is completed, the biggest issue that should be considered moving forward is ease-of-use. To simplify the initial steps of the assay, I anticipate that magnetophoretic separation will be incorporated upstream of the detection zones using another transparency-based device that is currently under development in our laboratory.

Finally, Chapter Four reports on a disposable ELISA (dELISA) system used to detect SARS-CoV-2 antibodies. The device uses a combination of polyester transparency film, double-sided adhesive, nitrocellulose, and glass fiber membrane to form hydrophilic channels that automatically perform sequential reagent delivery and washing steps. In this way an ELISA can be performed with only two end-user steps: sample addition followed by buffer addition. The dELISA enables ELISA level sensitivity in a device that is as easy to use as a lateral flow assay. Due to the success of the SARS-CoV-2 serology assay in the dELISA we will continue to use the dELISA system to explore the detection of other relevant biomolecules sensitivity greater than

what μPADs or lateral flow assays can provide is needed. Future studies outlining possible new targets for the dELISA, including a SARS-CoV-2 viral antigen assay that is currently under development, can be found in Appendix 5. Although rapid and inexpensive SARS-CoV-2 testing is currently the most urgent need in the world of diagnostics, the dELISA could be used to detect many more targets. The novelty of the dELISA is that with one or two end-user steps, an assay with ELISA-level sensitivity can be run outside of a centralized laboratory, so detection of targets that were previously impossible to detect with typical point-of-care devices will be possible in remote settings. Therefore, I expect much of the future research with dELISA will involve optimizing assays for new analytes like protein biomarkers, micro-RNA, or bacteria and viruses. To expand the reach of the dELISA further, I also expect next steps will include changes in the device configuration for handling of multiple sample types like saliva and urine.

I am fascinated by technology that can accomplish sophisticated and sensitive analysis with limited resources and untrained users. Useful devices require thoughtful and elegant designs from an engineering and chemistry perspective, and those that combine ease of use with high analytical performance have tremendous potential to improve access to high quality healthcare for billions of people. In the future I am interested in continuing to work on medical diagnostics. Of specific interest are assays that screen for biomarkers of non-infectious diseases like heart-failure, stroke, or cancer. Appendix 6 proposes a microfluidic assay to detect micro RNA to screen for lung cancer. The proposed assay is a shift from the work that I have done at CSU as it requires a power source and precise volume is not designed for use in all environments. Instead it is tailored for a clinic or doctor's office for rapid and inexpensive screening.

This thesis is a collection of published and unpublished works that have helped advance the field of low-cost analysis at the point-of-need. The most glaring issue with current point-of-

need analysis is the inability to achieve the necessary analytical performance for a given application. Efforts to improve metrics like sensitivity and specificity have worked, but almost always come at the cost of user-friendliness, portability, or price. This pattern is especially visible in the field of paper-based microfluidics, which our laboratory is intimately involved with. My Ph.D. was spent attempting to improve the analytical performance of μPADs without sacrificing the other qualities necessary for point-of-need analysis.

The major theme of my thesis is that multiple sensing technologies and device types must be combined to develop point-of-need devices that are sufficiently sensitive and specific, but also portable, inexpensive, and easy-to-use. Whether this means using a rotational housing to achieve immunomagnetic separation in a μPAD; combining paper for reagent storage, channels made of transparency film for particle transport, and electrochemical sensing using thermoplastic electrodes; or stacked transparency film channels embedded with glass fiber pads and nitrocellulose for automating immunoassay steps. The fields of μPADs, traditional microfluidics, 3D-printing, and immunoassays are too segregated. The most successful academic projects I have been involved with have all been collaborations with engineers, biologists, computer scientists, and chemists. The same sort of collaboration must occur with the technology that we use to solve the problems facing the field of point-of-need analysis. I believe that my work as a Ph.D. student has demonstrated the potential of this strategy and am hopeful that it will have a lasting impact on the field moving forward.

APPENDIX ONE: SUPPLEMENTARY INFORMATION - SEALING 3D-PRINTED PARTS TO POLY(DIMETHYLSILOXANE) FOR SIMPLE FABRICATION OF MICROFLUIDIC DEVICES

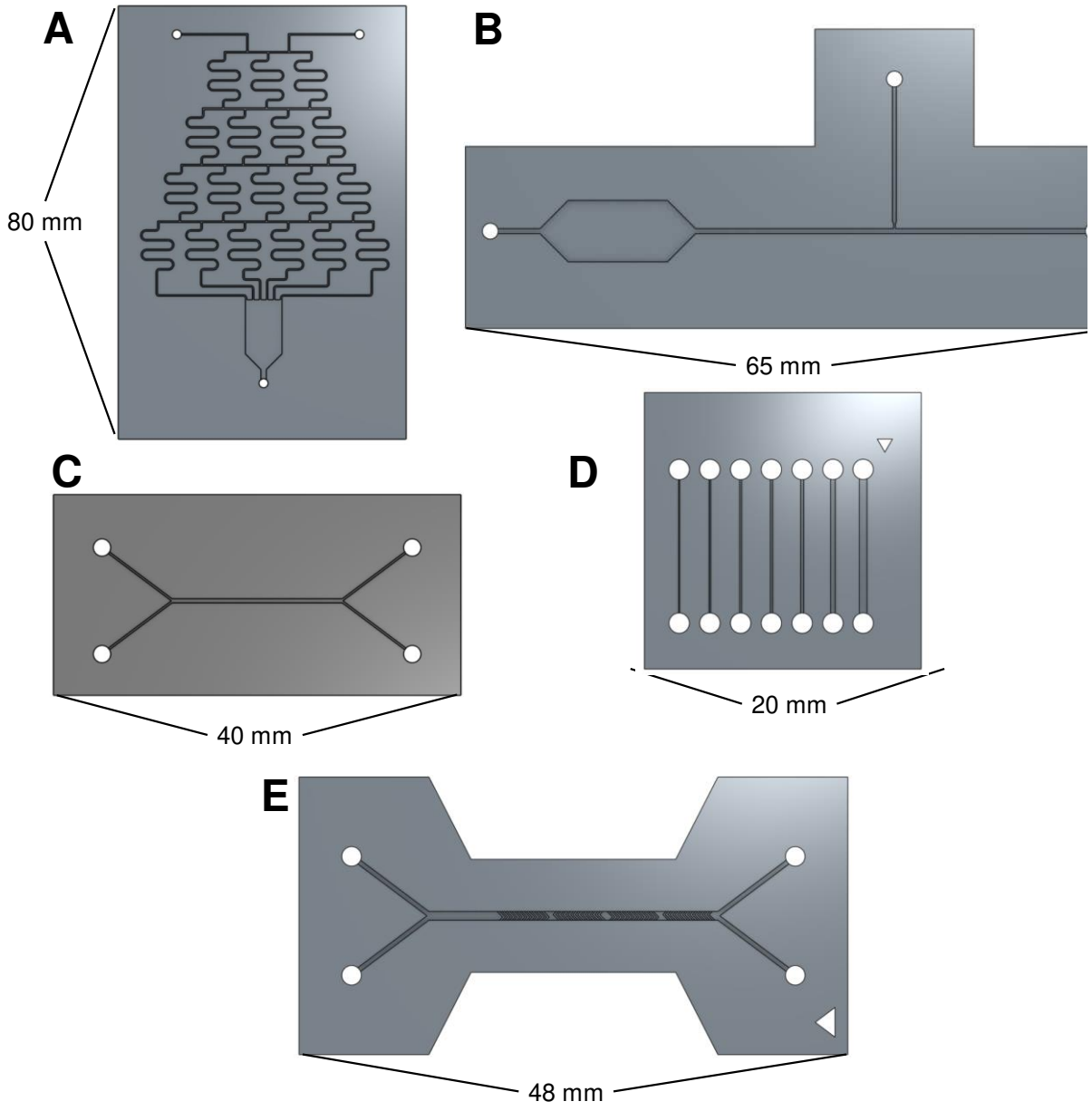

Figure A1.1. CAD renderings of all open-faced 3DPPs used to create microfluidic devices in this manuscript. Gradient generator (A), droplet generator (B), H-cell device (C), Seal and channel dimension testing device (D), Herringbone mixer (E).

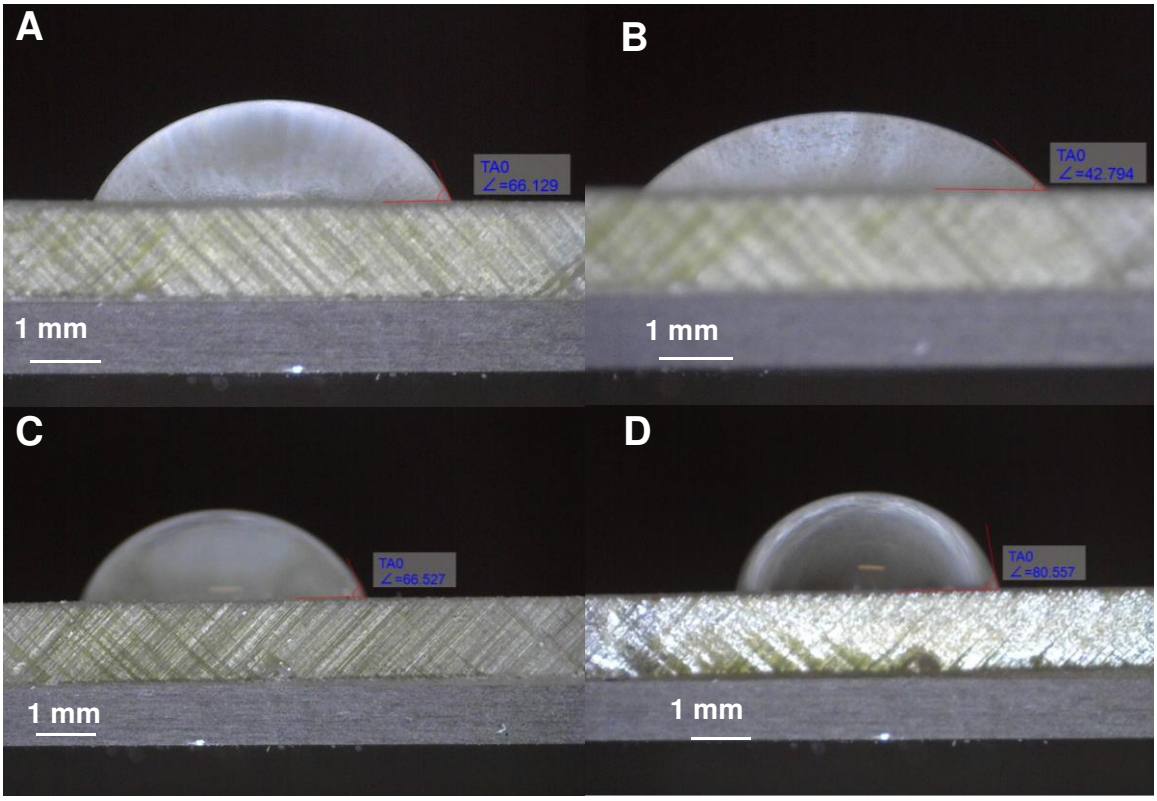

	Before	After
APTES	**66°**	**43°**
Silicone Spray	**67°**	**81°**

Figure A1.2. 20 µL of DI water was pipetted onto the surface of a 3DPP before modification with APTES and Silicone spray. Before modification with APTES the 3DPP had a contact angle of 66° (A). After modifying with APTES, the 3DPP had a contact angle of 43° (B). Before modification with silicone spray the 3DPP had a contact angle of 67° (C). After modifying with silicone spray, the 3DPP had a contact angle of 81° (D)

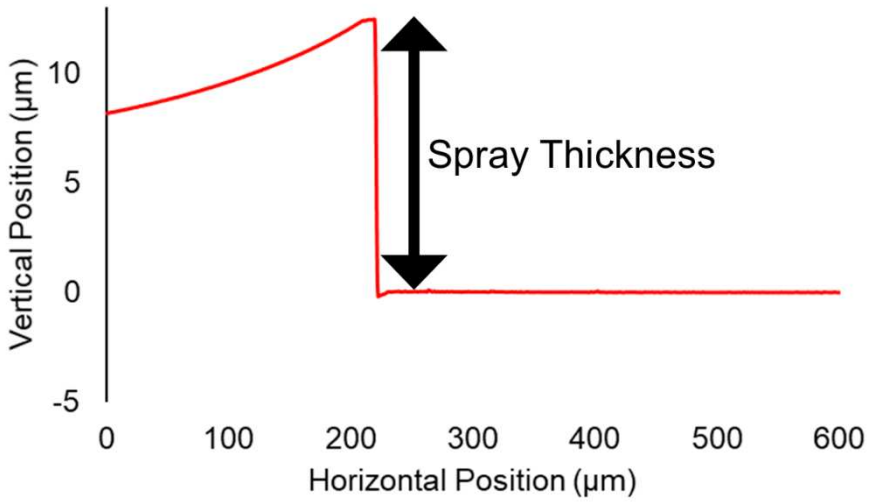

Device Number	1	2	3	4	5	**Average**
Spray thickness	8.7	5.9	1.1	4.4	12.5	**6.5±4.3**

Figure A1.3. Silicone spray thickness of five different devices sprayed at five different times. Each device was a glass slide partially covered with a piece of scotch tape. After spraying, the tape was removed and the ledge formed at the tape-spray interface was measured with an optical profilometer. The figure shows a representative optical profilometer profile and the table shows the data for all devices tested

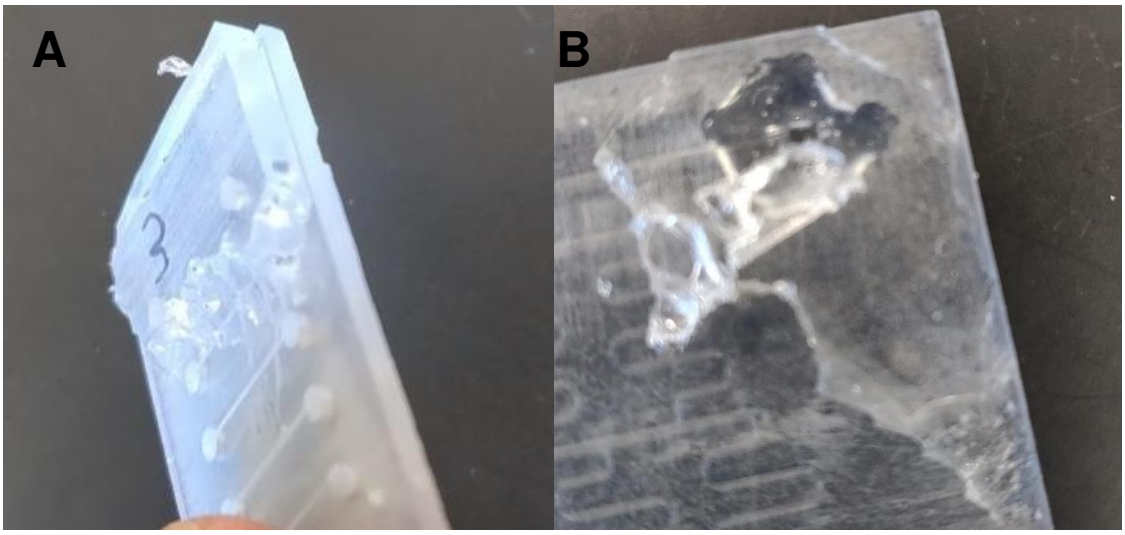

Figure A1.4. Images of PDMS bound to a 3DPP after spray sealing (A) and APTES-sealing (B). Both seals shown here were considered 'Strong' seals because the PDMS ripped while trying to peel the PDMS from the 3DPP. In many cases it was impossible to completely remove the PDMS from the 3DPP without the aid of a scraping tool.

Table A1.1. Channel heights and depths before and after spraying with Si Spray (n=6).

Channel	**1**	**2**	**3**	**4**	**5**
Designed Width/Depth	500/200	300/200	200/200	150/200	125/200
Before spray	626.0 ± 71.7/ 179.6 ± 11.8	321.4 ± 41.2/ 111.9 ± 13.6	294.8 ± 16.4/ 51.6 ± 5.3	238.7 ± 18.2/ 26.6 ± 6.1	146.2 ± 19.1/ 15.9 ± 4.6
After Spray	636.9 ± 70.3/ 149.1 ± 10.0	411.3 ± 43.6/ 71.2 ± 6.2	324.9 ± 53.6/ 27.0± 1.7	271.0 ± 45.3/ 10.7 ± 1.7	230.0 ± 30.0/ 6.9 ± 2.3
Difference	10.9 ± 100.4 /-30.5 ± 15.4	89.0 ± 60.0/ -40.7 ± 15.0	120.1 ± 56.1/ -24.6 ± 5.6	32.3 ± 48.8/ -15.9 ± 6.4	83.8 ± 35.6/ -9.0 ± 5.1
% Difference	2%/-17%	28%/-36%	59%/-48%	14%/-60%	57%/-57%

Table A1.2. Channel heights and depths before and after spraying modifying with APTES (n=6).

Channel	1	2	3	4	5
Designed Width/Depth	500/200	300/200	200/200	150/200	125/200
Before spray	597.5 ± 22/ 198.5 ± 7.4	400.4 ± 8.1/ 173.4 ± 2.2	292.8 ± 9.4/ 116.2 ± 1.2	230.3 ± 4.9/ 76.0 ± 5.4	204 ± 8.7/ 42.8 ± 1.3
After Spray	601.5 ± 16.5/ 195.8 ± 1.9	388.5 ± 11.1/ 173.8 ± 0.5	301.3 ± 18.5/ 123.4 ± 3.5	241.3 ± 23.4/ 77 ± 1.4	205.3 ± 22.9/ 37.0 ± 4.1
Difference	5.8 ± 27.5/ -2.7 ± 7.6	-11.8 ± 13.7/ 0.3 ± 2.2	8.5 ± 20.7/ 7.2 ± 3.7	10.9 ± 23.9/ 1.0 ± 5.6	1.3 ± 24.5/- 5.8 ± 4.3
% Difference	2%/-1%	-3%/-0.2%	3%/6%	5%/-1%	1%/-14%

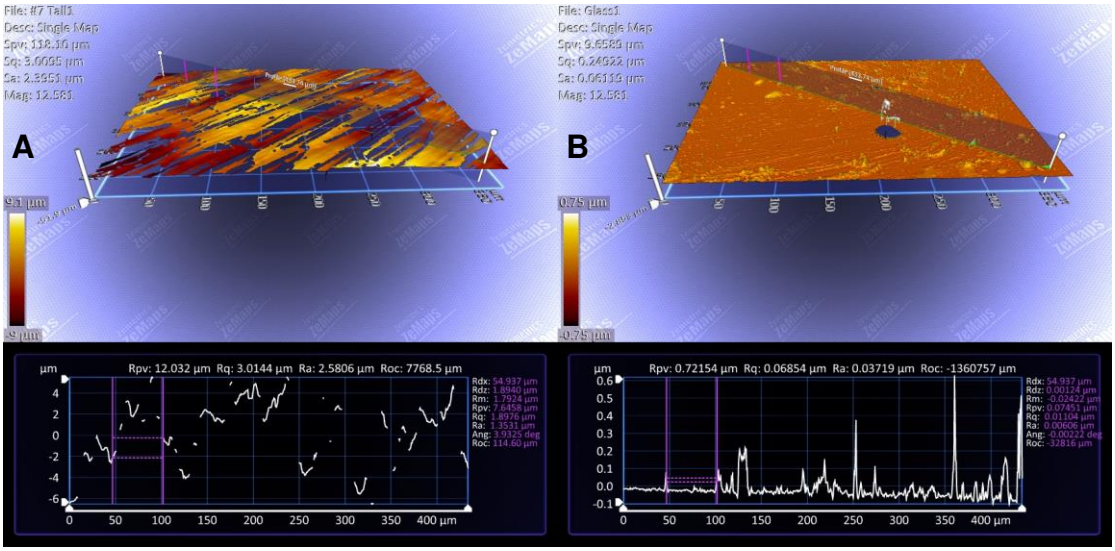

Figure A1.5. Profilometer maps of a 3DPP (A) and a glass slide (B). Distinct ridges are visible on the 3DPP from the 3D-printing process. The surface roughness of the 3DPP is therefore much larger than for a glass slide or PMMA.

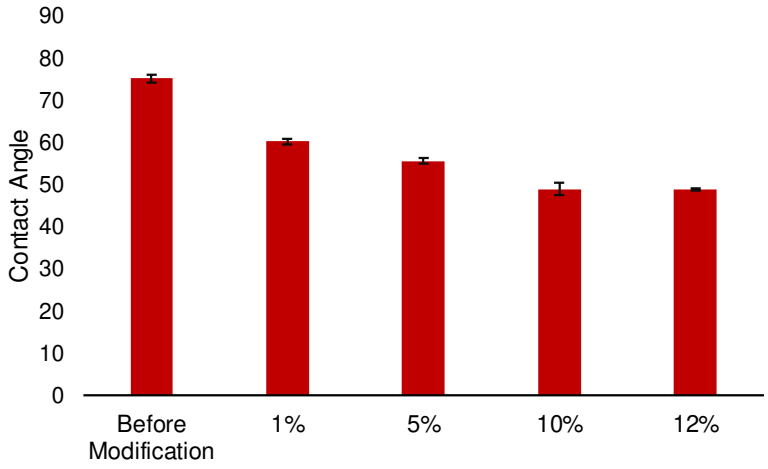

Figure A1.6. Contact angle of 3DPPs treated with different concentrations of APTES. Past 10% APTES, increasing the concentration did not impact the contact angle, so 10% was chose as the optimal APTES concentration

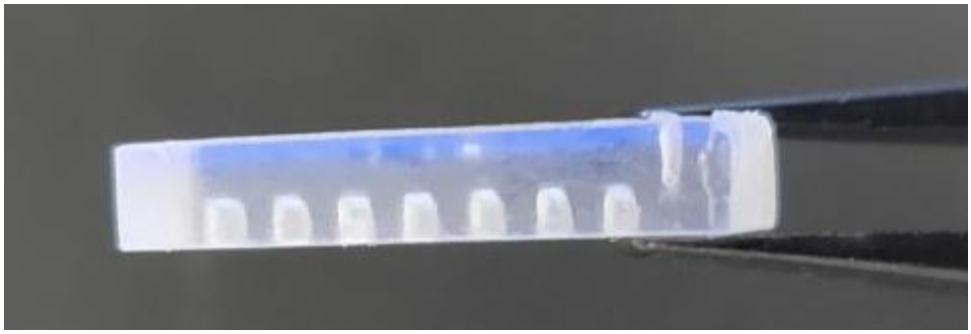

Figure A1.7. Cross sectional view of a 3DPP printed with enclosed channels. The 6mm holes leading into the channels can be seen, but the channels themselves are all clogged with cured resin. The 3DPP was cut in half with a laser cutter and no channels are observable. The specified channel dimensions are shown in Figure 3 and Tables S1 and S2

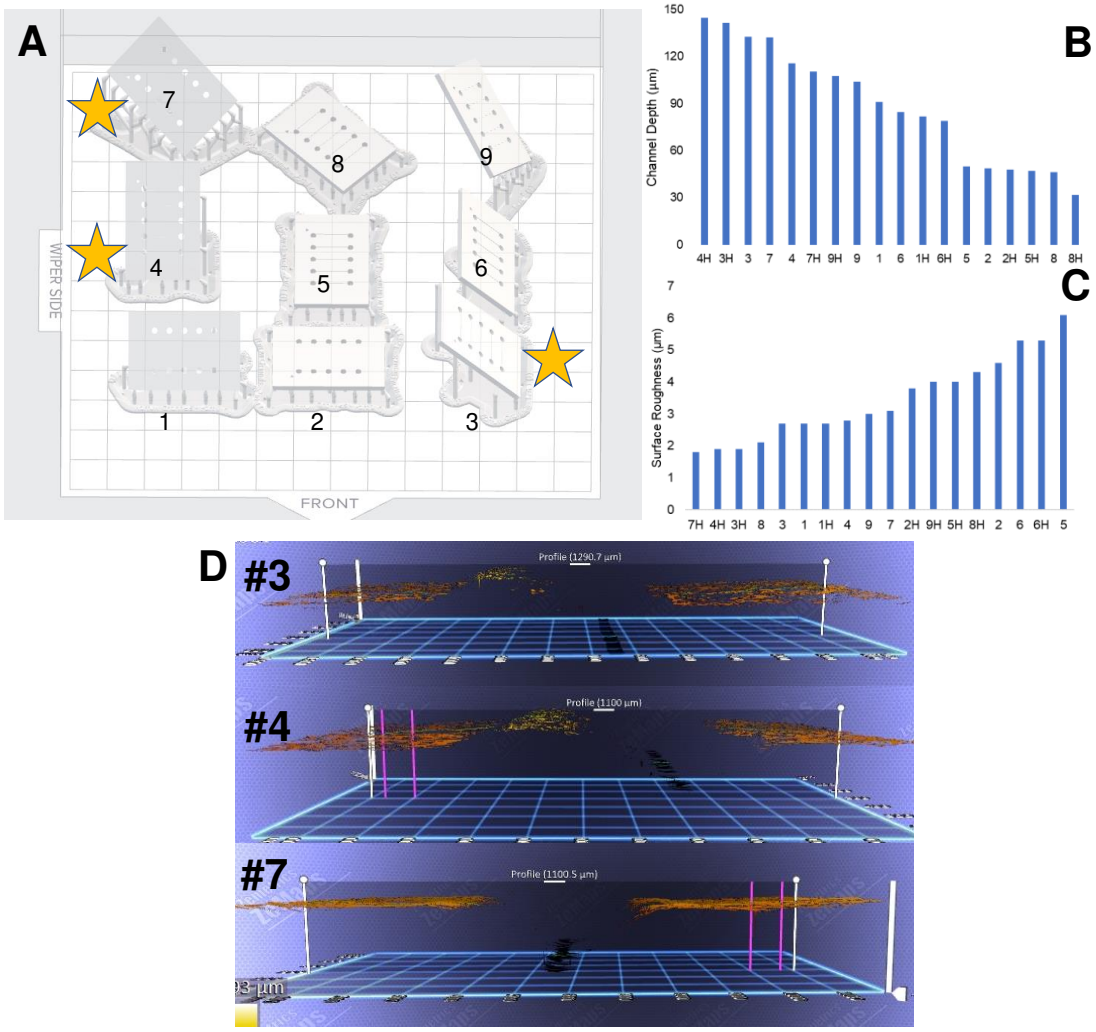

Figure A1.8. Layout of the 9 different orientations on the 3D printer (A). Channel depth determined by optical profilometry (B). 150 µm was the printed theoretical depth, therefore, the higher values are preferred. The H after certain numbers denotes high resolution (25 µm z-height) vs standard resolution (50µm Z-height). Surface roughness determined by optical profilometry, where lower values are preferred (C). Optical profilometer maps of channels for orientations 3, 4, and 7 (D). Number 7 has a channel depth close to the theoretical value, a low surface roughness value, and does not have a peak next to its channel.

APPENDIX TWO: SUPPLEMENTARY INFORMATION - ROTARY MANIFOLD FOR AUTOMATING A PAPER-BASED *SALMONELLA* IMMMUNOASSAY

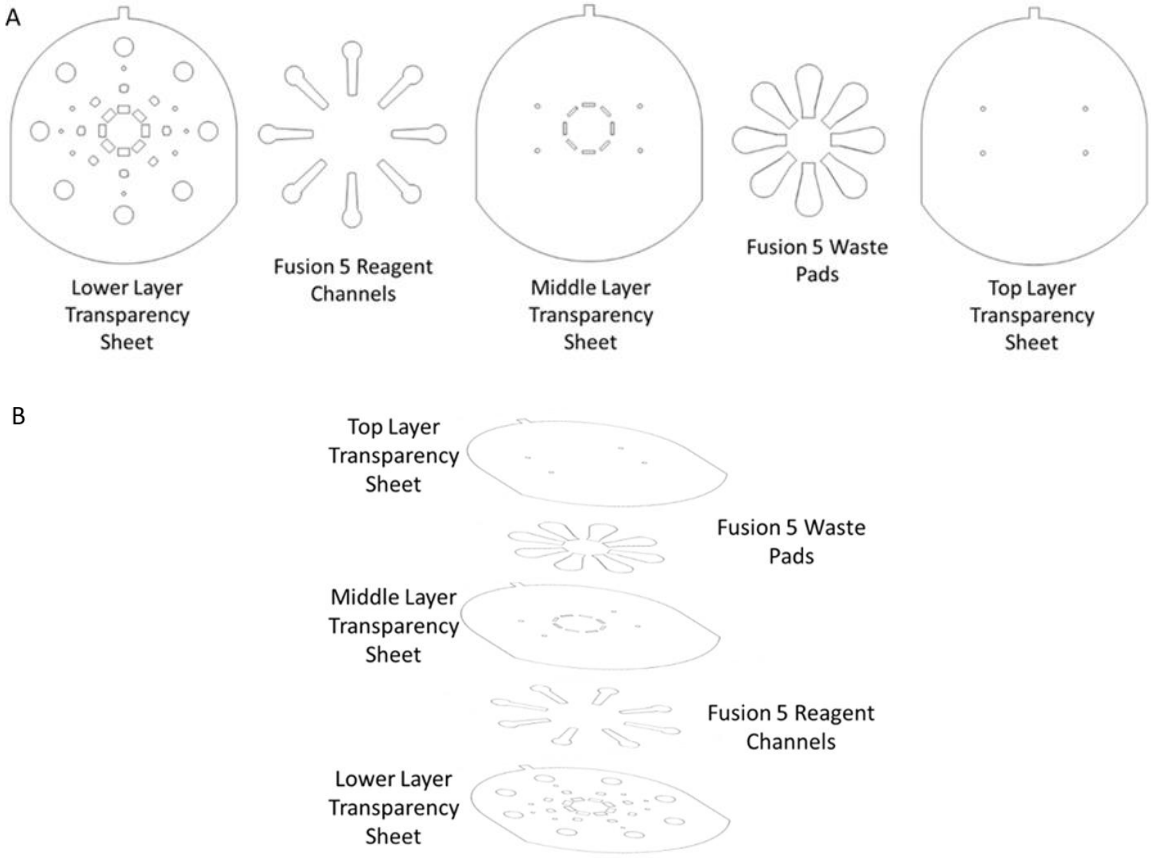

Figure A2.1: Designs for the different layers of transparency and paper pieces that make up the reagent card (A) and their stacking orientation before lamination (B). The lower transparency sheet is coated with a hydrophobic coating called NeverWet from Rust-Oleum.

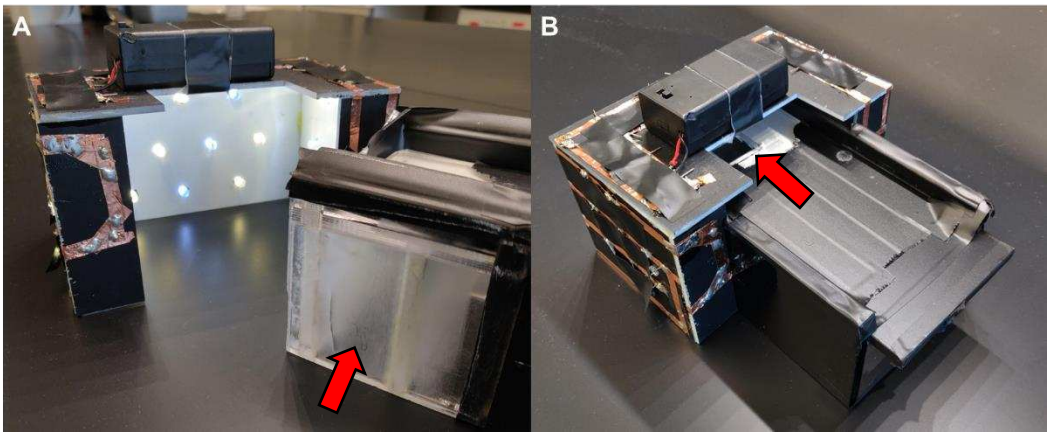

Figure A2.2. Light box opened to show lighting inside. Red arrow highlighting area where sample layer sits (A). Light box put together - red arrow highlighting the hole used to take a picture with a smartphone (B).

Video 1: In the included video three food coloring dyes are dried on different reagent layers. When the device is assembled, the buffer washes the dye from the reagent layer, through the sample layer and into the waste pad. The video shows the food coloring washing into the waste pad. The order of colors is Yellow, green, and purple and the video is sped up 8x. The nut that is placed on the device was used to hold the sample layer insert in place. Further iterations of the device did not require the nut, but the new devices made it more difficult to visualize the flow of food coloring into the waste pad. The video also shows how different sized waste pads could be incorporated into the device to increase or decrease the volume of washing buffer.

Image processing algorithm: The image processing employs a standard flood-fill algorithm available in the OpenCV computer vision library (see citation #45 in main paper). Flood-fill is an example of a region segmentation algorithm. As used here, flood-fill finds a single contiguous region of pixels grown out from a seed pixel known to be in our sample. This is typically the center pixel in the image. Flood-fill starts with the seed and then recursively adds adjacent pixels

to the region until no similar adjacent pixels are left to include. Because there is a distinct border around the color sample, at which the addition of pixels stops, the resulting region nicely contains the pixels from the sample and does not include extraneous pixels of the border or from elsewhere in the image. The precise settings used for flood-fill are captured in the following example of our call to the OpenCV algorithm:

```
cv2.floodFill(image, mask, seed, (255, 0, 0), (4,4,4), (4,4,4), floodflags)
```

The above line of the floodFill function call takes the following inputs:

1. RGB image of the sample layer.
2. Mask is a pixel padding added to the four sides of the image.
3. Seed represents the starting point of the floodfill algorithm.
4. The fourth parameter represents the color by which the flood-filled region needs to be repainted.
5. The next two parameters represent the lower and upper color difference between the current pixel and its neighboring pixel. As we are dealing with RGB space, so we have 3 values representing threshold for each of the color space.
6. The final parameter defines the connectivity value that is the number of pixels to be considered around the current pixel.

The blue masked region in Figure A2.3 shows the region of a sample layer that was analyzed with the flood-fill algorithm. The automated flood-fill algorithm was compared to the analysis performed with NIH ImageJ (Fig. A2.3). When plotted against each other, the manual and automated analysis are nearly identical with a slope of 0.986±0.014 and an r^2 of 0.9996. In addition to reducing manual labor, the automated analysis can discard pixels that are inconsistent with neighboring pixels due to glare, increasing analysis accuracy.

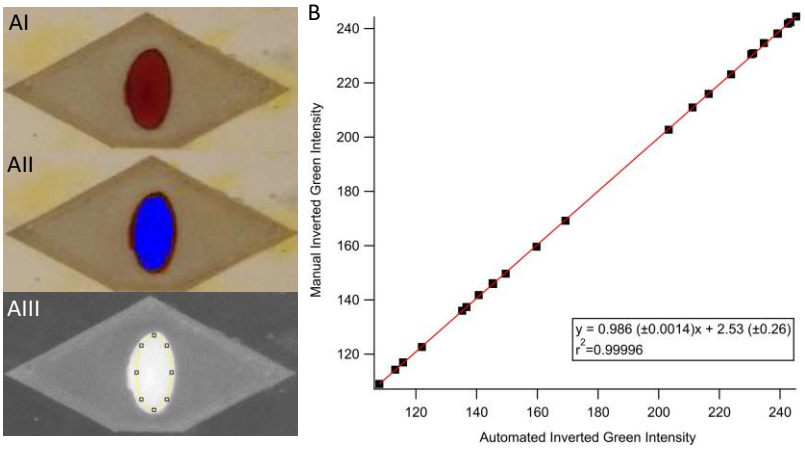

Figure A2.3. Original image (AI), area of original image analyzed by flood fill algorithm (AII), Manual analysis of one -color channel. Inverted green intensity found using a manual analysis vs the inverted green intensity found with the automated algorithm.

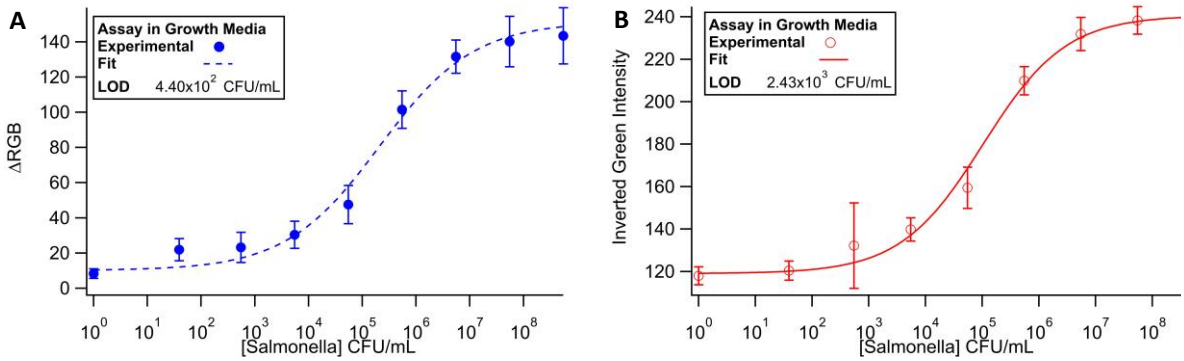

Figure A2.4. Dose response curves created using ΔRGB (A) and inverted green (B).

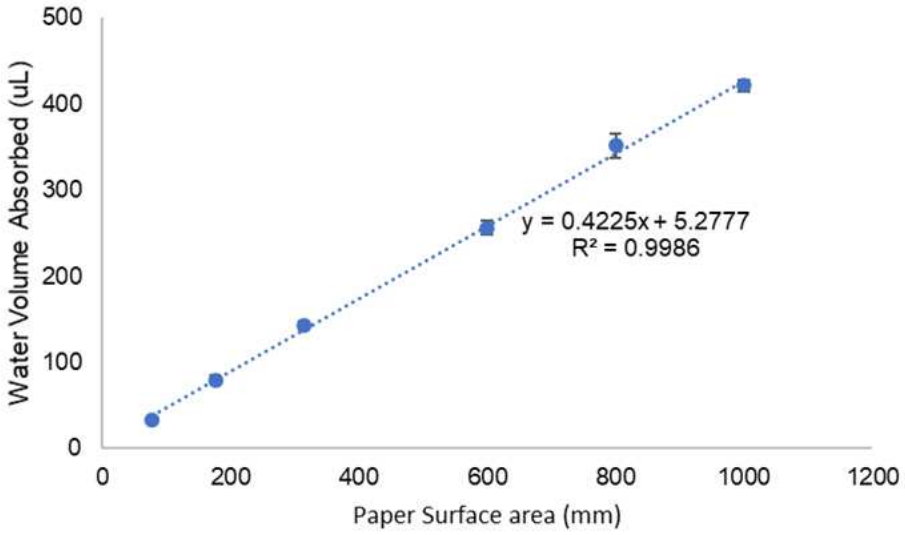

Figure A2.5. Buffer volume/mm^2 absorbed by Fusion 5

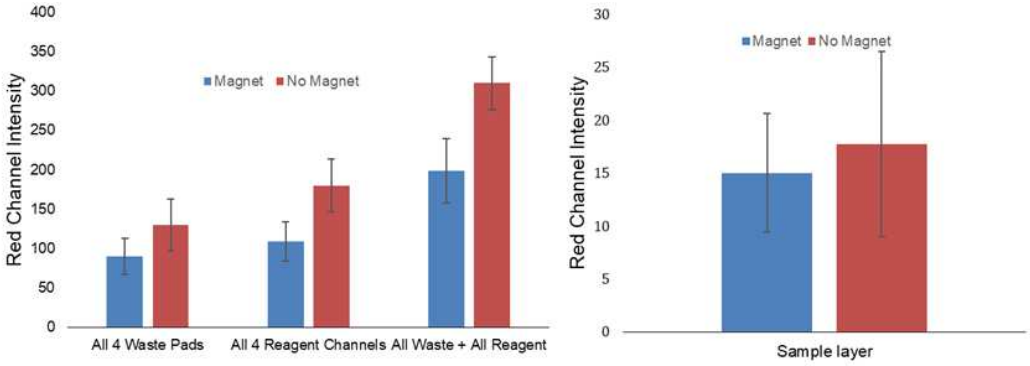

Figure A2.6. Magnetic bead retention with and without a magnet. A) Fluorescent intensity of sample layer before and after 4 washes in the device. B) Summed fluorescent intensities of the reagent layer and waste pads used for washing.

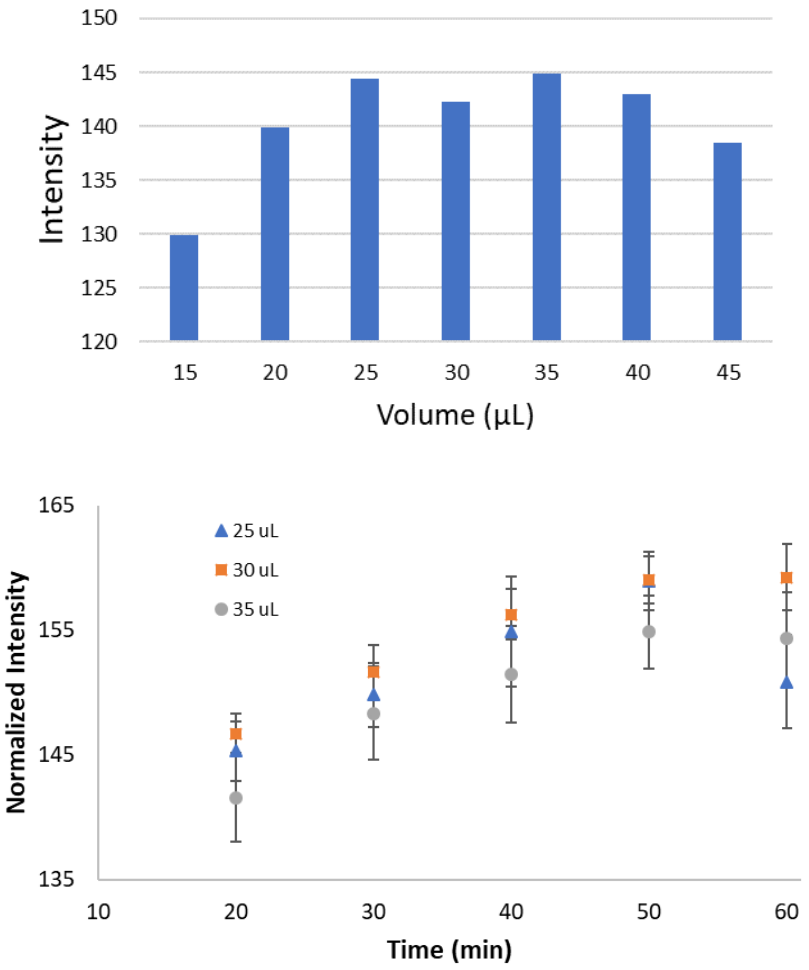

Figure A2.7. CPRG volume (a) and time(b) optimization. CPRG concentration was 2.5 mM and 0.2 µg of Streptavidin β-galactosidase was reacted on each sample layer. The volume of CPRG and reaction time were varied.

Table A2.1

	Ambient Light	Light Box
Image 1: Fluorescent light	111.1	126.2
Image 2: Traditional bulb	163.1	126.1
Image 3: Direct sunlight	158.2	133.5
Average	144.1	128.5
SD	28.7	4.2
%RSD	**19.9%**	**3.3%**

Inverted green intensity of the same sample layer in multiple ambient light environments inside and outside the light box

$$\boldsymbol{Signal = d + \frac{a - d}{1 + \left(\frac{T}{c}\right)^{b}}}$$

Equation A3.1: Signal is the intensity of the colored sample layer, T is the target (Salmonella) concentration, and a – d are the 4 parameters defining the shape of the curve. The parameter a is the expected signal at T=0, b is the slope of the line at the center/steepest part of the curve, c is the target concentration at the center of the curve, and d is the maximum signal, i.e. when T is infinitely high. The coefficients assigned to the curve in Figure 3.5 are:

a=10.12 ± 2.7; b=0.496 ± 0.116; c=2.10 ± 1.45 $\times 10^5$ ± 0.001; d=151.42 ± 14.1

The coefficients from the curve in figure 3.6 are:

a=10.413 ± 8.46; b=0.32644 ± 0.138; c=3.4086e+005 ± 5.4e+005 d=173.04 ± 37.2

APPENDIX 3: SUPPLEMENTARY INFORMATION – POINT-OF-NEED DISPOSABLE ELISA SYSTEM FOR COVID-19 SEROLOGY TESTING

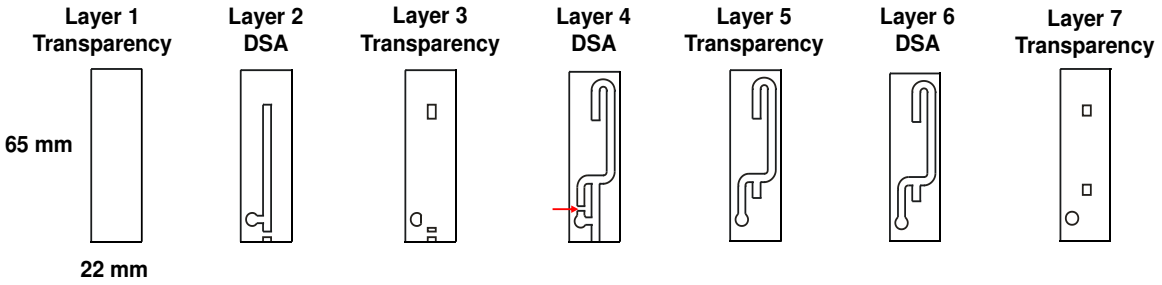

Figure A3.1. Design of each layer of the dELISA. Layers are currently assembled by hand with the aid of a cold-press laminator. During assembly, the marked section on layer 4 of DSA is cut out to complete the connection in the channel. The DSA material that is cut is included initially to hold all layers together.

Equation A3.1. 4-Parameter Logistic model used to fit the data from the dose-response curve. Y is the signal, x is the target concentration, a is the expected response (Y) at x=0, b is the slope of the curve at point c, which is the target concentration that corresponding to Y=(a+d)/2, and d is the expected response when the target concentration is infinitely high (Assuming no hook effect).

$$Y = d + \frac{a - d}{1 + \left(\frac{x}{c}\right)^{b}}$$

Equation A3.2. The equation used to calculate the detection limit from the 4-parameter logistic fit. Parameters a, b, c, and d are defined in Equation S1 above. SD_b is the standard deviation of the blank and R_b is the response or signal of the blank.

$$LOD = c \times \left(\left(\frac{(a - d)}{(3 \cdot SD_b + R_b) - d} \right) - 1 \right)^{\frac{1}{b}}$$

APPENDIX 4: SIMULTANEOUS ELECTROCHEMICAL DETECTION OF *E.COLI, SALMONELLA,* AND *LISTERIA* WITH A TRANSPARENCY AND PAPER-BASED ANALYTICAL DEVICE

Introduction

Bacterial infections pose a significant risk to global health, and as antimicrobial resistance continues to grow the threat will expand even further.[1] The World Health Organization estimates that by 2050, death bacterial infections will become the number one cause of death worldwide.[2] A limiting factor in preventing large bacteria outbreaks is the cost and time required to detect specific bacteria from complex samples, and the WHO specifically recommends improved diagnostic testing as a means to combat the threat of antimicrobial resistant bacteria.[3] Ideally, samples would be tested with a rapid and easy-to-use screening platform for analysis at the point-of-need. Rapid screening techniques enable informed decisions on how to treat an infected individual or contaminated product more quickly, which can slow or stop the spread of disease. Traditionally, culture-based methods are used to grow and identify bacteria. Although well-established, sensitive, and selective, culturing can take days to complete and requires a centralized laboratory and trained end users.[4-6] Alternative testing methods include polymerase chain reaction, enzyme-linked immunosorbent assays (ELISA), loop-mediated isothermal assays, and lateral flow immunoassays.[4] Unfortunately, these techniques all come with their own disadvantages, such as cost, power and temperature requirements, lack of sensitivity, and complexity, which limits their use outside of a centralized laboratory.[7-9] Microfluidic paper based analytical devices (μPADs) are a promising technology that have been studied intensely since they were introduced in 2008.[10] μPADs offer several advantages including pump-free fluid manipulation, reagent storage

capabilities, low-cost, disposability, ease of use, and the ability to integrate with electrochemical sensors.[11-13]

However, paper also has multiple disadvantages as a testing platform, especially when considering bacteria assays. One disadvantage is the inability to handle complex matrices. Sample characteristics such as pH, viscosity, color, opacity, and interfering biological components all impact assay performance dramatically in μPADs.[12] A common method used to isolate bacteria from complex matrices is immunomagnetic separation (IMS). Here, bacteria are captured by magnetic particles modified with antibodies or other recognition elements.[14, 15] Once captured, the bead-bacteria complex is removed from the sample solution with an external magnet and re-constituted in a clean buffer with ideal properties for testing. Importantly, IMS also concentrates bacteria for more sensitive detection limits and increases capture efficiency over probes immobilized on 2-dimensional surfaces.[16] IMS has been used in conjunction with μPADs multiple times.[17-20] In these reports a single bacteria strain was captured with magnetic beads and labeled with enzymes before adding the complex to a paper detection zone with a dried substrate for colorimetric detection. These bead-based ELISA assays work well for one analyte, but struggle when multiplexed detection is required.

Multiplexed bead-based assays typically use beads with unique characteristics (size, emission, etc.) and measure analyte capture using a bulky and expensive flow cytometer.[21] Multiplexed bacteria detection in μPADs has been accomplished by lysing bacteria and detecting intracellular components like proteins or DNA, but lysis adds a minimum of one extra step after IMS and often lacks specificity.[20] In this work three bacteria species from the same sample will be labeled with different enzymes instead of lysing cells or using flow cytometry to distinguish between species. To do so, labeled bacteria separated via IMS must be delivered to different

detection zones where substrates specific to each enzyme label are stored. In traditional μPADs manipulation of bacteria-bead complexes to different zones is not possible. Although bacteria are smaller than the average pore size in many μPADs (~1 μm vs >10 μm respectively), the bacteria-bead complexes are retained in paper fibers as solutions wick multiple centimeters through paper channels.[22]

To combat this fundamental problem of μPADs we designed a hybrid-μPAD (HμPAD) made of transparency sheets, double-sided adhesive (DSA), acrylic, and paper detection zones. Hollow channels between the transparency sheets and acrylic are created with walls of DSA to define the gap height and passively wick solutions along the channels without a pump. Large particles like bacteria-bead complexes can move through these channels without being retained as they would in traditional μPADs. The ability to manipulate these large particles through channels enables multiplexed detection at different detection zones. The HμPAD in this work is integrated with carbon composite electrodes for multiplexed electrochemical detection of *Salmonella, E. Coli, and Listeria,* which are the three most harmful foodborne pathogens.[23] After IMS each bacteria species will be labeled with a different enzyme and added to the HμPAD. The labeled complexes are transported along channels to a detection zone made of paper with immobilized substrate and buffering reagents specific to the given enzyme. Each labeling enzyme has a different optimal pH, and the design of the HμPAD enables enzymatic detection at the appropriate conditions with the correct substrate. Electrochemical detection was chosen to increase sensitivity, but the technique described here could be used for colorimetric detection as well. We believe that HμPADs have the same advantages as traditional μPADs and can solve inherent problems that have plagued the field for years, like the ability to transport large particles.

Experimental Design

Device Design: The device in this work incorporates thermoplastic electrodes (TPEs) developed by our laboratory.[24, 25] The electrodes are made from inexpensive graphite and poly(methyl methacrylate) (PMMA). The fabrication process for these electrodes has been described previously.[25] Briefly, PMMA is dissolved in methylene chloride and mixed with graphite at a 2:1 graphite:PMMA ratio. Once mixed, the solvent is slowly evaporated until the mixture is a paste that has a gum-like texture and can be handled without sticking to gloves. At that point, the paste is hand-pressed into an electrode template cut from a sheet of ¼" PMMA using a laser cutter. The paste is dried under 1000 PSI at 160ºC for two hours. Excess electrode material is sanded off the top of the PMMA until the individual electrodes are separated from one another. Using this method, many electrodes can be created in one day that outperform commercially available screen-printed electrodes.[25] Unlike screen printed electrodes, TPEs can be re-used after simply sanding

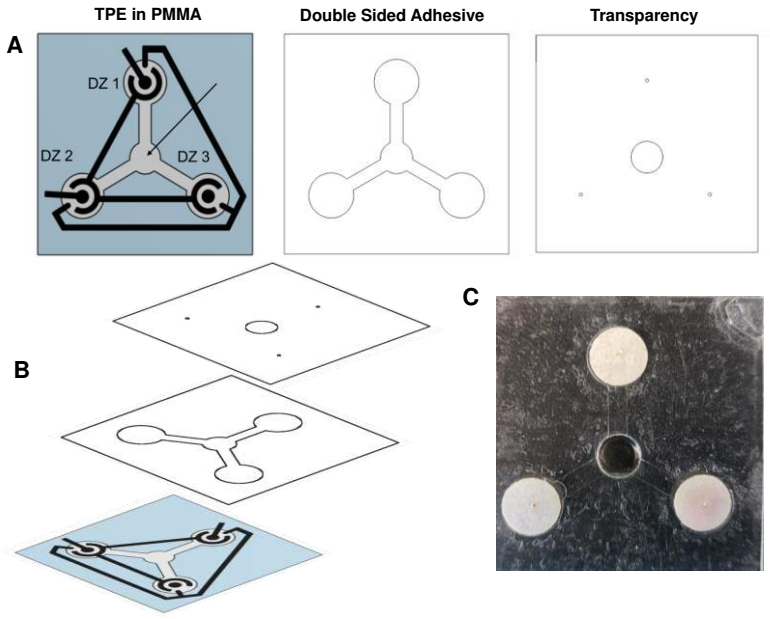

Figure A4.1. Three layers used to construct the multiplexed electrochemical device (A). Orientation of the three layers needed to make enclosed channels (B). Image of the full device with paper pads integrated above the electrodes for substrate storage.

the surface with fine-grit sandpaper (>600 grit). This is especially important for detection of biological analytes where electrode fouling is common.

Here, a three-electrode design will be used to detect bacteria at three different detection zones (Figure A4.1). Above each electrode will be a Whatman 4 paper pad that contains a substrate specific to the enzyme label for a particular bacteria. After immunomagnetic separation and enzyme labeling, the bacteria-bead mixture will be added to an inlet with three channels leading to each electrode. The channels are made from transparency sheets (3M PP2500) and double sided adhesive (3M MP467). The transparency sheet forms the top of the channel and the PMMA that is part of the TPE template forms the bottom of the channel. The channel height is set by the thickness of the double-sided adhesive, which is 50 μm. Small holes in the transparency above the electrodes allow for air to escape from the channels and enable flow.

Assay Parameters: The sandwich ELISA scheme used for each bacteria is shown in Figure A4.2. *E.Coli* will be labeled with alkaline phosphatase and the substrate para-aminophenyl phosphate (PAPP) will be used for electrochemical detection. *Salmonella* will be labeled with β-galactosidase and the substrate para-aminophenol- β-D-galactopyranoside (PAPG) will be used for electrochemical detection. The enzyme label and substrate for *Lysteria* are still being decided. Both PAPP and PAPG will produce para-aminophenol (PAP) after reacting with their specific enzyme. PAP is electrochemically active and can be oxidized at roughly +150 mV. Because each bacteria will be labeled with a different enzyme, the optimal pH at each detection zone is different. For example, β-galactosidase has a maximum reactivity at pH 6.8, while alkaline phosphatase is most active at pH 9.5. Therefore, in addition to storing the substrate for each label in the paper pads a buffering agent must also be dried and stored.

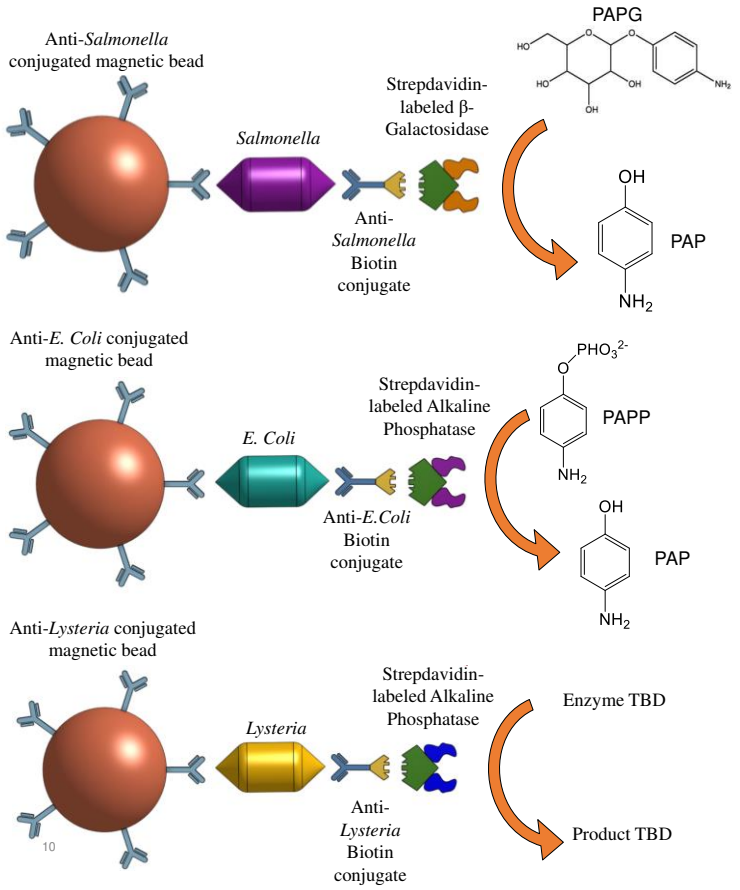

Figure A4.2. Detection scheme for *Salmonella, E. Coli, and Lysteria* using an electrochemical immunomagnetic separation enzyme linked immunosorbent assay

The wide pH range for the enzyme labels (6.8-9.5) necessitated the use of Bis-Tris-Propane as a buffer for the entire system. Bis-tris-propane has a useful pH range from 6.3 to 9.5, which covers the optimal pH values for β-galactosidase and Alkaline phosphatase. However, as we will only be using one sample, the pH of the buffer needs to be adjusted at each electrode. To adjust the pH at each electrode, small volumes of NaOH or H_3PO_4 are dried onto the paper pad along with the substrate. The specific amount of NaOH or H_3PO_4 on each pad is still being optimized. 5 µL of substrate at 2.5 mM is added and dried on each pad as well.

A total of 30 µL of the bead-bacteria solution is added to the inlet. Roughly 5 µL fills each detection zone and channel. Bead-bacteria complexes are transported to each detection zone

through the channel and the reaction between the enzyme label and substrate begins as soon as the substrate is wetted in the detection zone. Over time, solution evaporates from the small hole above the detection zone, which wicks additional bead-bacteria solution towards the electrodes. After 20 minutes a square wave voltammogram will be take at each electrode to detect the PAP produced during the enzymatic reaction. Samples containing bacteria will result in a peak at +150 mV.

Preliminary Data and Future Directions

The ability to perform electrochemical bacteria detection after immunomagnetic separation and enzymatic labeling was confirmed with *Salmonella* and β-galactosidase. In previous work, the same capture and labeling system was used with a colorimetric substrate and detection limits of 440 colony forming units (CFU)/mL. Here, the substrate para-aminophenol- β-D-galactopyranoside (PAPG) was used. In the presence of β-galactosidase, PAPG is cleaved to form para aminophenol (PAP), which is detected through square wave voltammetry. Figure A4.3 shows the dose-response curve and corresponding voltammograms. The curve was fit to a 4-parameter logistic model commonly used for sandwich immunoassays and a detection limit of 50 CFU/mL was calculated. The electrochemical LOD is an order of magnitude lower when using colorimetric detection, which is expected. Although these results were not obtained in the three-electrode device, they are encouraging for the final multiplexed application.

Currently the same experiment is being optimized for *E. Coli* detection using alkaline phosphatase and para-aminophenyl phosphate (PAPP) as an enzyme substrate pair. Initial detection limits are high ($>10^4$ CFU/mL), which we believe is a function of the capture and secondary antibody. Additional antibodies will be screened to lower the detection limit before moving to multiplexed detection in the device.

Finally, a suitable enzyme-substrate pair for *Listeria* detection will be determined. There are multiple pairs that are under consideration and each will be screened using TPEs in bis-tris-propane buffer to establish which is the most sensitive in our system. Next, capture and secondary antibodies for *Listeria* will be screened to determine the optimal pair. Antibodies must be screened to find capture antibodies that bind to a different epitope than the secondary antibody and vice versa. Once the assays for *Listeria* and *E. Coli* are satisfactory (LOD of 10^2 CFU/mL or less), we will move to optimizing multiplexed detection within the three-electrode device.

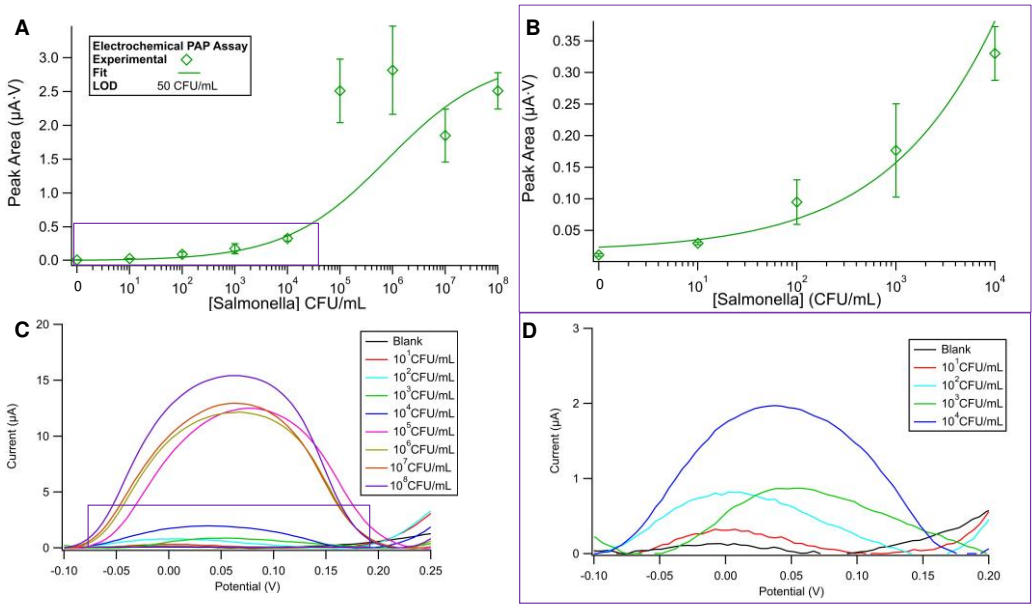

Figure A4.3. Dose response curve for *Salmonella* captured and labeled using immunomagnetic separation and detected using TPEs (A). Lower portion of the dose-response curve from 0 to 10^4 CFU/mL (B). Square wave voltammograms for each concentration of *Salmonella* (C). Square wave voltammograms for *Salmonella* concentration from 0 to 10^4 CFU/mL

REFERENCES

1. Roca, I.; Akova, M.; Baquero, F.; Carlet, J.; Cavaleri, M.; Coenen, S.; Cohen, J.; Findlay, D.; Gyssens, I.; Heure, O., The global threat of antimicrobial resistance: science for intervention. *New microbes and new infections* **2015,** *6*, 22-29.

2. Organization, W. H. *Antimicrobial Resistance: Global Report on Surveillance* 2014.

3. WHO, Global action plan on antimicrobial resistance. WHO Geneva: 2015.

4. Law, J. W. F.; Ab Mutalib, N. S.; Chan, K. G.; Lee, L. H., Rapid methods for the detection of foodborne bacterial pathogens: principles, applications, advantages and limitations. *Front. Microbiol.* **2015,** *5*, 19.

5. Velusamy, V.; Arshak, K.; Korostynska, O.; Oliwa, K.; Adley, C., An overview of foodborne pathogen detection: In the perspective of biosensors. *Biotechnol. Adv.* **2010,** *28* (2), 232-254.

6. Bohaychuk, V. M.; Gensler, G. E.; King, R. K.; Wu, J. T.; McMullen, L. M., Evaluation of detection methods for screening meat and poultry products for the presence of foodborne pathogens. *Journal of Food Protection* **2005,** *68* (12), 2637-2647.

7. Mori, Y.; Notomi, T., Loop-mediated isothermal amplification (LAMP): a rapid, accurate, and cost-effective diagnostic method for infectious diseases. *J. Infect. Chemother.* **2009,** *15* (2), 62-69.

8. Posthuma-Trumpie, G. A.; Korf, J.; van Amerongen, A., Lateral flow (immuno) assay: its strengths, weaknesses, opportunities and threats. A literature survey. *Anal. Bioanal. Chem.* **2009,** *393* (2), 569-582.

9. Zhao, X.; Lin, C. W.; Wang, J.; Oh, D. H., Advances in Rapid Detection Methods for Foodborne Pathogens. *J. Microbiol. Biotechnol.* **2014,** *24* (3), 297-312.

10. Martinez, A. W.; Phillips, S. T.; Butte, M. J.; Whitesides, G. M., Patterned paper as a platform for inexpensive, low-volume, portable bioassays. *Angew. Chem.-Int. Edit.* **2007,** *46* (8), 1318-1320.

11. Carrell, C.; Kava, A.; Nguyen, M.; Menger, R.; Munshi, Z.; Call, Z.; Nussbaum, M.; Henry, C., Beyond the lateral flow assay: A review of paper-based microfluidics. *Microelectronic Engineering* **2019,** *206*, 45-54.

12. Yamada, K.; Shibata, H.; Suzuki, K.; Citterio, D., Toward practical application of paper-based microfluidics for medical diagnostics: state-of-the-art and challenges. *Lab Chip* **2017,** *17* (7), 1206-1249.

13. Gong, M. M.; Sinton, D., Turning the page: advancing paper-based microfluidics for broad diagnostic application. *Chemical reviews* **2017,** *117* (12), 8447-8480.

14. Skjerve, E.; Rørvik, L. M.; Olsvik, O., Detection of Listeria monocytogenes in foods by immunomagnetic separation. *Applied and environmental microbiology* **1990,** *56* (11), 3478-3481.

15. Suh, S. H.; Jaykus, L.-A., Nucleic acid aptamers for capture and detection of Listeria spp. *Journal of biotechnology* **2013,** *167* (4), 454-461.

16. Zhang, J.; Wu, D.-Z.; Cai, S.-X.; Chen, M.; Xia, Y.-K.; Wu, F.; Chen, J.-H., An immobilization-free electrochemical impedance biosensor based on duplex-specific nuclease assisted target recycling for amplified detection of microRNA. *Biosensors and Bioelectronics* **2016,** *75*, 452-457.

17. Carrell, C. S.; Wydallis, R. M.; Bontha, M.; Boehle, K. E.; Beveridge, J. R.; Geiss, B. J.; Henry, C. S., Rotary manifold for automating a paper-based Salmonella immunoassay. *RSC Adv.* **2019,** *9* (50), 29078-29086.

18. Srisa-Art, M.; Boehle, K. E.; Geiss, B. J.; Henry, C. S., Highly Sensitive Detection of Salmonella typhimurium Using a Colorimetric Paper-Based Analytical Device Coupled with Immunomagnetic Separation. *Analytical Chemistry* **2018,** *90* (1), 1035-1043.

19. Schaumburg, F.; Carrell, C. S.; Henry, C. S., Rapid Bacteria Detection at Low Concentrations Using Sequential Immunomagnetic Separation and Paper-Based Isotachophoresis. *Analytical Chemistry* **2019,** *91* (15), 9623-9630.

20. Hossain, S. Z.; Ozimok, C.; Sicard, C.; Aguirre, S. D.; Ali, M. M.; Li, Y.; Brennan, J. D., Multiplexed paper test strip for quantitative bacterial detection. *Anal. Bioanal. Chem.* **2012,** *403* (6), 1567-1576.

21. Khan, S. S.; Smith, M. S.; Reda, D.; Suffredini, A. F.; McCoy Jr, J. P., Multiplex bead array assays for detection of soluble cytokines: comparisons of sensitivity and quantitative values among kits from multiple manufacturers. *Cytometry Part B: Clinical Cytometry: The Journal of the International Society for Analytical Cytology* **2004,** *61* (1), 35-39.

22. Choi, G.; Choi, S., Cellular flow in paper-based microfluidics. *Sensors and Actuators B: Chemical* **2016,** *237*, 1021-1026.

23. Scallan, E.; Hoekstra, R. M.; Angulo, F. J.; Tauxe, R. V.; Widdowson, M. A.; Roy, S. L.; Jones, J. L.; Griffin, P. M., Foodborne Illness Acquired in the United States-Major Pathogens. *Emerg. Infect. Dis* **2011,** *17* (1), 7-15.

24. Noviana, E.; Klunder, K. J.; Channon, R. B.; Henry, C. S., Thermoplastic Electrode Arrays in Electrochemical Paper-Based Analytical Devices. *Analytical Chemistry* **2019,** *91* (3), 2431-2438.

25. Klunder, K. J.; Nilsson, Z.; Sambur, J. B.; Henry, C. S., Patternable Solvent-Processed Thermoplastic Graphite Electrodes. *Journal of the American Chemical Society* **2017,** *139* (36), 12623-12631.

APPENDIX 5: SARS-CoV-2 VIRAL ANTIGEN ASSAY USING THE dELISA

The next application that has been targeted with the dELISA is a viral antigen assay for SARS-CoV-2. Rather than detecting antibodies that indicate a prior infection, a viral antigen assay detects proteins from live virus to determine active infections. Along with a point-of-care serology test, the WHO has listed a point-of-care test for active infections as one of their four target products still needed to combat the virus.[1] Viral antigen assays are an alternative to polymerase chain reaction tests that detect viral RNA. Although less sensitive than PCR, these assays are cheaper, faster, and easier to deploy at scale. Several public health experts are advocating for the development and mass production of these tests to slow the spread of the disease and help society return to normalcy.[2] Although they cannot detect all active infections, viral antigen assays will flag a person when they are most infectious (Figure A5.1). Frequent, inexpensive, and rapid testing is considered more important than high test sensitivity.[3]

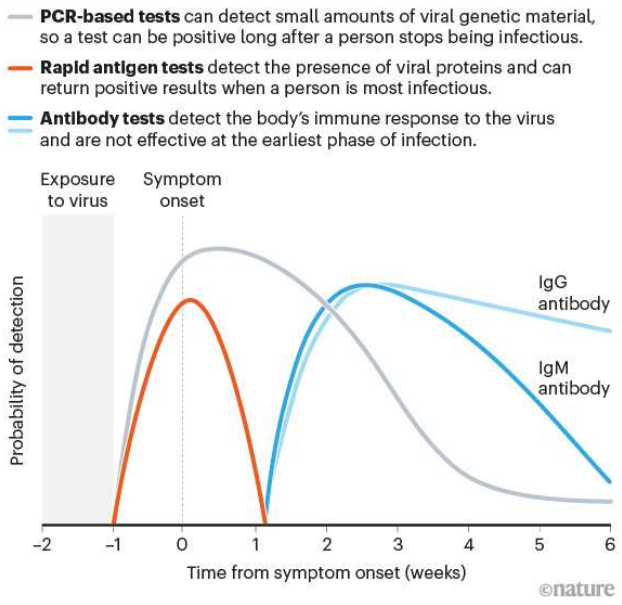

Figure A5.1. Timeline for potential detection of active SARS-CoV-2 infection and antibodies using PCR, antigen testing, and ELISAs.[1]

The dELISA is now being used to perform a viral antigen assay by targeting SARS-CoV-2 Nucleocapsid protein (N Protein). The sandwich ELISA scheme used to detect N Protein in the dELISA is shown in Figure A5.2. Rather than using whole blood as a sample matrix, as was used for the serology test (Chapter Four), the live virus is more likely to be found in the respiratory system. Therefore, the N protein assay and device have been modified to use mid-nasal swabs as a sample. Fortunately, the change in sample matrix allows for a simpler end-user workflow and device. In the serology assay, blood was added to a plasma separation membrane to remove red-blood cells and decrease matrix-effects. After the sample was added, the end user then needed to add a buffer to the buffer inlet, so there were two end-user steps. In the N protein assay, virus from the nasal swab is captured in an extraction buffer containing surfactant to disrupt the viral membrane and release soluble N protein. Because the conditions of the transport media can be controlled, the final sample solution is relatively clean, and interference from the matrix is negligible. Therefore, the sample in extraction buffer can be used as the sample and as the wash buffer so only one sample addition step is necessary.

To further simplify the assay, we proposed a device design that incorporates the extraction buffer into a sealed well above the sample addition inlet. Here, the nasal swab will be placed in

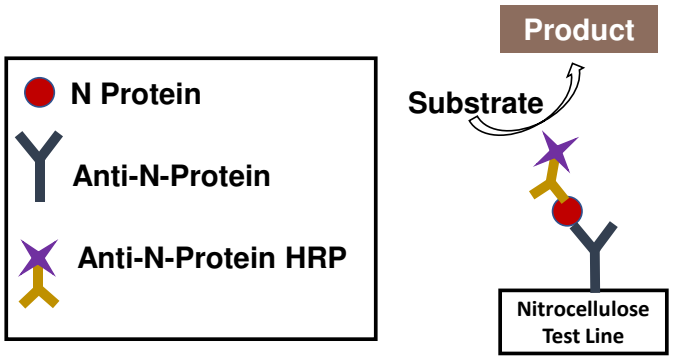

Figure A5.2. Sandwich ELISA detection scheme for the SARS-CoV-2 N-Protein assay.

the well containing extraction buffer. The swab will then be used to puncture a foil seal that releases the media and any virus into the device to start the assay. This process along with a 3D-printed prototype device housing containing a buffer well are shown in Figure A5.3. Flow from the housing into the device has been confirmed, but we are still in the process of creating a foil seal to hold the buffer.

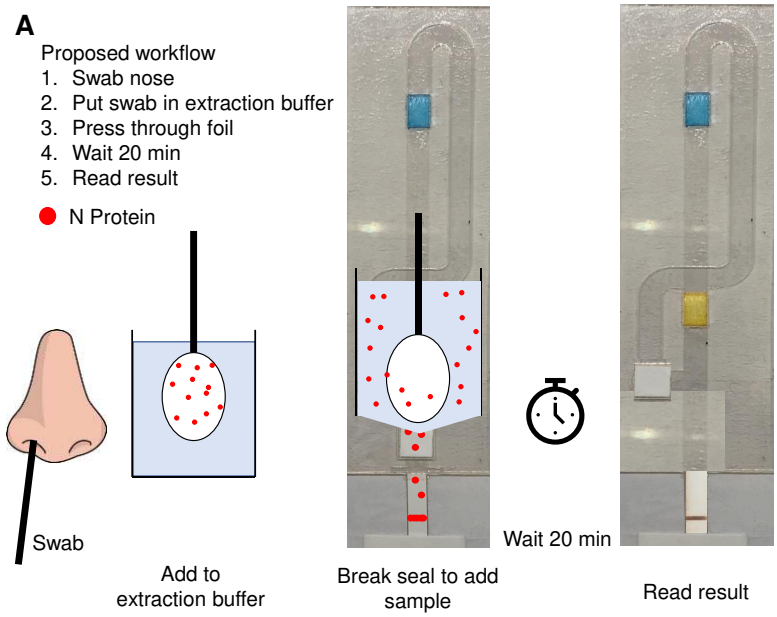

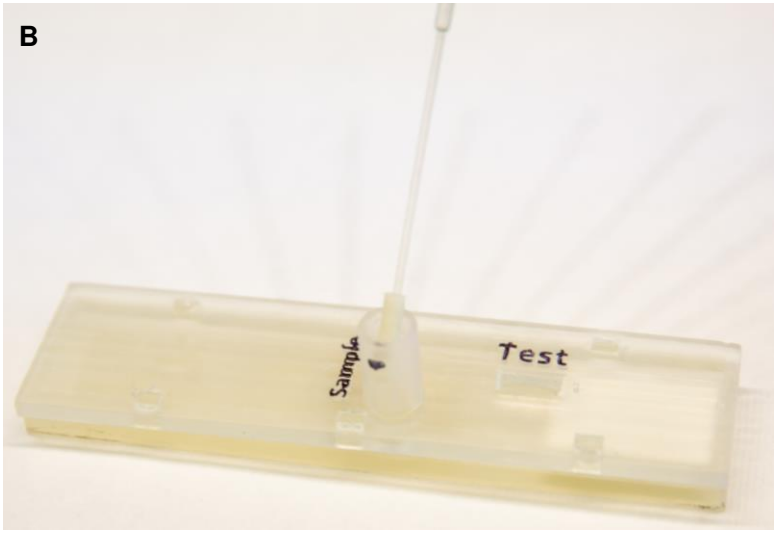

Figure A5.3. Proposed workflow for N Protein assay using the dELISA and a 3D-Printed housing (A). Image of housing with dELISA enclosed and a nasal swab in the extraction buffer well (B).

Along with device design and ease-of-use considerations the assay must also detect low levels of viral antigen to avoid false negative results (high clinical sensitivity). To this end, the assay is being optimized like the serology assay was optimized in Chapter Four. Results for these studies are ongoing and not available to present in this document. Once the assay has been optimized for maximum sensitivity, it will be tested against high concentrations of other common viruses (norovirus, influenza, and other corona viruses) to ensure a low false positive rate (high clinical specificity). Patient samples will then be acquired to determine a clinical sensitivity and specificity. If the assay meets criteria set by the WHO in their target product profile (>90% sensitivity and >99% specificity) after the clinical trial, we envision the dELISA and the N protein assay to be used around the planet to screen individuals for an active infection. It is difficult to overstate the importance of this technology, as it has the potential to help slow the spread of SARS-CoV-2 and save hundreds of thousands of lives in the coming years.

REFERENCES

1. COVID-19 Target product profiles for priority diagnostics to support response to the COVID-19 pandemic v.0.1. Organization, W. H., Ed. 2020.

2. Guglielmi, G., Fast coronavirus tests: what they can and can't do. *Nature*.

3. Larremore, D. B.; Wilder, B.; Lester, E.; Shehata, S.; Burke, J. M.; Hay, J. A.; Tambe, M.; Mina, M. J.; Parker, R., Test sensitivity is secondary to frequency and turnaround time for COVID-19 surveillance. *MedRxiv* **2020**.

APPENDIX 6: A MICROFLUIDIC MAGNETOPHORETIC DUPLEX SPECIFIC NUCLEASE MICRO RNA ASSAY FOR LUNG CANCER SCREENING

Specific Aims: Lung cancer is the most common (2.09 million cases) and deadly (1.76 million deaths) of all cancers (WHO, 2018).[1] Lung cancer is unusually lethal because it is difficult to diagnose at early stages and is frequently only detected after progressing to a late stage.[2, 3] The most common early stage screening method is radiography or computer tomography (CT) scans, which are only recommended for high-risk patients (e.g. smokers) because they are expensive, prone to false positives, and pose other health risks.[3] Therefore, a non-invasive and inexpensive screening tool for early-stage lung cancer detection is needed. To this end many lung-cancer biomarkers that could be used for screening have been found.[4-9] A promising and relatively new class of cancer biomarkers are micro-RNA (miRNA). miRNA are small, non-coding, RNA sequences that are most often detected using nucleic acid amplification techniques, like quantitative reverse transcriptatse PCR (qRT-PCR). However, these techniques are expensive, complex, bulky, and time-consuming (2-6 h). These limitations relegate qRT-PCR to specialized laboratories and decrease the chance of widespread use as a screening tool. In fact, **no miRNA assays that combine ease-of-use, affordability, and sensitivity exist.** This proposal will describe a novel immunomagnetic separation duplex specific nuclease assay (IMS-DSNA) that will meet the needs for low cost screening of miRNA. Here, magnetic beads will be conjugated to 100 nm polystyrene beads (PSBs) through nucleic acid probes (**Fig A6.2**). The probes will bind to miRNA target during a short incubation period (~20 min). The miRNA-bound beads will be removed from the sample and concentrated on an electrode. The enzyme duplex specific nuclease (DSN) will be introduced to the beads and any probes bound to miRNA will be cleaved by the enzyme, removing the PSBs from the electrode surface. miRNA will then bind to a second probe and undergo DSN

cleavage again, thereby amplifying the signal. The number of PSBs remaining after incubation with DSN will be quantified using impedance spectroscopy. Multiplexing will be enabled by using different sized beads for each miRNA target, which will be sorted by size in a magnetophoretic microfluidic cell. Three electrodes in the device will be used to detect three miRNA (**Fig. A6.3**). The IMS-DSNA will be inexpensive, rapid, and easy to use for use in traditional hospital laboratories, clinics, and resource-limited settings. The assay will detect three miRNA that have a positive correlation with lung cancer. This project is an optimal candidate for a small-scale R03 study because the scope will be limited to the demonstration a successful proof-of-concept device before moving to larger scale studies including real patients and/or device commercialization. To accomplish the goals of this proposal, two aims will be tested:

Aim 1: Develop an IMS-DSNA that can detect miRNA with an impedance-based sensor. We will develop a magnetic-bead/probe/PSB complex capable of capture and detection of miRNA-21. Assay conditions such as reagent concentrations, reaction time, pH, etc. will be studied. Once the assay for miRNA-21 is optimized, the same optimization will be performed for miRNA-210 and miRNA-126.

Significance: miRNA are biomarkers for many different diseases, including lung-cancer. Our system will detect miRNA without a nucleic-acid amplification step like PCR, which will decrease equipment cost, time, and assay complexity. Although this proposal is focused on detecting lung cancer biomarkers, in the future it could be used to detect miRNA to screen for other cancers, Alzheimer's, diabetes, and more.

Innovation: To the best of our knowledge, a multiplexed, impedance IMS-DSNA does not exist. The proposed system will allow for the detection of miRNA without nucleic acid amplification

because the cyclic cleavage of large beads from the surface will result in large changes at the electrode surface and enhanced signals.

Aim 2: Develop a microfluidic device capable of running multiplexed IMS-DSNA in real blood samples: Alongside Aim 1, we will design a microfluidic system that separates magnetic beads by size, can handle real blood samples, and runs an impendence-based assay on three electrodes for multiplexed miRNA detection. The goal of this aim is to create a device that minimizes user input and automates most assay steps.

Significance: miRNA are typically detected in a panel to increase their prognostic or diagnostic capabilities. To increase useful as a screening tool, we must design a system that can detect multiple miRNA simultaneously.

Innovation: Magnetophoresis, the separation of magnetic beads by size, has not been used to detect miRNA and offers a new method to multiplex in a portable and easy-to-operate device. The device will also handle whole blood to decrease sample preparation steps.

Significance: We aim to create a platform for simple, rapid, multiplexed, and amplification-free detection of miRNA from a small blood sample for the diagnosis of lung cancer. Lung cancer is the most common and deadly cancer worldwide.[1, 2] To decrease the death rate it is imperative to detect the disease before it progresses to a late stage.[1-3] The incidence of lung cancer may also rise in the coming years because of the increased use of e-cigarettes among non-smokers in the last decade.[10] Unfortunately, the current diagnostic methods (CT scans) are so invasive and expensive that they are not recommended for anyone but those at the highest risk for lung cancer.[3] To improve early detection methods, researchers have identified specific lung cancer biomarkers that can be detected in blood.[11] Of these biomarkers, miRNA have shown significant promise as diagnostic and prognostic indicators for lung cancer and many other diseases like Alzheimer's, heart failure,

and other cancers.[9, 12-14] They have also been used to determine tumor progression and a patient's response to treatment.[13] miRNA have traditionally been detected using Northern Blot methods, microarrays, or amplification methods like quantitative real-time reverse transcriptase PCR (qRT-PCR).[15] Of these methods, qRT-PCR is the most common and is considered the gold standard that is used to validate the results of other methods. qRT-PCR is widely used because, as an amplification-based technique, the detection limits are very low (<10 copies).[16] The only commercial products for miRNA detection are also qRT-PCR based.[11, 17] However, considerable and tedious sample processing is necessary, costly thermal cycling is used (~$5000/instrument), and careful primer design is essential to reduce the risk of non-specific amplificaiton.[15, 18, 19] Furthermore, the sensitivity of PCR assays are unnecessarily low for circulating miRNA in the bod (~1 fM) and take upwards of six hours.[20, 21] To increase the use of miRNA as cancer screening biomarkers in clinics and hospitals the assays must become easier to use, less expensive, and faster, while achieving detection limits of 1 fM.

In this project we will design a less invasive alternative to current lung-cancer screening techniques like CT scans, and a more user-friendly and faster assay than qRT-PCR by detecting miRNA with a microfluidic device. Currently, easy to use and sensitive molecular diagnostics do not exist, which limits the adoption of molecular techniques for cancer screening in clinics without a dedicated clinical laboratory.[22] The proposed device will be designed to use at clinics so samples do not need to be sent to external laboratories. Here, a multiplexed miRNA assay will be developed using a microfluidic device to decrease the complexity, instrument size, and cost. The assay will be based on a DNase enzyme called duplex specific nuclease (DSN), which facilitates miRNA detection *without nucleic acid amplification*. DSN was recently discovered and has been used to detect miRNA at 60 aM.[15, 23] Performing amplification free molecular detection decreases assay

times, removes the need for primers, thermal cyclers, and other PCR other reagents, and reduces false positive rates. Low detection limits are achieved with DSN using an isothermal enzymatic cycling process that releases upwards of 10^7 probes for every one miRNA captured.[24] However, to reach these limits the samples must be incubated with a capture probe for upwards of two hours at high temperatures and multiplexing is difficult. The assay proposed here will eliminate the need for high temperatures and long incubation times by increasing the sensitivity through a novel electrochemical impedance-based detection method using polystyrene beads as signal probes. Impedance assays measure the change in resistance to charge transfer with a redox probe at an electrode surface based on surface changes caused by analyte binding to the electrode. Importantly, impedance assays are label free so only one binding step is necessary.[25] The assay will also enable multiplexing via magnetophoretic separation of magnetic beads by size and will automate sample pre-treatment so whole blood can be introduced to the system without user intervention. Our assay will detect three miRNA that have shown impressive diagnostic capabilities when detected simultaneously: miRNA-21, miRNA-210, and miRNA-126.[14] These miRNA have been used to diagnose lung-cancer patients with >85% sensitivity and >95% specificity.[16] **We hypothesize that microfluidic impedance-based DSN assays can be used to sensitively and specifically detect miRNA at clinically relevant levels in complex samples in under 30 min.**

Innovation: Our proposal is innovative in the following ways:

- An impedance-based approach using polystyrene beads will increase sensitivity over current methods that only use the binding of ssDNA to induce a change in charge transfer resistance

- All DSN assays to date use multiple time and labor intensive pipetting steps for miRNA detection. We will automate the assay using a microfluidic device so only one sample addition step is necessary.
- Current multiplexed DSN assays have only detected two miRNA at once and qRT-PCR can only detect one. This proposal aims to simultaneously detect three.
- Our device will use whole blood to detect miRNA instead of tumor cells, which is more applicable to a clinical screening test.
- The device in this proposal is re-useable as electrode regeneration can occur by simply washing away magnetic beads.

Approach

Overview: Multiplexed detection of three miRNA from whole blood will be accomplished in two aims. The first aim consists of developing an IMS-DSNA for three miRNA. This aim will focus on optimizing the target capture sequence for each miRNA, the conjugation chemistries to link magnetic beads to polystyrene beads via miRNA, and the assay conditions such as pH and reagent concentrations. In the second aim we will create a microfluidic device capable of magnetophoretic separation of magnetic beads onto three separate electrodes based on their size. This aim will also focus on creating a microfluidic system capable of delivering reagents and handling whole blood to improve ease-of-use and sensitivity.

Preliminary Results. The Henry and Geiss labs are experienced in target sequence design, microfluidic fabrication, EIS detection strategies, and magnetic bead immunoassays.[26-30] Although our groups have not targeted miRNA in the past, the following results are relevant to this proposal and demonstrate the capabilities of our laboratories to perform the proposed experiments.

Impedance detection of polystyrene beads on gold electrodes. In a 2018 publication, trace detection of virus particles captured on a gold mircowire in a paper channel was demonstrated.[26] In this work, 10 virus particles could be detected in a 50 µL sample using impedance spectroscopy. Virus particles were initially modeled using streptavidin-coated polystyrene beads, which after binding to a biotin modified gold electrode, showed a large change in resistance to charge transfer (Fig. A6.1a). Similarly, in this work we will modify a gold-coated magnetic bead with a biotinylated miRNA probe and streptavidin-coated polystyrene beads (Fig. A6.2). Using a permanent magnet, the gold coated magnetic beads will be concentrated on the electrode surface. After miRNA bind to the probes that are used as a linkage between the polystyrene beads and the magnetic bead, DSN will cleave that linkage, which will release the polystyrene beads from the electrode surface and create a change in resistance to charge transfer.

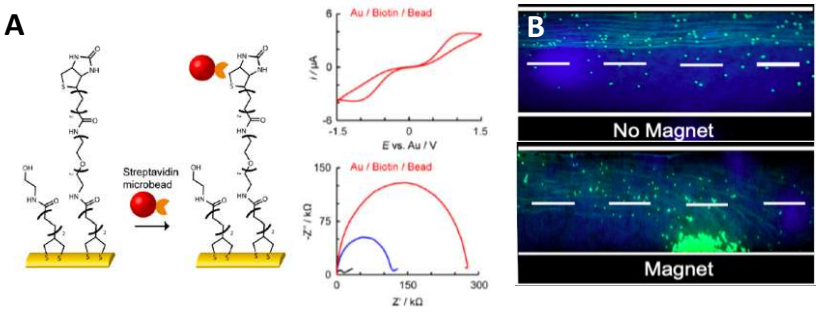

Figure A6.1. Immobilization scheme, cyclic voltammogram, and Nyquist plot showing the impact of binding polystyrene beads to an electrode surface for the detection of virus particles (A). Magnetophoretic separation of fluorescent magnetic particles across a laminar flow barrier in a paper-based channel (B). Calibration curve for the detection of a West Nile virus sequence using an affinity sensor on a gold electrode (C).

Magnetic separation for bacteria detection in solution and in paper channels. In 2018 and 2019 publications, our groups demonstrated the ability to capture and separate bacteria from complex sample matrices like bird feces, milk, and apple juice.[27, 28] These experiments were performed in a microcentrifuge tube with multiple pipetting steps. To increase user-friendliness, we have

recently demonstrated separation of magnetic beads from urine samples using a microfluidic paper-based channel (Fig. A6.1b). More precise separation and capture is possible in a traditional device, which will enable separating beads by size as discussed below.

Proposed Experiments

Aim 1: **In this aim we will create a novel electrochemical impedance spectroscopy (EIS)-based assay to detect miRNA using DSN to amplify the signal.** The goal of this aim is to develop assay conditions in a test tube and with manual reagent addition steps to demonstrate a proof-of-concept assay for three different miRNA. In this aim, the miRNA will be detected individually instead of simultaneously to determine the viability of the proposed technique and to hone the assay conditions for improved sensitivity.

Objective 1: Create magnetic mead-target probe conjugates for miRNA-21, miRNA-210, and miRNA-126. These three miRNA have been shown in multiple studies to be elevated in lung-cancer patients.[14, 16, 31-33] Importantly, they can all be found as circulating miRNA in plasma samples instead of in tissue/tumor samples, which increases their usefulness for minimally-invasive sampling. Combined, the three miRNA have an increased diagnostic capability over any single miRNA, so it is imperative to detect all three instead of only one.[14, 34, 35]

Table A6.1. miRNA and corresponding probe Sequences

miRNA	miRNA Sequence (5'-3')	Probe (3'-5')
21	UAGCUUAUCAGACUGAUGUUGA	ATCGAATAGTCTGACTACAACT
210	AGCCCCUGCCCACCGCACACUG	TCGGGGACGGGTGGCGTGTGAC
126	CAUUAUUACUUUUGGUACGCG	GTAATAATGAAAACCATGCGCC

The sequences of the three miRNA and their corresponding capture probe sequences are shown in Table 1. The probes and miRNA sequences will be purchased from Integrated DNA Technologies. The probe must be completely complementary to each miRNA because DSN will distinguish

between 0 and 1 mismatched base pairs.[23] Each probe will have a thiol terminus at the 5' end and a biotinylated terminus at the 3' end. The thiol end of the probe will be conjugated to gold-coated magnetic beads (Nanocs or similar). Binding efficiency of probe to Au-MBs will be determined by gel electrophoresis. The beads are coated with gold for two reasons: 1) for facile modification with thiolated probes and 2) we hypothesize that the conductive gold-magnetic beads will increase the electrode surface area, which will enhance the electrochemical sensitivity of the assay. To test this hypothesis, we will compare the peak current of ferri/ferrocyanide ($Fe(CN)_6^{3/4}$) on a bare carbon electrode, a carbon electrode coated with polystyrene magnetic beads, and a carbon electrode coated with gold-magnetic beads. Probe-conjugated magnetic beads will be used in this project to increase the binding efficiency to miRNA in solution versus methods that modify an electrode surface with capture probes. Here, binding is not limited to only the diffusion of miRNA to the electrode surface. Instead, the additional diffusion of beads in solution will enhance binding efficiencies.[20] After conjugation of the miRNA probes, the Au-MBs will be blocked with mercaptoethanol to prevent non-specific interactions with the gold surface. Three different sizes of magnetic beads will be used for each probe: 0.5, 1, and 5 μm. The size difference of the beads will allow for separation and multiplexing in the microfluidic device, which is discussed in Aim 2. The 3' end of the probe will be biotinylated and conjugated to 50 nm streptavidin-coated polystyrene beads (PSBs) (Nanocs) (Figure A6.2). To determine conjugation success and surface coverage of the PSBs on the Au-coated magnetic beads, we will add a biotin-FITC complex (Thermo Fisher) and the fully conjugated system will be imaged with a fluorescent microscope (Evos or Dinoscope).

Objective 2: Optimize miRNA capture and DSN signal amplification using EIS for miRNA-21.

After magnetic bead probes have been synthesized in Objective 1 the detection of miRNA-21 will

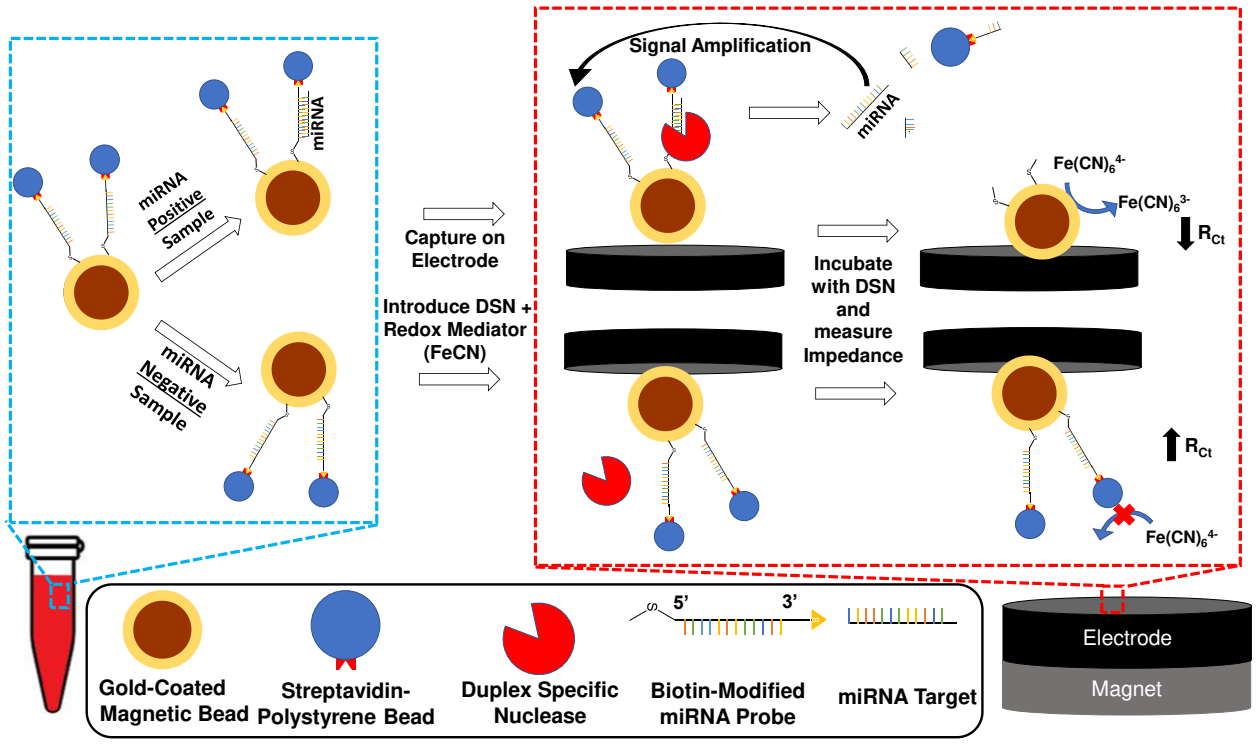

Figure A6.2. Schematic demonstrating the proposed assay. When a miRNA target is present (top), DSN will cleave the probe-miRNA complex and a polystyrene bead will be washed away, decreasing the resistance to charge transfer in the presence of the redox probe $Fe(CN)_6^{4-}$. The miRNA that was cleaved by DSN is free to bind to another probe and is cleaved by DSN a second time. This process repeats and the signal is amplified. When no target miRNA is present (bottom), DSN will not cleave the single-stranded probe and the resistance to charge transfer remains large.

be optimized. Standard conditions that will be studied include the magnetic bead concentration, electrode size and composition, redox mediator identity and concentration, pH, temperature, and incubation times. All experiments will be performed in 10 fM solutions of miRNA buffered with PBS. Due to previous reports on EIS miRNA detection, 10 fM should be near the lower end of the linear range for the proposed technique.[20] Initially, the assay will be performed in a microcentrifuge tube on a roller for binding of miRNA to probes. The solution will then be transferred to a well with an electrode and magnet at the bottom. Once the beads are concentrated on the electrode using the permanent magnet, the sample solution will be removed and replaced with a solution of DSN. The DSN cleavage kinetics will be studied to determine ideal DSN

concentration and the impact of concentrating beads on an electrode vs performing enzymatic amplification in solution.

After an incubation period (<30 min), the DSN solution and cleaved PSBs will be replaced with a $Fe(CN)_6^{3/4}$ solution and an impedance spectrum collected. Ideally the beads will form a monolayer on the electrode surface. If there are too many beads, DSN will be blocked from reaching the beads on the bottom, and if there are too few the $Fe(CN)_6^{3/4}$ will reach the base electrode and assay sensitivity will decrease. Electrode coverage as a function of bead concentration will be explored during this aim by finding the concentration with maximum impedance before a plateau in the presence of only beads and $Fe(CN)_6^{3/4}$.

The optimal probe surface coverage on the Au-MBs will also be explored to determine the probe concentration and conjugation time that will deliver the largest signal. If the probe concentration on the Au-MBs is too large, it is possible that PSBs will not bind to all probes due to steric hinderance and electrostatic repulsion. miRNA targets that bind to probes without PSBs will not be measured, and sensitivity will decrease. Conversely, if the probe concentration is too low, the number of possible binding events will be limited, and the sensitivity will decrease. To determine the appropriate probe coverage on the Au-MBs, they will be conjugated to PSBs and concentrated onto a gold-electrode and impedance measurements will be collected. The probe concentration that results in the largest resistance to charge transfer before a plateau will be chosen as the optimal probe concentration.

The electrode material will also be explored in this objective. As we are tailoring this assay for point-of-care applications the initial electrode materials tested will be inexpensive composite carbon materials of which our lab has extensive experience developing.[36] Importantly, these composite materials can be implemented into microfluidic devices with ease and have been used

to perform EIS assays in the past.[37] If the composite electrodes have poor sensitivity, we will explore other materials like glassy carbon, gold, or platinum.

Once the above parameters have been established, a detection limit will be determined for the assay. Because of the expected enhancement in signal from large beads being released in each binding step, it is expected that the LOD will decrease over current DSN methods. The sample volume will be 100 µL so that the necessary volume of blood can be collected with a single finger-prick. The typical circulating concentration of miRNA in blood is between 0.1 and 100 fM, therefore our limit of detection should be ~10^3 miRNA molecules in 100 µL. Our group has previously demonstrated the detection of 10 polystyrene beads in 50 µL of solution using EIS, so detecting 10^3 copies in 100 µL is feasible.[26] Additionally, capturing miRNA in solution with suspended beads has proven more efficient than capturing target sequences with probes immobilized on an electrode surface.[20] If the desired LOD is reached, binding and reaction times will be minimized as is preferred in a point-of-care assay.

Finally, the specificity of the assay will be tested using miRNA with one mis-matched base pair. Because miRNA are short (22 nucleotides), the chance that similar sequences with one mis-matched base pair exist in the same sample is relatively high. DSN has been shown to differentiate between double stranded DNA with one mis-matched base pair in the past, but this will need to be verified in our system.[20, 23] The miRNA with one mis-matched base pair will be synthesized and purchased from Integrated DNA Technologies.

Objective 3: Capture and detect for miRNA-210 and 26. Once the detection of miRNA-21 is optimized in Objective 2, the same experiments will be performed for miRNA-210 and 26. Bead concentration as it relates to electrode coverage will need to be determined for each size bead The bead concentration/coverage can be estimated from the results in Objective 2, but will need to be

determined experimentally. The specificity of the assays for miRNA-210 and 26 will be confirmed using miRNA with one mis-matched base pair will be purchased from Integrated DNA Technologies. The specificity will also be tested against the other two miRNA in the panel.

Potential pitfalls and workarounds: 1) In previous work from our lab we demonstrated that thiolated probes immobilized on gold electrodes are not stable over time.[26] In that work, the Au-thiol bond was not stable in the presence of $Fe(CN)_6^{3/4-}$, which is the same redox mediator we will use in this project. However, the same instability is not expected because the Au-thiol bonds will be exposed to $Fe(CN)_6^{3/4-}$ for <1 min. If poor stability is observed, we will use a di-thiol linkage, which was successful in preventing degradation in our previous work. 2) Although the loss of one PSBs will result in a large ΔR_{ct} compared to other probes, the total number of PSBs immobilized on the surface of each Au-MB could be too small to observe a significant difference, or the linear range will be cut off too quickly (poor upper limit of detection). If this is the case, there are multiple solutions. The first is to decrease the size of the PSBs so more can be immobilized on each Au-MB. Next the concentration of Au-MBs in solution will be increased so there are more probes to bind to and PSBs to cleave during DSN signal amplification. Finally, the probe length will be modified using a polyethylene glycol linker so multiple probe lengths can exist on the same Au-MB, and multiple PSBs can be immobilized at different lengths from the Au-MBs. 3) The third concern is that the PSBs will block the electrical connection between the Au-MBs and the electrode material. Polystyrene is insulating and if the surface of the Au-MBs is saturated with PSBs, direct contact between Au-MBs and the electrode will be difficult. Ideally, the magnet that will concentrate the beads on the electrode surface will be strong enough to force contact between with the beads. However, if poor electrical connections are observed, there are several workarounds. The first is to decrease the concentration of PSBs on the surface of the Au-MBs to create "holes"

in the coverage and allow transfer of electrons between beads. If decreasing PSB coverage is not successful, some PSBs can be replaced with gold nanoparticles. Here the outer shell of the Au-MBs would be conductive enough to transfer electrons to the interior Au-MB. The gold nanoparticles used would be the same size as the PSBs, coated with streptavidin, and attached to the surface via a thiol and biotin linker. 4) The final potential pitfall is that the miRNA will have difficultly binding to the probes because of steric hinderance from the PSBs. If this is the case, the first workaround is to decrease the concentration of PSBs on the surface of the bead to create areas for miRNA to interact with the probes. The second is to conjugate the miRNA to free PSB-probe complexes in solution before binding to magnetic beads.

Aim 2: **Create a microfluidic device capable of handling whole blood and magnetophoretic sorting of magnetic beads for multiplexed miRNA detection.** miRNA are valuable biomarkers for many different diseases and disease states. However, certain miRNA are elevated or suppressed for many diseases, so it is difficult to specifically screen for a single disease with one miRNA target. To improve diagnostic specificity multiple miRNA must be detected simultaneously. Incorporating the assay into a microfluidic device will also help automate sample preparation and detection steps for simple analysis by minimally trained end users.

Objective 1: Create a microfluidic device that can separate gold-coated magnetic beads by size.

Magnetophoretic separation of magnetic beads has been reported previously.[38, 39] The general concept of sorting magnetic beads by size is shown in Figure A6.3a. To separate magnetic beads by magnetophoresis, they must have different magnetic susceptibilities and or sizes. In a microfluidic channel, a magnet perpendicular to the flow will deflect beads at an angle dependent on the flow rate and properties of the bead.[39] Larger beads will have more magnetic material and larger magnetic susceptibilities, and will be deflected further than smaller beads. The device we

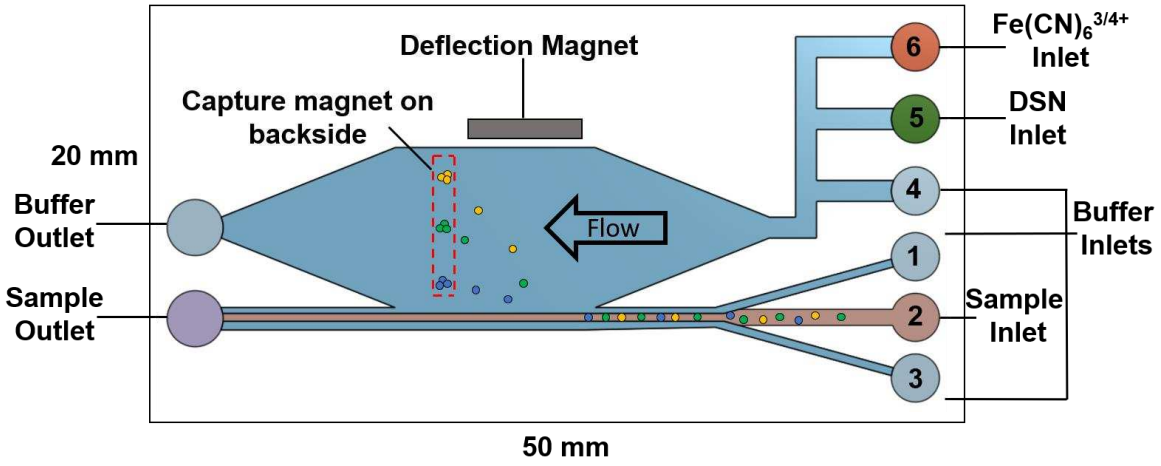

Figure A6.3. Schematic representing the proposed microfluidic device Focusing and magnetic separation/sorting of Au-MBs based on size will occur in the first step (inlets 1-4), followed by DSN addition (inlet 5) and $Fe(CN)_6^{3/4-}$ addition (inlet 6)

create will have the same general shape as the device in Figure A6.3. Before size sorting can occur, the beads will be focused into a line so deflection will be consistent. Sheath flow will be used to focus the beads.[40] After focusing, the beads will enter the deflection region and be separated by size with a permanent magnet placed above the deflection region. Once sufficient spatial separation (>2mm) has been achieved the beads will be captured on carbon composite electrodes using a permanent magnet underneath each electrode.

In this aim the flow rate, magnet size, and magnet placement will be optimized for maximum spatial separation in <5 min. During these experiments, inlets 1-4 (Figure A6.3a) will be pumping at experimentally determined flow rates. To image the beads in the device, the streptavidin-coated PSBs will be labeled with a biotin-FITC probe and imaged with a fluorescent microscope (Dinoscope or similar). A permanent magnet under the device will capture the beads in the flow chamber after deflection from the inlet. The final location of captured beads will determine where electrodes are placed in future device designs.

The microfluidic device will be created with soft lithography techniques to create channels in polydimethylsiloxane (PDMS).[41] Because 5 µm magnetic beads will be the largest used, channels will initially be 10 µm high channels with varying widths depending on the section of the device. Limiting the channel height to roughly the size of the largest particle will result in more consistent deflection angles. The PDMS will then be bound to a poly(methyl methacrylate) (PMMA) backing. Although glass is traditionally used as a backing, PMMA will be used instead so we can incorporate inexpensive thermoplastic electrodes (TPEs) into the device. Our lab pioneered the development of TPEs and their fabrication process can be found elsewhere.[36] PMMA will be bound to PDMS through a silanization and plasma treatment process reported in 2012.[42, 43] Our lab is experienced in this technique and has recently published a similar method for binding PDMS to 3D-printed parts.[44]

Objective 2: Incorporate reagent delivery steps into magnetophoretic device and demonstrate multiplexed detection of all three analytes. Conjugation of target miRNA to the probe-coated Au-MBs will be performed off-chip in a microcentrifuge tube in PBS buffer (Aim 1). After conjugation, the beads will be introduced to inlet 2 and separated as described in Objective 1. Once the beads are separated in the device, DSN and $Fe(CN)_6^{3/4+}$ must be introduced. These reagents will be added to the device by stopping the flow from inlets 1-4, and beginning the flow from inlet 5 (Fig. A6.3). Inlet 5 will contain a solution of DSN and flow will be stopped once the chamber is filled. The DSN incubation time will have been determined in Aim one. Due to the increased sensitivity expected from the cleavage of large PSBs and the incubation times used in previous DSN studies (30-90 min), we anticipate the time needed to detect the objective concentration of 100 aM will be 30 min or less.[20, 23, 24] After the incubation period with DSN, inlet 4 will be turned on again and PSBs that have been cleaved from the magnetic beads will be washed away from the

electrode surfaces. Inlet 4 will then be stopped and inlet 6 turned on. Once the chamber is filled with $Fe(CN)_6^{3/4+}$ from inlet 6, the flow will be stopped and EIS will be performed on each electrode using $Fe(CN)_6^{3/4+}$ as a redox probe. Next, the surface of the electrodes will be regenerated by removing the magnet from the back of the device and flushing the channels with buffer from all 5 inlets. The concentrations of DSN and $Fe(CN)_6^{3/4+}$ found in Aim one will also be used here. Once other conditions in the device (flow rates, channel geometries, etc.) are optimized for sensitive detection of each miRNA, calibration curves will be created and a detection limit and linear range reported.

Objective 3: Detect miRNA from whole blood with the microfluidic device. In this assay the magnetic beads serve two purposes: 1) To capture and sort miRNA for multiplexed detection and 2) to separate miRNA from complex matrices like whole blood. In this objective we will switch from buffered miRNA solutions to pooled whole blood (Lee biosolutions or similar). Real patient samples are not in the scope of this proposal. Instead miRNA will be spiked into whole blood at concentrations determined by the linear range from Aim 2, Objective 2. The blood will be treated with an RNAse inhibitor (Murine or similar commercial product) to protect the miRNA from any RNAse present in the blood sample. Because miRNA will be spiked into the blood, no lysis steps are necessary. However, in studies with real patient samples a cell lysis step will be needed to remove miRNA from cells and exosomes.[45] Ideally, both the lysis and RNAse inhibition will be performed on-chip, which has been accomplished previously.[46] Incubation time of Au-MBs in blood will be determined here. After incubation, a 100 µL blood sample will be injected into inlet 2 and the remaining assay will be identical to the assay developed in Objective 2. The specificity of the assay will be tested again with different combinations of each miRNA along with single base pair mis-matched miRNA. A LOD and linear range in whole blood will also be determined.

Potential pitfalls and workarounds: 1) Reproducible, and precise spatial separation of the magnetic beads may be difficult to achieve. Magnetophoretic separation has been reported, but beads have not been captured on top of electrodes. Spatial separation could be increased by increasing the length of the deflection zone in the device. However, this would increase variability in the final capture location. If enhanced precision is needed, the beads will be collected in secondary channels that narrow over an electrode. 2) miRNA capture efficiency in blood may be poor because of steric hinderance from the PSBs. If miRNA capture is inefficient, the surface coverage of the Au-MBs by PSBs as discussed in Aim 1. 3.) Whole blood may interfere with miRNA capture. If we observe a significant decrease in sensitivity after switching to whole blood samples, we will perform a plasma separation step to remove blood cells that may contribute to the inefficient miRNA capture. Plasma separation has been reported on microfluidic chips previously and a similar separation step will be used here.[47, 48]

Summary: This proposal aims to create a microfluidic device for multiplexed detection of three miRNA specific to lung cancer. Multiplexing will be accomplished via magnetic beads that are separated by size in a microfluidic chamber. miRNA will be detected via EIS after signal amplification with DSN. Importantly, the proposed technique could be adapted to detect other miRNA for screening of other cancers or diseases. Several important innovations for miRNA detection are presented here. First, sensitive detection of miRNA will be accomplished without the need for expensive and complicated nucleic acid amplification techniques. Instead, isothermal capture and detection will take place on a small microfluidic chip with a 100 μL sample. Second, the sensitivity of this assay will be improved over current DSN-amplification techniques by using polystyrene beads bound to the target probe. The loss of PSBs when cleaved by DSN will result in larger changes in impedance than by simply losing the probe. The increased sensitivity will

enable the assay to be shortened and/or the temperature to be reduced. Finally, this proposal will create a fully functioning microfluidic device that will detect a miRNA panel from whole blood. To the best of our knowledge a microfluidic chip for multiplexed miRNA detection does not exist and the proposed device will enable simple, inexpensive, and re-useable miRNA screening assays in settings without access to a centralized laboratory. We are hopeful that the proposed device can provide the type of screening assay that is needed to decrease the lung cancer death rate by improving early detection.

REFERENCES

1. Ferlay, J.; Soerjomataram, I.; Dikshit, R.; Eser, S.; Mathers, C.; Rebelo, M.; Parkin, D. M.; Forman, D.; Bray, F., Cancer incidence and mortality worldwide: sources, methods and major patterns in GLOBOCAN 2012. *International journal of cancer* **2015,** *136* (5), E359-E386.

2. Howlader N, N. A., Krapcho M, Miller D, Brest A, Yu M, Ruhl J, Tatalovich Z, Mariotto A, Lewis DR, Chen HS, Feuer EJ, Cronin KA (eds), SEER Cancer Statistics Review. Institute, N. C., Ed. Bethesda, MD, 2019.

3. Detterbeck, F. C.; Mazzone, P. J.; Naidich, D. P.; Bach, P. B., Screening for lung cancer: diagnosis and management of lung cancer: American College of Chest Physicians evidence-based clinical practice guidelines. *Chest* **2013,** *143* (5), e78S-e92S.

4. Amann, A.; Corradi, M.; Mazzone, P.; Mutti, A., Lung cancer biomarkers in exhaled breath. *Expert review of molecular diagnostics* **2011,** *11* (2), 207-217.

5. Hu, Z.; Chen, X.; Zhao, Y.; Tian, T.; Jin, G.; Shu, Y.; Chen, Y.; Xu, L.; Zen, K.; Zhang, C., Serum microRNA signatures identified in a genome-wide serum microRNA expression profiling predict survival of non-small-cell lung cancer. *J Clin Oncol* **2010,** *28* (10), 1721-1726.

6. Kosaka, N.; Iguchi, H.; Ochiya, T., Circulating microRNA in body fluid: a new potential biomarker for cancer diagnosis and prognosis. *Cancer science* **2010,** *101* (10), 2087-2092.

7. Lee, C. K.; Brown, C.; Gralla, R. J.; Hirsh, V.; Thongprasert, S.; Tsai, C. M.; Tan, E. H.; Ho, J. C. M.; Chu, D. T.; Zaatar, A.; Sanchez, J. A. O.; Vu, V. V.; Au, J. S. K.; Inoue, A.; Lee, S. M.; Gebski, V.; Yang, J. C. H., Impact of EGFR Inhibitor in Non-Small Cell Lung Cancer on Progression-Free and Overall Survival: A Meta-Analysis. *JNCI-J. Natl. Cancer Inst.* **2013,** *105* (9), 595-605.

8. Zamay, T. N.; Zamay, G. S.; Kolovskaya, O. S.; Zukov, R. A.; Petrova, M. M.; Gargaun, A.; Berezovski, M. V.; Kichkailo, A. S., Current and prospective protein biomarkers of lung cancer. *Cancers* **2017,** *9* (11), 155.

9. Zheng, D.; Haddadin, S.; Wang, Y.; Gu, L.-Q.; Perry, M. C.; Freter, C. E.; Wang, M. X., Plasma microRNAs as novel biomarkers for early detection of lung cancer. *International journal of clinical and experimental pathology* **2011,** *4* (6), 575.

10. Gostin, L. O.; Glasner, A. Y., E-cigarettes, vaping, and youth. *Jama* **2014,** *312* (6), 595-596.

11. Chu, G. C.; Lazare, K.; Sullivan, F., Serum and blood based biomarkers for lung cancer screening: a systematic review. *BMC cancer* **2018,** *18* (1), 181.

12. Mitchell, P. S.; Parkin, R. K.; Kroh, E. M.; Fritz, B. R.; Wyman, S. K.; Pogosova-Agadjanyan, E. L.; Peterson, A.; Noteboom, J.; Briant, K. C.; Allen, A.; Lin, D. W.; Urban, N.; Drescher, C. W.; Knudsen, B. S.; Stirewalt, D. L.; Gentleman, R.; Vessella, R. L.; Nelson, P. S.; Martin, D. B.; Tewari, M., Circulating microRNAs as stable blood-based markers for cancer detection. *Proceedings of the National Academy of Sciences* **2008,** *105* (30), 10513.

13. Cho, W. C., MicroRNAs: potential biomarkers for cancer diagnosis, prognosis and targets for therapy. *The international journal of biochemistry & cell biology* **2010,** *42* (8), 1273-1281.

14. Wang, W.; Ding, M.; Duan, X.; Feng, X.; Wang, P.; Jiang, Q.; Cheng, Z.; Zhang, W.; Yu, S.; Yao, W., Diagnostic Value of Plasma MicroRNAs for Lung Cancer Using Support Vector Machine Model. *Journal of Cancer* **2019,** *10* (21), 5090.

15. Qiu, X.; Zhang, H.; Yu, H.; Jiang, T.; Luo, Y., Duplex-specific nuclease-mediated bioanalysis. *Trends in biotechnology* **2015,** *33* (3), 180-188.

16. Shen, J.; Todd, N. W.; Zhang, H.; Yu, L.; Lingxiao, X.; Mei, Y.; Guarnera, M.; Liao, J.; Chou, A.; Lu, C. L.; Jiang, Z.; Fang, H.; Katz, R. L.; Jiang, F., Plasma microRNAs as potential biomarkers for non-small-cell lung cancer. *Lab Invest* **2011,** *91* (4), 579-587.

17. Sozzi, G.; Boeri, M.; Rossi, M.; Verri, C.; Suatoni, P.; Bravi, F.; Roz, L.; Conte, D.; Grassi, M.; Sverzellati, N., Clinical utility of a plasma-based miRNA signature classifier within computed tomography lung cancer screening: a correlative MILD trial study. *Journal of clinical oncology* **2014,** *32* (8), 768.

18. McDonald, J. S.; Milosevic, D.; Reddi, H. V.; Grebe, S. K.; Algeciras-Schimnich, A., Analysis of circulating microRNA: preanalytical and analytical challenges. *Clinical chemistry* **2011,** *57* (6), 833-840.

19. Bustin, S. A.; Nolan, T., Pitfalls of quantitative real-time reverse-transcription polymerase chain reaction. *Journal of biomolecular techniques: JBT* **2004,** *15* (3), 155.

20. Zhang, J.; Wu, D.-Z.; Cai, S.-X.; Chen, M.; Xia, Y.-K.; Wu, F.; Chen, J.-H., An immobilization-free electrochemical impedance biosensor based on duplex-specific nuclease assisted target recycling for amplified detection of microRNA. *Biosensors and Bioelectronics* **2016,** *75*, 452-457.

21. Moltzahn, F.; Olshen, A. B.; Baehner, L.; Peek, A.; Fong, L.; Stöppler, H.; Simko, J.; Hilton, J. F.; Carroll, P.; Blelloch, R., Microfluidic-based multiplex qRT-PCR identifies diagnostic and prognostic microRNA signatures in the sera of prostate cancer patients. *Cancer research* **2011,** *71* (2), 550-560.

22. Drain, P. K.; Hyle, E. P.; Noubary, F.; Freedberg, K. A.; Wilson, D.; Bishai, W. R.; Rodriguez, W.; Bassett, I. V., Diagnostic point-of-care tests in resource-limited settings. *Lancet Infect Dis* **2014,** *14* (3), 239-249.

23. Yin, B.-C.; Liu, Y.-Q.; Ye, B.-C., One-step, multiplexed fluorescence detection of microRNAs based on duplex-specific nuclease signal amplification. *Journal of the American Chemical Society* **2012,** *134* (11), 5064-5067.

24. Bai, Y.-Y.; Wu, Z.; Xu, C.-M.; Zhang, L.; Feng, J.; Pang, D.-W.; Zhang, Z.-L., One-to-Many Single Entity Electrochemistry Biosensing for Ultrasensitive Detection of microRNA. *Analytical chemistry* **2019,** *92* (1), 853-858.

25. Lisdat, F.; Schäfer, D., The use of electrochemical impedance spectroscopy for biosensing. *Anal. Bioanal. Chem.* **2008,** *391* (5), 1555.

26. Channon, R. B.; Yang, Y.; Feibelman, K. M.; Geiss, B. J.; Dandy, D. S.; Henry, C. S., Development of an electrochemical paper-based analytical device for trace detection of virus particles. *Analytical chemistry* **2018,** *90* (12), 7777-7783.

27. Carrell, C. S.; Wydallis, R. M.; Bontha, M.; Boehle, K. E.; Beveridge, J. R.; Geiss, B. J.; Henry, C. S., Rotary manifold for automating a paper-based Salmonella immunoassay. *RSC Adv.* **2019,** *9* (50), 29078-29086.

28. Srisa-Art, M.; Boehle, K. E.; Geiss, B. J.; Henry, C. S., Highly Sensitive Detection of Salmonella typhimurium Using a Colorimetric Paper-Based Analytical Device Coupled with Immunomagnetic Separation. *Analytical Chemistry* **2018,** *90* (1), 1035-1043.

29. Rattanarat, P.; Suea-Ngam, A.; Ruecha, N.; Siangproh, W.; Henry, C. S.; Srisa-Art, M.; Chailapakul, O., Graphene-polyaniline modified electrochemical droplet-based microfluidic sensor for high-throughput determination of 4-aminophenol. *Analytica chimica acta* **2016,** *925*, 51-60.

30. Wang, L.; Veselinovic, M.; Yang, L.; Geiss, B. J.; Dandy, D. S.; Chen, T., A sensitive DNA capacitive biosensor using interdigitated electrodes. *Biosensors and Bioelectronics* **2017,** *87*, 646-653.

31. Geng, Q.; Fan, T.; Zhang, B.; Wang, W.; Xu, Y.; Hu, H., Five microRNAs in plasma as novel biomarkers for screening of early-stage non-small cell lung cancer. *Respir Res* **2014,** *15* (1), 149-149.

32. Shen, J.; Liu, Z.; Todd, N. W.; Zhang, H.; Liao, J.; Yu, L.; Guarnera, M. A.; Li, R.; Cai, L.; Zhan, M., Diagnosis of lung cancer in individuals with solitary pulmonary nodules by plasma microRNA biomarkers. *BMC cancer* **2011,** *11* (1), 374.

33. Feng, S.; He, A.; Wang, D.; Kang, B., Diagnostic significance of miR-210 as a potential tumor biomarker of human cancer detection: an updated pooled analysis of 30 articles. *OncoTargets and therapy* **2019,** *12*, 479.

34. Kunz, M.; Wolf, B.; Schulze, H.; Atlan, D.; Walles, T.; Walles, H.; Dandekar, T., Non-coding RNAs in lung cancer: Contribution of bioinformatics analysis to the development of non-invasive diagnostic tools. *Genes* **2017,** *8* (1), 8.

35. Tsujiura, M.; Ichikawa, D.; Komatsu, S.; Shiozaki, A.; Takeshita, H.; Kosuga, T.; Konishi, H.; Morimura, R.; Deguchi, K.; Fujiwara, H.; Okamoto, K.; Otsuji, E., Circulating microRNAs in plasma of patients with gastric cancers. *British Journal of Cancer* **2010,** *102* (7), 1174-1179.

36. Klunder, K. J.; Nilsson, Z.; Sambur, J. B.; Henry, C. S., Patternable Solvent-Processed Thermoplastic Graphite Electrodes. *Journal of the American Chemical Society* **2017,** *139* (36), 12623-12631.

37. Klunder, K. J.; Clark, K. M.; McCord, C.; Berg, K. E.; Minteer, S. D.; Henry, C. S., Polycaprolactone-enabled sealing and carbon composite electrode integration into electrochemical microfluidics. *Lab Chip* **2019,** *19* (15), 2589-2597.

38. Munaz, A.; Shiddiky, M. J. A.; Nguyen, N.-T., Recent advances and current challenges in magnetophoresis based micro magnetofluidics. *Biomicrofluidics* **2018,** *12* (3), 031501-031501.

39. Pamme, N.; Wilhelm, C., Continuous sorting of magnetic cells via on-chip free-flow magnetophoresis. *Lab Chip* **2006,** *6* (8), 974-980.

40. Xuan, X.; Zhu, J.; Church, C., Particle focusing in microfluidic devices. *Microfluidics and Nanofluidics* **2010,** *9* (1), 1-16.

41. Qin, D.; Xia, Y.; Whitesides, G. M., Soft lithography for micro- and nanoscale patterning. *Nature Protocols* **2010,** *5* (3), 491-502.

42. Sunkara, V.; Park, D. K.; Hwang, H.; Chantiwas, R.; Soper, S. A.; Cho, Y. K., Simple room temperature bonding of thermoplastics and poly(dimethylsiloxane). *Lab Chip* **2011,** *11* (5), 962-965.

43. Sunkara, V.; Cho, Y. K., Investigation on the Mechanism of Aminosilane-Mediated Bonding of Thermoplastics and Poly(dimethylsiloxane). *ACS Appl. Mater. Interfaces* **2012,** *4* (12), 6537-6544.

44. Carrell C.S., M. C. P., Feeny R.W., Henry C.S., Sealing 3D-Printed Parts and PDMS for Simple Fabrication of Microfluidic Devices. *Analytica Chimica Acta, Accepted for Publication* **2020**.

45. Gallo, A.; Tandon, M.; Alevizos, I.; Illei, G. G., The majority of microRNAs detectable in serum and saliva is concentrated in exosomes. *PLoS One* **2012,** *7* (3).

46. Kim, J.; Johnson, M.; Hill, P.; Gale, B. K., Microfluidic sample preparation: cell lysis and nucleic acid purification. *Integrative Biology* **2009,** *1* (10), 574-586.

47. Yang, S.; Ündar, A.; Zahn, J. D., A microfluidic device for continuous, real time blood plasma separation. *Lab Chip* **2006,** *6* (7), 871-880.

48. Amasia, M.; Madou, M., Large-volume centrifugal microfluidic device for blood plasma separation. *Bioanalysis* **2010,** *2* (10), 1701-1710.